NASA Contractor Report 185278

# The Entrainment Rate for a Row of Turbulent Jets

Eliott B. Gordon and Isaac Greber
*Case Western Reserve University*
*Cleveland, Ohio*

September 1990

NASA
National Aeronautics and
Space Administration

# THE ENTRAINMENT RATE FOR A ROW OF TURBULENT JETS

by

ELIOTT B. GORDON and ISAAC GREBER

DEPARTMENT OF MECHANICAL AND AEROSPACE ENGINEEERING

CASE WESTERN RESERVE UNIVERSITY

## ACKNOWLEDGEMENTS

# TABLE OF CONTENTS

# GLOSSARY OF TERMS AND SYMBOLS

$A_i$      Incremental area of one and two dimensional velocity distribution grids

B      Slot jet width

S      Distance between jet centerlines (units in feet)

D      Jet diameter (ft.)

Q      Volume flux (cu.ft./sec)

$Q_o$      Initial volume flux (cu.ft./sec)

J      Momentum flux (ft.$^4$/sec$^2$)

$J_o$      Inital momentum flux (ft.$^4$/sec$^2$)

X      Axial distance downstream of jet source. See Fig. 1

Y      Direction parallel to axis perpendicular to and through centerlines of the row of jets. See fig. 1

Z      Direction perpendicular to X-Y plane of jet array. See fig. 1

Jet array      Row of jets

Radial      Perpendicular to jet axis

U      Velocity component along jet axis or X axis (ft./sec)

V      Velocity component along Y axis

W      Velocity component along Z axis

$U_o$      Maximum initial jet velocity as measured at jet source (ft./sec)

$U_m$      Maximum axial jet velocity as measured at a given downstream cross-section (ft./sec)

$U(r=1/2R_o)$      Axial velocity measured at midpoint bet-

ween jet centerline and nozzle wall at jet source.

Section      Y-Z plane in which velocity distributions fall

$U_i$      Average of 200 instantaneous velocity readings that is assigned to a one or two dimensional coordinate in the velocity distribution grid (ft./sec)

$U_{iave}$      Average velocity found by $[U(i) + U(i+1)]/2$ in the one dimensional grid and by $[U(i,j) + U(i+1,j) + U(i,j+1) + U(i+1,j+1)]/4$ for the two dimensional velocity distribution grid. (ft./sec)

Re      Reynold's number, based on maximum nozzle velocity at the jet source and on the jet diameter

r      Correlation coefficient

# Chapter I

## Introduction

The subject of this study is the free jet which results from the injection of a fluid through a row of equally spaced nozzles (at turbulent Reynold's numbers) into an unbounded resevoir in which a second fluid is initially at rest. The focus of attention is on one particular property of the free jet - the mass flow rate across a section at right angles to the jet axis:

$$m = \int \rho \, U \, dA \qquad \text{eqn. (1)}$$

As fluid is injected into the quiescent environment, the second fluid of this resevoir is drawn radially inwards towards the jet axis (in the case of the circular jet) or is drawn in along the Z axis (in the case of the slot jet) until it becomes part of the jet. This process is known as entrainment.

The entrainment rate for a fluid issuing into a quiescent environment can be varied between the limiting entrainment rates of the single circular and slot jet by changing the jet spacing to jet diameter ratio (S/D). Choosing smaller S/D's results in entrainment rates closer to that of the slot jet, while larger S/D's result in entrainment rates which approach that of the circular jet.

In a study of dilution jet mixing in compact reverse flow combustors for gas turbines, Lipshitz and Greber noted the need for and absence of information on the entrainment rate for a row of jets (ref. 6).

It is the intent of this study to provide fundamental data and its results on the effect that jet spacing in a row of jets has upon the entrainment rate. Chimney spacing required to givea specified dilution rate of exhaust gases into the environment, fuel to air mixing ratios in injection and carburation systems, the determination of jet interaction behavior in cases such as V/STOL aircraft and jet engine combustion chambers represent only a few of the many applications that require basic information on jet array entrainment rates.

This study undertakes as its primary objective the establishment of entrainment rates for array spacing ratios of S/D = 2.5, 5, 10, and 20. Velocity distributions are determined at X/D = 16.4, 32.8, 65.6, 98.4, 131.2, and 164 at Reynold's numbers ranging from 5,110 to 17,000. Centerline velocity decay rates are also presented in the results.

## Chapter II

## PREVIOUS STUDIES

Numerous measurements of the axial velocity pro-
files have been made in studies of isothermal air jets.
Inserting U(y,z) into equation (1), the mass flow can
be determined by numerical quadrature. This is, how-
ever, a time consuming and difficult procedure that
many authors have circumvented by assuming a profile
that permits analytical integration. Then by measuring
the jet velocity at the axis and the distance from the
axis at which the velocity is half of the center line
velocity, the assumed velocity profile can then be
scaled to that section. Obviously, the mass flux then
becomes dependent on the `theoretical' curve chosen by
the author.

The difficulties in determining detailed velocity
distributions are largely a result of the limitations
of the instrument used to make the velocity measure-
ments - the pitot tube (ref. 9). At large distances
from the jet axis, where the velocity of jet becomes
very small and increasingly intermittant, the pressure
differences are difficult to read because of their
small and constantly changing magnitude.

The limitations involved in determining detailed

velocity distributions and in curve fitting the velocity profile into an analytical form that can than be integrated prompted Ricou and Spalding to formulate an experimental procedure that bypasses the integration of a velocity profile altogether. The two researchers devised their method on the basis of the following considerations (ref. 9):

> "In the ideal free jet which is under consideration, the surrounding resevoir is large and, except in the vicinity of the jet axis, at uniform pressure; the entrained fluid flows radially inward towards the jet axis. If, however, a turbulent jet is partially enclosed in circular walls, the radial inflow is impeded; the fluid entrained by the enclosed part of the jet has to flow axially in the annular space between the cylindrical wall and the conical `boundary'of the jet; the corresponding axial pressure gradients can be be measured.
> Now let us suppose that the cylindrical wall is made porous, and that a controlled and measured amount of fluid can be caused to flow through it in a radially inward direction. Then, if this flow is equal in quantity to that which would have passed through the area occupied by the wall if the wall had been absent, the axial pressure gradients reffered to in the last paragraph would disappear.
> This recognition underlies the experimental method which has been used: the flow rate through the porous wall is varied until no axial pressure gradients can be detected; this flow rate is then measured and presumed to be equal to that which would be entrained if the jet were unenclosed."

A detailed discription of their apparatus and procedure may be found in reference 9.

If we take the case of the isothermal free jet - where the temperature of the resevoir air is equal to that of

fluid issuing into the resevoir - the entrainment rate reduces to the rate of change in the volume flux. The volume flux itself can be expressed as a function of the initial volume flux, $Q_o$, the distance from the jet source, $X$, the jet diameter or width, $D$ or $B$, and the jet Reynold's number, $Re$, and the initial velocity profile. In nondimensional form, the expression becomes:

$$Q/Q_o = f(X/D \text{ or } X/B, Re, \text{initial profile})$$

For a given nozzle geometry, a measure of the initial velocity profile, called the coefficient of jet structure, has been defined as $a = 0.066(U_m/U_o)$ where $U_m/U_o$ is a centerline velocity divided by the maximum initial velocity in a jet whose initial velocity profile is not uniform (fig. 2). The coefficient of jet structure increases from a base value of 0.066 (when the initial velocity profile is uniform) with increasing nonuniformity in the initial velocity profile. The product of $a/0.066$ and $U_m/U_o$ (where $U_m$ is a centerline velocity for a jet whose initial velocity profile is not uniform) now agrees with the theoretical curve (due to Tollmien) for the variation of velocity on the jet centerline. The dependence of the coefficient of jet structure on the initial velocity profile is shown in figure 3. The volume flux can then be expressed as:

$$Q/Q_o = f(X/D \text{ or } X/B, \text{ initial velocity profile})$$

Figure 25 shows a centerline velocity, decay rate
curve for the circular jet that has been adjusted to
the initial velocity profile of the S/D = 20 curve just
above. The correspondance was so exact that the circu-
lar jet curve had to be shifted slightly downward in
order to distinguish the two curves.

Analysis of the experiments of Trupel, Zimm, the
Gottingham Aerodynamics Institute, Turkus, and Syrkin
(ref. 1) has shown that for Reynold's numbers ranging
from 20,000 (or where the initial velocity distribution
becomes uniform) to 4,000,000 the plot of Um/Uo versus
X/D falls on the same curve, and the entrainment rate
can be reduced to:

$$Q/Qc = f(X/D \text{ or } X/B)$$

As the Reynold's numbers decrease and the nonuniformity
in the initial velocity distribution increases, the
axial velocities downstream of the jet source decay
more rapidly. The result is that the volume flux rates
of turbulent jets with an Re of less than 20,000 are
smaller than entrainment rates of turbulent jets with
uniform initial profiles. It should be noted that the
formulas given for the slot and single circular jet
(table 1) are generally valid for Reynold's numbers
in excess of 20,000.

The entrainment rates for the row of jets requires the

addition of the nondimensional parameter that takes into account the jet spacing. The functional relation for the row of jets is therefore represented by:

$$Q/Qo = f(X/D, S/D, \text{initial velocity profile})$$

Mary Nash, a graduate student at Case Institute of Technology, presented results for two spacing configurations (S/D = 5 and 10) for the row of jets. Her results are:

$$Q/Qo = (X/D)^{.665}$$

for S/D = 5, at Re = 5600, and

$$Q/Qo = (X/D)^{.692}$$

for S/D = 10, at Re = 7,000. These entrainment rates are limited to an X/D range of 70 to 220. For X/D < 70, Nash found her experimental values for volume fluxes (for both S/D = 5 and 10) to be higher than the rate for the single circular jet. As a result, she deemed her data valid only for X/D > 70.

## Chapter III

## EXPERIMENTAL METHOD

The volume flux is determined at the jet source,
Qo, and at cross sections 5, 10, 20, 30, 40, and 50 cm.
from the jet source. The volume flux, $\Sigma \Delta Y \Sigma$ Uiave$\Delta$ Z,
is found by integrating the velocity distributions that
have been measured across the entire width of the jet
and from the midpoint between the central jet being
surveyed and its neighbor underneath to the midpoint
between the center jet and the neighboring jet above,
as shown in figure 4. In all cases, the hot wire probe
is oriented along the Y axis.

### 2.1  Apparatus

41 jet apertures, .3 inches on center, are drilled
and reamed to .12 inches in diameter in a 2.25 x 13 x 1
inch block of polyvinylchloride. Thisspacing between
adjacent jets gives an original S/D ratio of 2.5, with
larger S/D ratios obtained by simply plugging ever
other jet. The row of jets is mounted on an adjustable
support, and is connected to a plenum chamber that
evenly divides the flow from the compressor (supplied
through 1 inch O.D. tubing) to each one of the aper-
tures.

The row of jets is bounded by a three sided enclo-

sure (figure 5) that constrains the entrainment air to be drawn in along the Z axis, and that prevents the flow from spreading along the Y axis. The setup not only approximates flow in a section of an infinite row of jets, but prohibits the axial entrainment of air from behind the jet source. The enclosure is constructed out of quarter inch plexiglas, glued together with thermal adhesive.

A three foot diameter axial compressor supplies air to the plenum chamber through a Jamesbury valve used to adjust flow as read on a 28 cfm. full scale, Fischer-Porter rotameter.

A three foot hot wire probe support is mounted on a three directional tracking mechanism that is powered along the Z and Y axis by Superior Electric MO62-FD03 stepping motors. The stepping motors are connected to screw and follower mechanisms that drive the probe at 1 inch per 16 shaft revolutions along the Z axis and at 1 inch per 13 shaft revolutions along the Y axis. Operating at 1.8 degree steps per pulse, the steppers are capable of moving the probe incremental distances which are on the order of the thickness of the hot wire probe diameter - .002 inches. Even at such small distances, the error due to hysterisis in the follower mechanism, a double follower is employed in the Z direction

mechanism, while the weight of the probe mount assures
no hysterisis along the Y axis (figure 6). Smooth
tracking, resulting in minimal torque required from
the stepping motors, is obtained by mounting the Z and
Y axis traversing components on linear tracking bearings.

A Tecmar Labmaster A/D board supplies the square
wave pulses that are amplified by a single driver card
which powers the stepper motors. A pulse rate of just
under 400 per second (the maximum allowable for accu-
rate operation of the stepping motors) is generated by
a timer source on the A to D board, and is in turn
gated by a second timer that determines the duration of
the square wave form. In this way, the distance that
the probe is moved can be controlled by varying the
duration set by the second or gating timer.

The probe support is fixed to the traversing
mechanism so that it moves the hot wire probe into the
jet wake along the Z axis. This probe support orienta-
tion places the traversing mechanism the farthest pos-
sible distance from the jet, while minimizing the ob-
struction that the probe support itself introduces into
the flow field of the jet.

2.2   Instrumentation

A TSI model 1054B constant temperature linearized
hot wire anemometer is paired with a model 1210-20 hot

wire probe that produces a voltage signal which is proportional to air speed. The analog voltage signal generated by the anemometer is then sampled by the Labmaster A/D board at a 50 hertz frequency, and processed by an IBM XT personal computer (256k with one hard and one floppy disk drive).

All plots are made on a Hewlett-Packard 7470A plotter.

## 2.3  Experimental Procedure

The initial volume and momentum fluxes are experi-
mentally determined at the exit of the jet nozzle
through the establishment of a highly detailed velocity
distribution across the jet nozzle. The hot wire probe
sensor element is positioned at centerline of the jet,
just inside the nozzle. The program is initialized, and
the probe is positioned at .003 inch increments across
the mouth along the Z axis (from the jet centerline to
the nozzle wall) of the jet for velocity readings. The
values for Qo and Jo are calculated by the following
formulas:

$$Qo = \Sigma \, (Uiave) \, (Ai)$$

$$Jo = \Sigma \, (Uiave)^2 \, (Ai)$$

$$Ai = \Sigma \, [R(i)^2 - R(i-1)^2]$$

The volume flux found by integrating the initial velo-
city profile is compared to the volume flux as indi-
cated by the rotameter.

Downstream cross sections at 5, 10, 20, 30, 40,
and 50 cm. are surveyed by locating the jet ` boundary'
using smoke to visualize the flow, positioning the hot
wire probe just outside the jet boundary, and initiali-
zing a program that positions the probe at .0625 inch
intervals across the jet wake in the Z direction until
the probe is 1/4 inch outside the jet `boundary' on the

otherside. The position of the probe is incremented up in the Y direction by .075 inches and the Z direction operation is performed again until the the probe has been moved up from the midpoint between the central jet and it neighbor below to the midpoint between the central jet and its neighbor above. The probe therefore sweeps out the area as shown in figure 4: where the area equals the distance from boundary to boundary times S. This procedure is repeated for all cross sections, although in S/D ratios of 10 and 20 the velocity grid is relaxed along the Y axis to .15 inches at far downstream cross sections. If, at any point in this operation, there is a question about the exact location of the jet `boundary', the program is momentarily stopped and the flow field of the jet is again visualized using smoke.

Having established values for the volume flux at the jet source and at the six downstream locations, functions of the form

$$Q/Qo = A(X/D)^C + B$$

are determined by choosing the exponent, C, and then performing a least squares fit which determines the constants A and B.

# Chapter IV

## RESULTS

The entrainment rates found for the four spacing ratios tested are presented in Table 2, along with the previously determined entrainment rates for the slot jet and the circular jet. Figure 7 is a graphical representation of the rates given in Table 2. Figures 8 - 11 show the least squares fit of the entrainment rate curves to the experimentally determined volume fluxes for each of the spacing ratios. As expected, the entrainment rates increase monotonically with increasing $S/D$, with small $S/D$ jet rows approaching the entrainment behavior of the slot jet and large $S/D$ jet rows approching the entrainment behavior of the circular jet.

The entrainment rates for the four spacing ratios are valid for $X/D$ greater than 10, because self-similarity in the velocity distributions generally begins at 10 nozzle diameters from the jet source (ref. 1). For $S/D = 5$, 10, and 20, the entrainment rates between $X/D = 10$ and lower value delineating the valid range for the use of the given rate formula may be calculated by using the entrainment rate formula for the circular jet.

For each of the four spacing to nozzle diameter

ratios tested, the upstream entrainment rate approaches
that of the individual circular jet, while the down-
stream entrainment rate approximates that of the slot
jet.

The least squares fit formulas for the velocity
decay rates are presented in table 3, and are graph-
ically represented in figure 12. The velocity decay
rate formulas for each of the spacing ratios are graph-
ed against the measured velocities in figures 13 - 16.
The decay rates also vary monotonically with
increasing S/D between the limiting cases of the slot
and circular jet, with the decay rate of the smaller
S/D row of jets approaching that of the slot jet and
the decay rate of the larger S/D row of jets approach-
ing the circular jet.

The dimensionless plots of Q/Qo versus Z/Z(1/2Um)
in figures 17 - 20 exhibit the self-similarity of the
velocity distributions recorded for each of four spa-
cing ratios.

Summaries of directly measured and calculated
quantities - listing values for S, Qo, Jo, Uo, Re, Um,
J, and Q - are given in tables 4 - 7.

Figure 21 presents a plot of Q/Qo (experimentally
determined) versus S/D for X/D = 65.6, 98.4, 131.2, and
164. A least squares curve is fit to the dimensionless

volume fluxes for each X/D in order to predict dimen-
sionless volume fluxes for S/D's ranging from 2.5 to
20. The X/D = 164 curve is proportional to $(S/D)^{.65}$,
the X/D = 131.2 curve is proportional to $(S/D)^{.60}$, the
X/D = 98.4 curve is proportional to $(S/D)^{.55}$, while the
X/D = 65.6 curve is proportional to the square root of
S/D. The curves for X/D = 164 and 131.2 are proportion-
al to S/D in the S/D range between 2.5 and 10.

# CHAPTER V

## DISCUSSION

The early stages of the present study were spent in an effort to assure the proper alignment of the jets first with respect to each other and second with respect to the traversing mechanism that moves the hot wire probe along each of the three axes. Misalignment in the row of jets itself can cause significant variations in centerline velocity and volume flux values for a section. These values will be larger than those for the perfectly aligned case if the nozzles converge in the X - Y plane, while the centerline velocities and volume fluxes for the divergent nozzles will be smaller.

Problems generated by jet misalignment were so severe that an original jet row assembly consisting of drilled and reamed threaded rod that screwed into tapped aluminum plate was discarded in favor of a solid block of aluminum in which jet apertures were drilled and reamed on a vertical milling machine. A number of jet row assemblies were drilled and tested, each one showing better symmetry in recorded velocities about the jet centerline along the Z axis and more uniform periodicity in velocities measured through the jet centerlines along the Y axis. Misalignment was further reduced by using a block of polyvinylchloride. The

softer plastic reduced drill over heating due to friction and required less load on the drill thereby reducing drill deflection during the machining operation.

After aligning the final row of jets assembly with traversing mechanism tests were performed to determine symmetry in velocity distributions about the jet centerline and to determine periodicity of velocity measurements taken through the jet centerlines along the Y axis. Figure 22 plots velocity measurements taken along the Y axis (through the jet centerlines) against the jet centerlines - as represented by the lines along the ordinate. The $S/D = 5$ case (shown in the lower half of the graph) shows the velocity distribution - at $X/D = 14$ - for 13 central jets out of a 20 jet row. The $S/D = 10$ case represents the velocity distribution - at $X/D = 65.6$ - for the 7 central jets in a 12 jet row. Tests conducted at $X/D = 164$ for $S/D = 2.5, 5$, and 10 resulted in velocity distributions (along the Y axis) that are uniform throughout a central 11 inch portion of the 13 inch distance from the top to bottom wall of the row of jet enclosure.

There is a fundamental difference in the velocity profiles of the slot and circular jet at and beyond $Y/Y(1/2Um) = \pm 1.85$ suggested in the comparison of figures 23 and 24. In both cases, the theoretical curve

due to Tollmien predicts a gradual decrease in axial
velocity from $Y/Y(1/2Um) = 2.0$ until it reaches a value
of zero at $Y/Y(1/2Um) = 2.5$. For the circular jet, ex-
perimental data is in excellent agreement with
Tollmien. Experimental data on the slot jet, however,
indicates that between $Y/Y(1/2Um) = 1.6$ and $1.85$ axial
velocities are presented only to $.2$ to $.1(Um)$, after
which no data appears to exist. Possible reasons for
this will be discussed below. Figure 25 shows qualita-
tively the streamline patterns for a circular, free
turbulent jet. At the jet 'boundary', marked by the
broken line, the streamlines vary from nearly radial to
nearly axial in direction. Farther downstream, this
streamline direction change is more gradual. There
seems to be little documentation in the literature on
streamline behavior for the slot jet. Figure 26 illus-
trates the results of flow visualization (using smoke)
for row of jet spacing to diameter ratios of up to and
including $S/D = 10$, and strongly suggests - as does
figure 23 - that there exists a point where the axial
velocity distribution goes to zero.

The flow visualization used in this study indi-
cates that there is not a monotonic decrease in axial
velocities to zero (as in the case of the circular
jet), but rather a region of oscillatory flow, as well

as back flow at a fairly well identified jet `boun-
dary'. Furthermore, it has been found that there is a
correlation between the `boundary' and the hot wire
anemometer voltage response at that location in the
flow field. Looking again at figure 26, the mean
streamlines approaching and crossing the jet `boundary'
(delimited by the broken line) are represented by a
smooth lines with both a radial and a somewhat smaller
negative axial component. As this entrained air ap-
proaches the jet `boundary', the back flow intensifies
until it becomes parallel to the `boundary'. The back
flow then ceases - as shown in figure 26 - oscillates
back and forth along the X axis with no net axial
velocity and with only a very small radial velocity. At
this point, Ui recordings drop from axial velocities of
approximately 2 fps. to readings that fluctuate between
1.5to .8 fps.. This represents the zone just outside
the jet `boundary' where no net axial velocity exists.
Because the anemometer voltage signal records only the
magnitude of the velocity and not the direction, an ap-
parent net velocity is indicated when in fact none
exists. As the probe moves farther out from the jet
axis, Ui readings rise again to 1.2 to 1.8 fps.. These
slightly higher readings show no fluctuation and repre-
sent the zone in which the back flow of the entrainment

air suddenly intensifies. Beyond this zone, velocity
readings fall back to under 1.0 fps. from which they
slowly decrease as the probe continues to move out from
the jet axis.

The velocity distributions shown in figures 1B -
52B represent total velocities. Within what has been
termed the jet `boundary', flow visualization has shown
that the velocities are axial. For the X/D locations of
65.6 only velocity points within $Y/Y(1/2Um) = \pm 1.85$
are summed over their respective area to yield a volume
flux. Farther downstream, the $Y/Y(1/2Um)$ bounds shrink,
until at $X/D = 164$ only the velocity points within
$Y/Y(1/2Um) = \pm 1.6$ are included in the axial velocity
distribution. Since the downstream flow behavior of the
row of jets approaches that of the slot jet, it is
encouraging to note the very close correspondance bet-
ween the velocity distribution cutoffs - as identified
by the flow visualization used in this study - and the
experimental data on the slot jet from previous re-
search. In the same way, the cutoff points for the X/D
= 16.4 and 32.8 cross sections are approximately at
$Y/Y(1/2Um) = 2.6$ and at $Y/Y(1/2Um) = 2.2$ respective-
ly. In the case of the more closely packed row of jets
- where streamline behavior approaches that of the slot
jet - it is easier to identify the characteristic sig-

nature recorded by the anemometer because the back flow and oscillating flow at the 'boundary' are more pronounced than in the case of the larger S/D row of jets, whose streamline behavior approaches that of the circular jet.

Figures 27 - 35 display the flow behavior of entrained air as it is drawn in towards the jet axes. In each of the figures, the row of jets is on the far right hand side of the photographs. The line of sight is almost at a right angle to the jet axis,and about 6 inches below the level at which the smoke is being injected. The locations of the smoke tests in the jet flow field are indicated in figure 26: for the X/D = 30 locations, smoke is injected into the jet as marked by "1", and for X/D = 120 as marked by "2". Only for the circular jet (figure 25) is the back flow - that characterizes the entrainment flow for the row of jets - absent. Even as far upstream as X/D = 32.8, the S/D = 20 row of jets exhibits a very slight back flow, while farther downstream (approximately X/D = 120) where significant mixing between the jets has begun the entrainment air is slowly oscillating along the X axis with a small net back flow. As the S/D ratio decreases, the strength of the back flow - both near upstream and downstream - increases. Compilation of data on the

initial momentum flux and its values for downstream cross sections of a row of jets suggests instead that, because very near upstream values and far downstream values of J can vary by as much as 5 - 10% from Jo, adjusting the volume flux to correspond with distribution that yield agreement with Jo would seriously inflate the near upstream and far downstream values of Q. Furthermore, the existence of backward entrainment flow along the boundary of the jet would indicate that the assumption upon which the conservation of axial momentum is founded - i.e. that the pressure everywhere in the flow field is uniform and ambient - is not entirely true. This study strongly suggests that pressure driven flows are in evidence at the boundary of the row of jets, and that consequently the conservation of axial momentum cannot be relied upon to furnish a cutoff for the axial velocity profile.

At S/D = 2.5 and 5 tests, the initial volume flux as calculated by integrating the initial velocity profile corresponded to the volume flux as read by the rotameter to within 2%. This excellent agreement broke down in the S/D = 10 and 20 tests when higher plenum chamber pressures apparently resulted in leaks that caused rotometer readings to indicate volume fluxes up to 10% higher than those calculated by integrating the

initial velocity profile. No other explanation is read-
ily available, sinse calibration of the rotameter indi-
cated perfect linearity in its 0 to 28 cfm. readings.
Because of the possibility of small leaks and the 6%
inaccuracy associated with reading the rotameter, the
initial volume flux as calculated by integrating the
initial velocity was relied upon as primary informa-
tion.

The results (given in table 2) indicate that the
entrainment for the row of jets behaves like the circu-
lar jet in the near upstream, while behaving like the
slot jet downstream. The `transition' point, marked by
the conjunction of the circular jet entrainment curve
and the curves that are proportional to the square root
of X/D, corresponds to an X/D at which the jets have
mixed sufficiently so that all velocities along the
Y axis, through the jet centerlines at that section,
are axial. Using data on the jet width growth from the
circular jet tests to predict the X/D at which this jet
mixing would take place for each of the spacing ratios,
excellent correspondance was found between the experi-
mental and predicted value of X/D at which the jet
`boundaries' cross. The predicted value is within 10%
of the experimental value.

# CHAPTER VI

## RECOMMENDATIONS

The following general recommendations concerning experiments on arrays of jets are based on the experience resulting from the experiments of this study.

The use of a three sensor probe anemometer would facilitate velocity measurement sinse it records the instantaneous direction as well as the speed of a flow.

Flow visualization techniques should be employed from the outset of the study so that velocity measurements may be interpreted in light of a previous understanding of general flow characteristics.

Extreme care must be taken in aligning the jets with respect to each other and with respect to the traversing mechanism.

Finally, it is useful to work with initial velocity profiles sinse entrainment rates found will generaly be valid over a wide range of Reynold's numbers in which the initial velocity profile is uniform.

TABLE 1: Turbulent jet rates from previous
studies (ref. 2, 7, and 9)

| Jet Type | Entrainment rate | Centerline Velocity |
|---|---|---|
| Slot Jet | $Q/Q_o = .62\sqrt{X/B}$ | $U_m/U_o = 2.28\sqrt{B/X}$ |
| Circular Jet | $Q/Q_o = .32(X/D)$ | $U_m/U_o = 6.2(D/X)$ |
| Row of Jets S/D = 5 | $Q/Q_o = (X/D)^{.665}$ | $U_m/U_o = .24(D/X)^{.17}$ |
| Row of Jets S/D = 10 | $Q/Q_o = (X/D)^{.692}$ | $U_m/U_o = .74(D/X)^{.50}$ |

TABLE 2: Entrainment Rates

| S/D | Re | Entrainment Rate | Range (X/D) | r |
|------|------|------|------|------|
| Slot Jet | | $Q/Q_o = .62 \sqrt{X/D}$ (ref. 2) | ——— | — |
| 2.5 | 5170 | $Q/Q_o = \sqrt{X/D} + .24$ | 16.4-164 | .998 |
| 5 | 8800 | $Q/Q_o = 1.26 \sqrt{X/D} + .44$ | 16.4-164 | .997 |
| 10 | 9730 | $Q/Q_o = 1.72 \sqrt{X/D} + .74$ | 36-164 | .999 |
| 20 | 12070 | $Q/Q_o = 2.44 \sqrt{X/D} + .13$ | 60-164 | .992 |
| Circular Jet | | $Q/Q_o = .32 \ (X/D)$ (ref. 2) | ——— | — |

TABLE 3: Centerline Velocity Rates

| S/D | Re | Velocity Decay Rate | Range (X/D) | r |
|-----|-----|---------------------|-------------|-----|
| 2.5 | 5170 | $U_m/U_o = 1.53(D/X)^{.55} + .0030$ | 16.4–164 | .999 |
| 5 | 8800 | $U_m/U_o = 3.65(D/X)^{.90} - .0169$ | 16.4–66 | .998 |
| 5 | 8800 | $U_m/U_o = 1.36(D/X)^{.60} - .0068$ | 32.8–164 | .999 |
| 10 | 9730 | $U_m/U_o = 5.21(D/X)^{.95} - .0079$ | 16.4–66 | .998 |
| 10 | 9730 | $U_m/U_o = 2.39(D/X)^{.80} + .0060$ | 65.6–164 | .998 |
| 20 | 12070 | $U_m/U_o = 4.77(D/X)^{.95} - .0030$ | 16.4–164 | .999 |

TABLE 4: Summary of Data for S/D = 2.5

| S/D = 2.5 | | | | |
|---|---|---|---|---|
| S | Qo | Jo | Uo | Re |
| .025 | .0057 | .425 | 84.5 | 5170 |

| X/D | Um | J | Q |
|---|---|---|---|
| 16.4 | 28.07 | .429 | .023 |
| 32.8 | 18.79 | .448 | .035 |
| 65.6 | 12.58 | .430 | .050 |
| 98.4 | 10.14 | .414 | .058 |
| 131.2 | 9.32 | .434 | .067 |
| 164 | 7.92 | .417 | .074 |

TABLE 5: Summary of Data for S/D = 5

| S/D = 5 | | | | |
|---------|---------|---------|---------|---------|
| S | Qo | Jo | Uo | Re |
| .050 | .010 | 1.07 | 142.5 | 8800 |

| X/D | Um | J | Q |
|---------|---------|---------|---------|
| 16.4 | 44.81 | .995 | .054 |
| 32.8 | 23.86 | 1.06 | .073 |
| 65.6 | 15.20 | 1.16 | .113 |
| 98.4 | 12.24 | 1.07 | .133 |
| 131.2 | 10.07 | 1.04 | .147 |
| 164 | 8.98 | 1.00 | .163 |

TABLE 6: Summary of Data for S/D = 10

| S/D = 10 | | | | |
|---|---|---|---|---|
| S | Qo | Jo | Uo | Re |
| .100 | .0110 | 1.30 | 158.0 | 9730 |
| X/D | Um | J | | Q |
| 16.4 | 57.00 | 1.30 | | .057 |
| 32.8 | 28.40 | 1.29 | | .111 |
| 65.6 | 14.33 | 1.30 | | .159 |
| 98.4 | 10.36 | 1.39 | | .203 |
| 131.2 | 8.40 | 1.30 | | .226 |
| 164 | 7.52 | 1.30 | | .253 |

TABLE 7: Summary of Data for S/D = 20

| S/D = 20 | | | | |
|---|---|---|---|---|
| S | Qo | Jo | Uo | Re |
| .200 | .0132 | 2.16 | 196.5 | 12070 |
| X/D | Um | J | Q | |
| 16.4 | 64.89 | 1.90 | .068 | |
| 32.8 | 33.44 | 2.20 | .135 | |
| 65.6 | 17.43 | 2.19 | .255 | |
| 98.4 | 10.86 | 1.91 | .332 | |
| 131.2 | 8.36 | 2.04 | .370 | |
| 164 | 7.29 | 2.11 | .409 | |
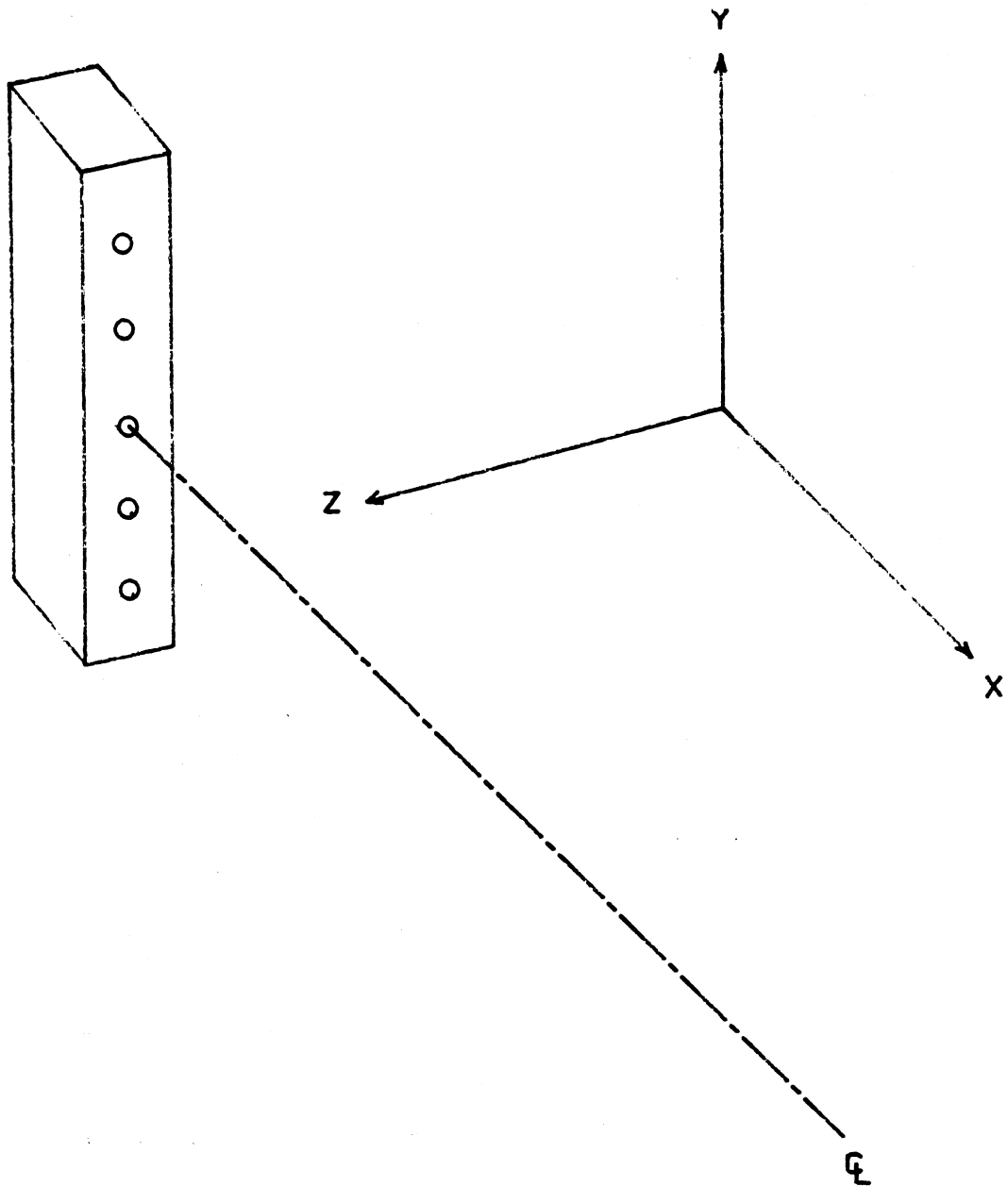
FIGURE 1: Definition of coordinates
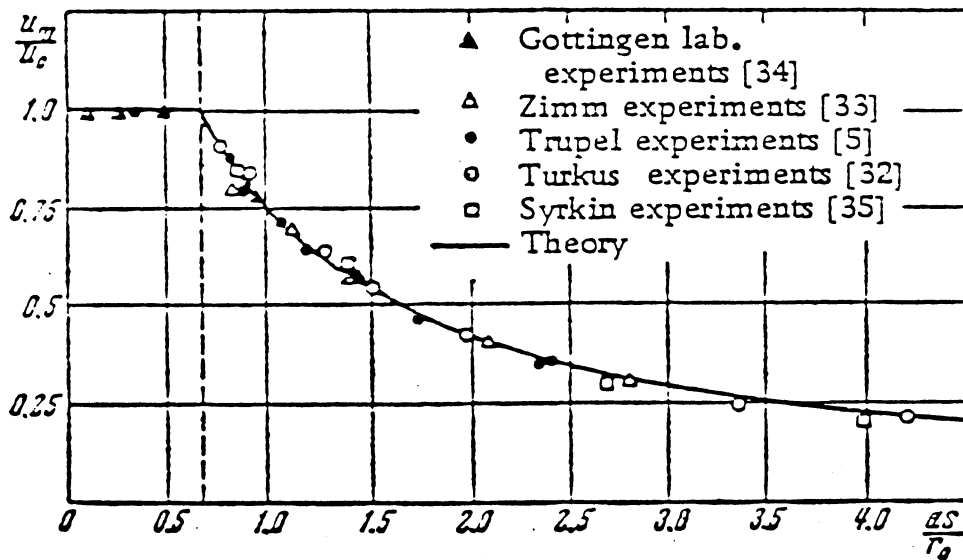
FIGURE 2: Variation of velocity on the axis
of a circular jet (ref. 1)
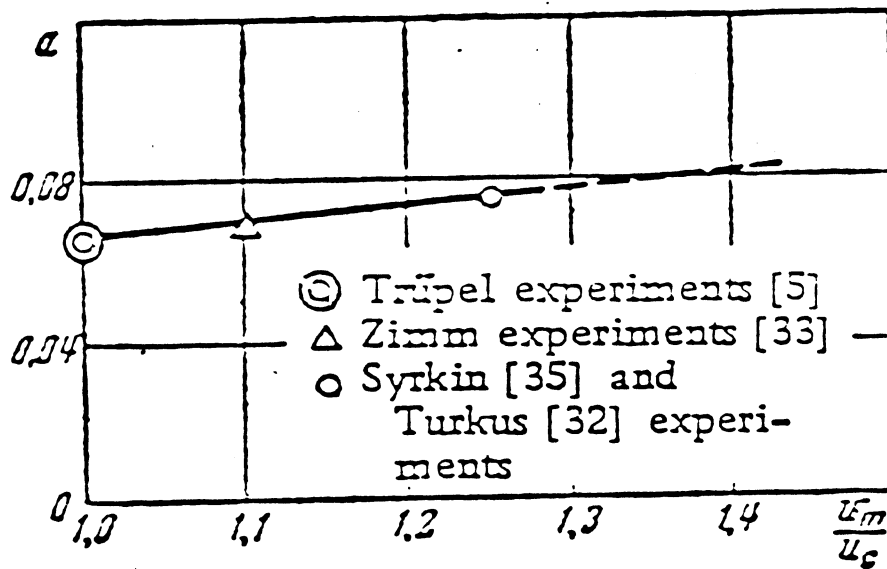


FIGURE 3: The dependence of the coefficient of
structure of a jet, a, on the initial
velocity profile (ref. 1)
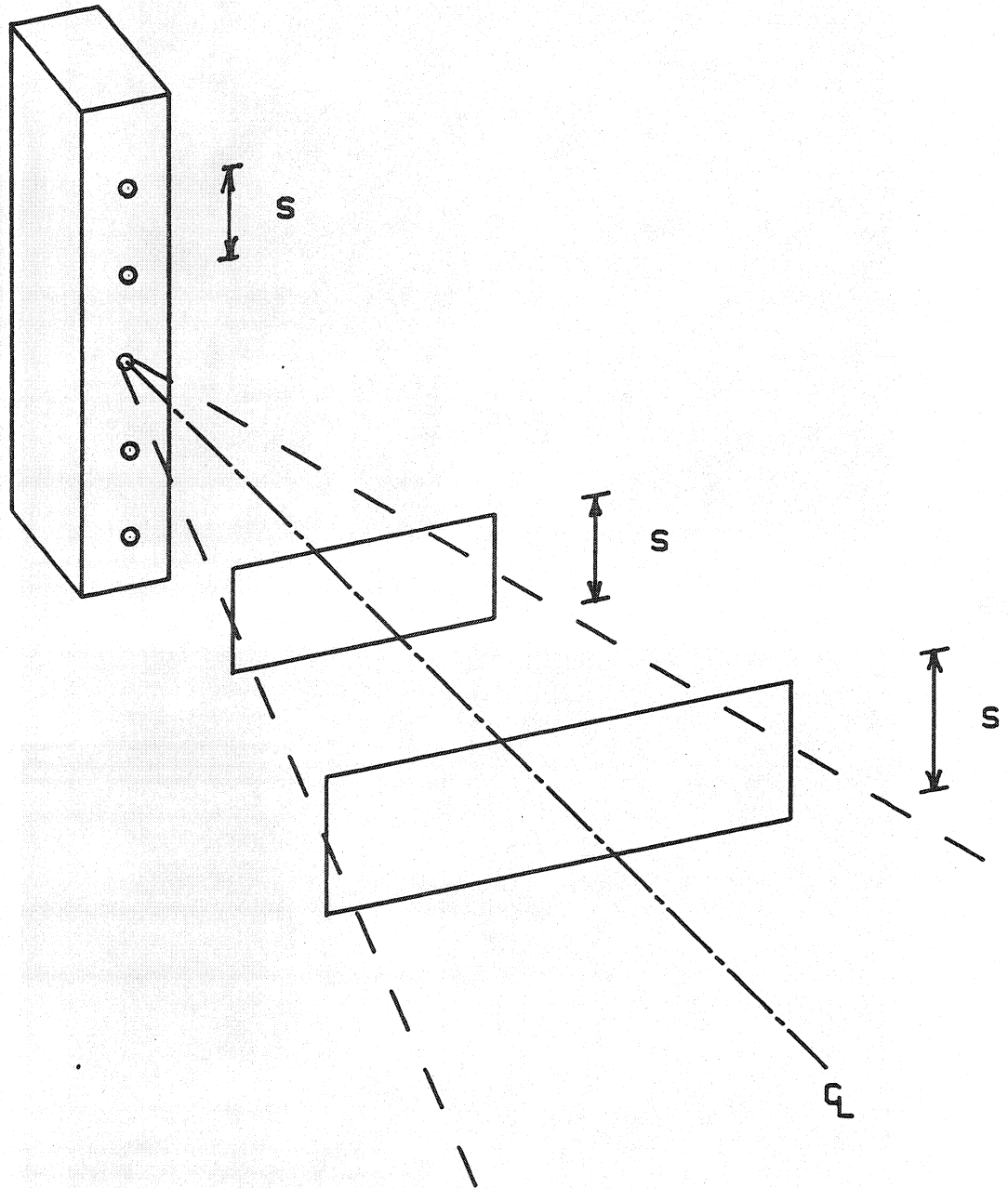
FIGURE 4: Area over which velocity
distribution is integrated
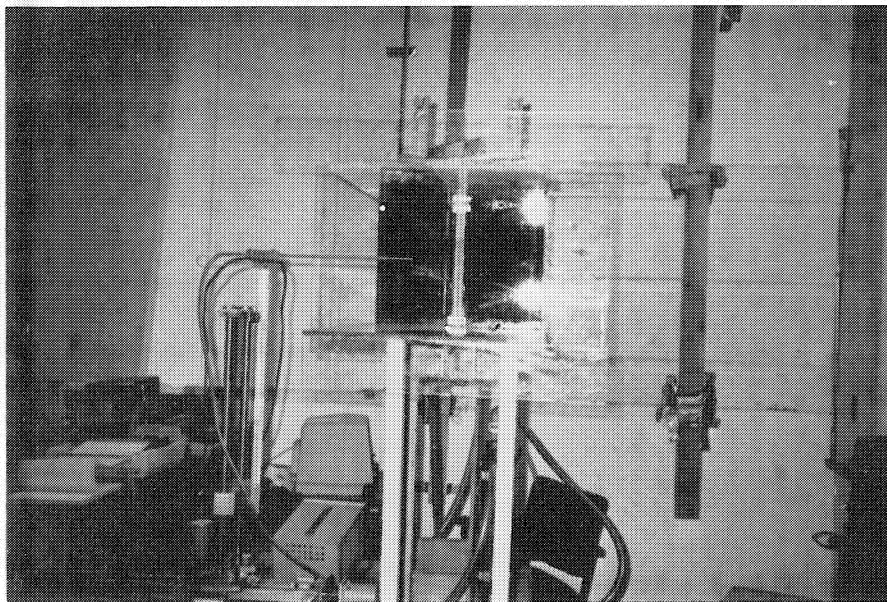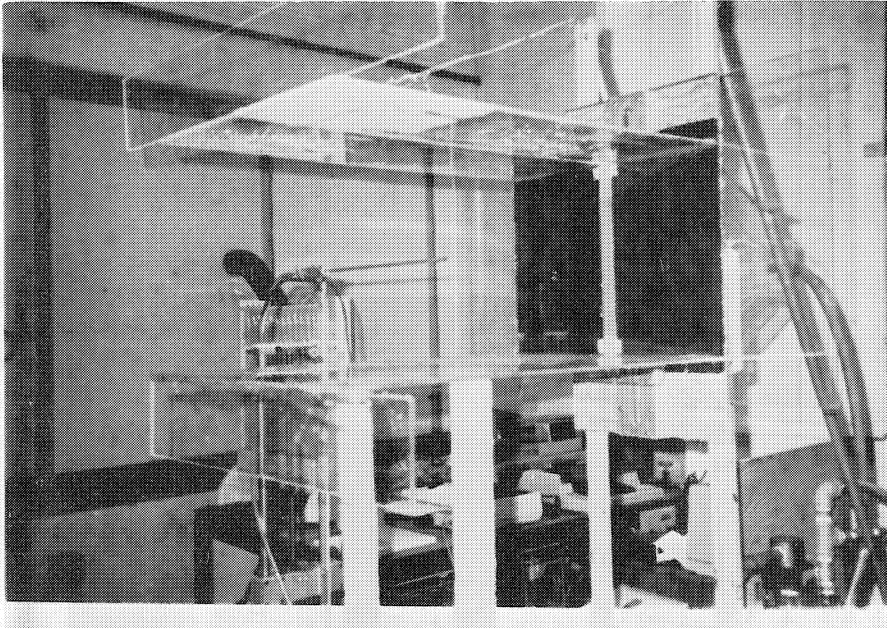
FIGURE 5:  Row of jets, enclosure, and smoke nozzle
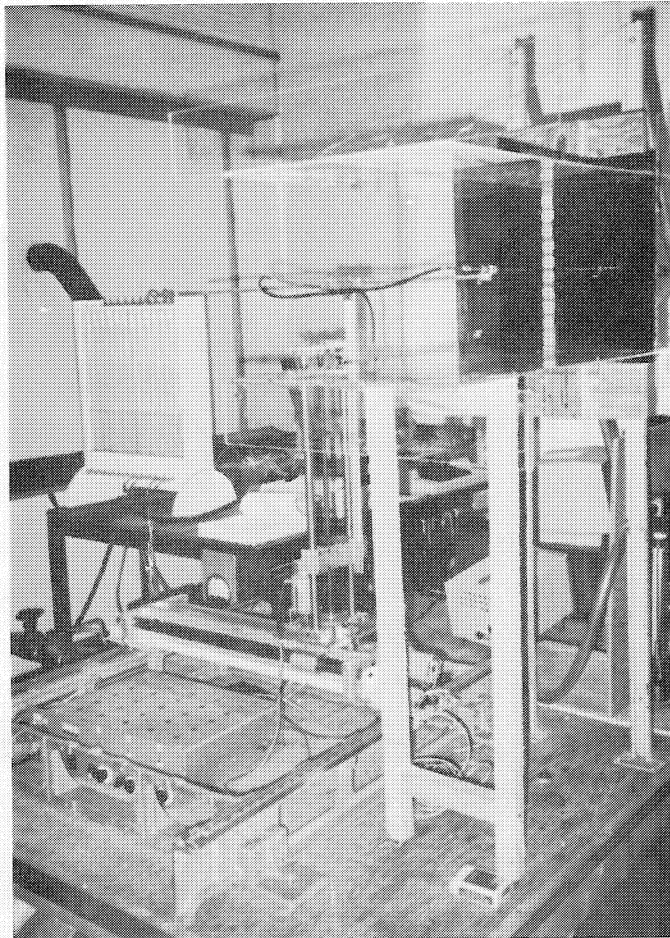
FIGURE 6: Row of jets, enclosure, and
traversing mechanism
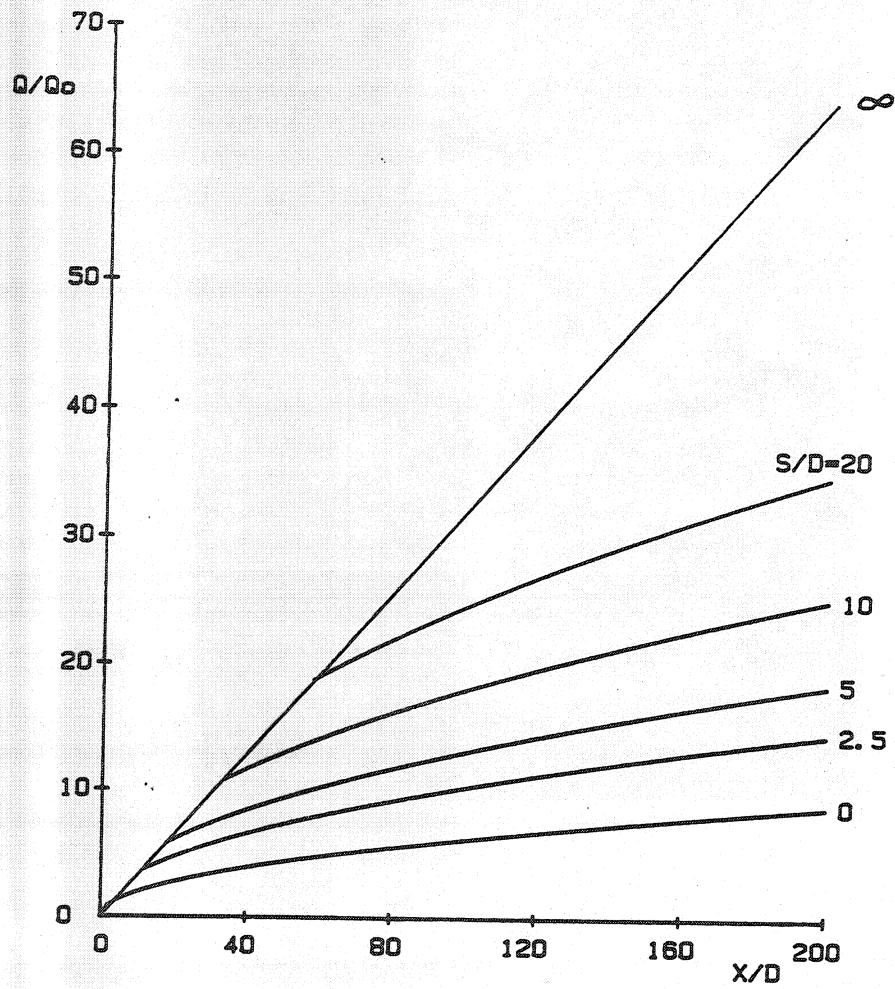
FIGURE 7: Entrainment curves for different
S/D's
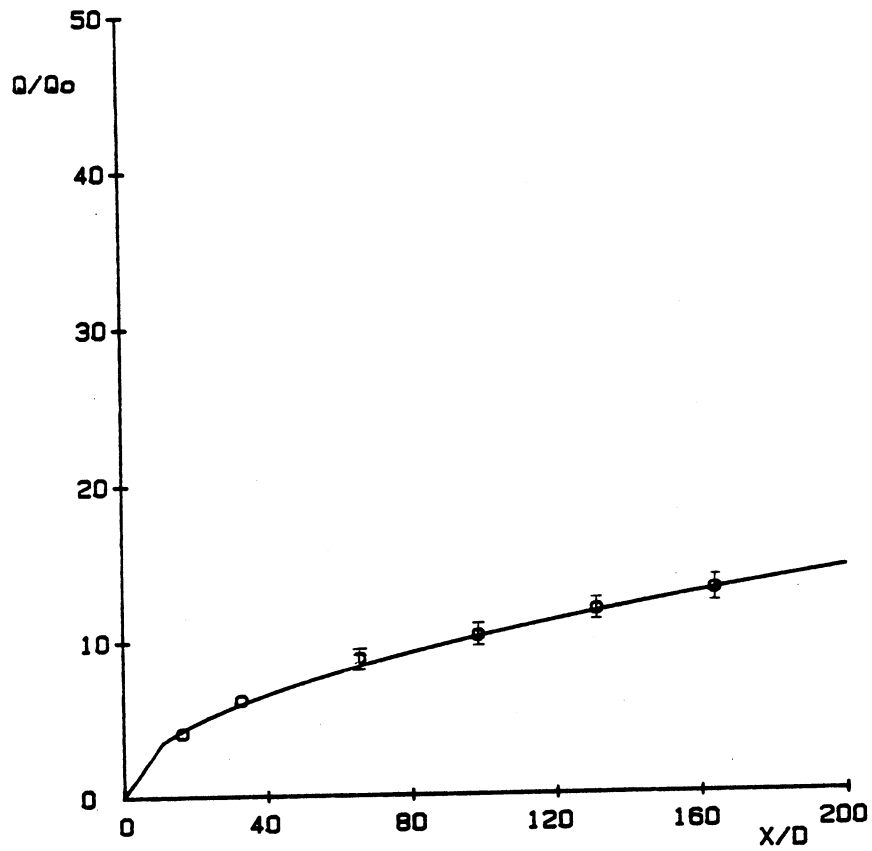
FIGURE 8 : Entrainment rate for S/D = 2.5
least squares fit to data
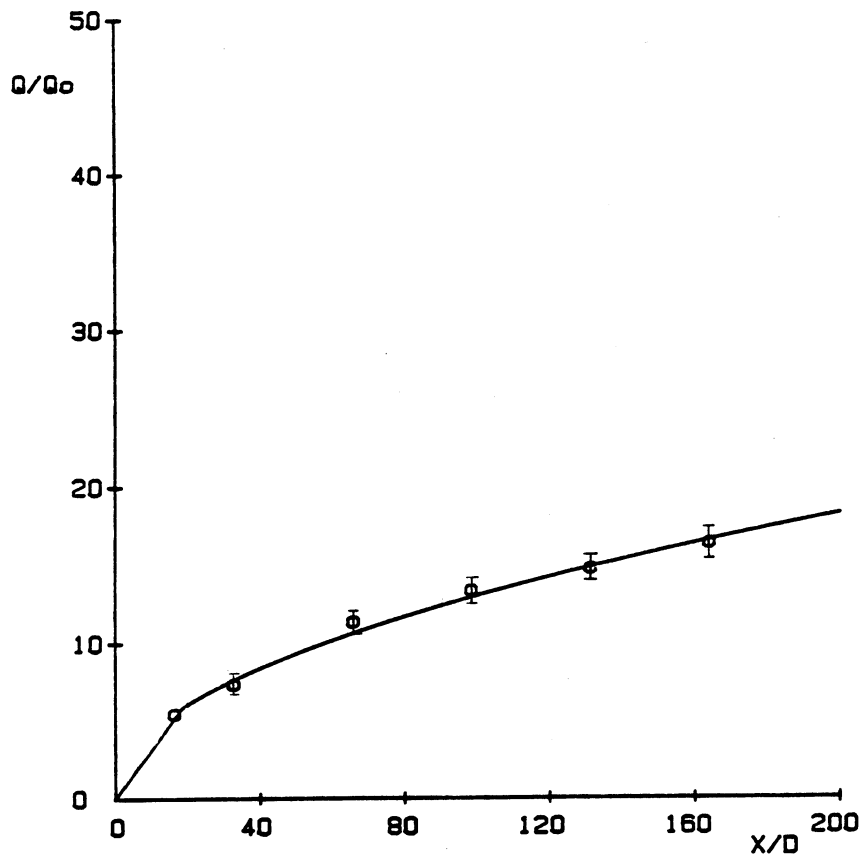
FIGURE 9 : Entrainment rate for S/D = 5
least squares fit to data
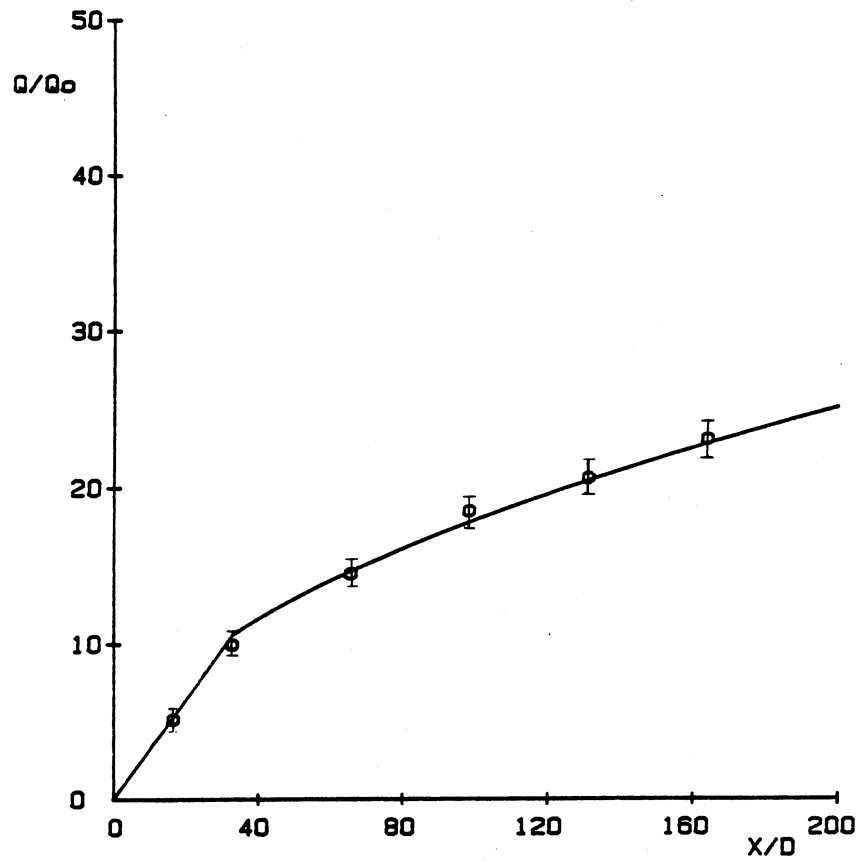
FIGURE 10: Entrainment rate for S/D = 10
least squares fit to data
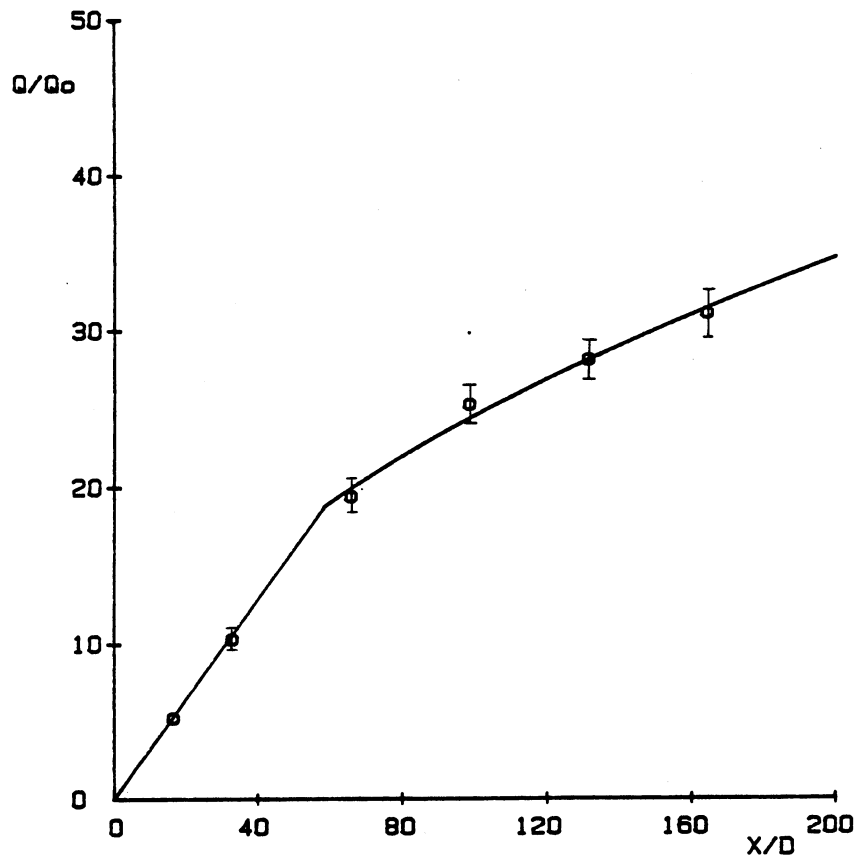
FIGURE 11: Entrainment rate for S/D = 20
least squares fit to data
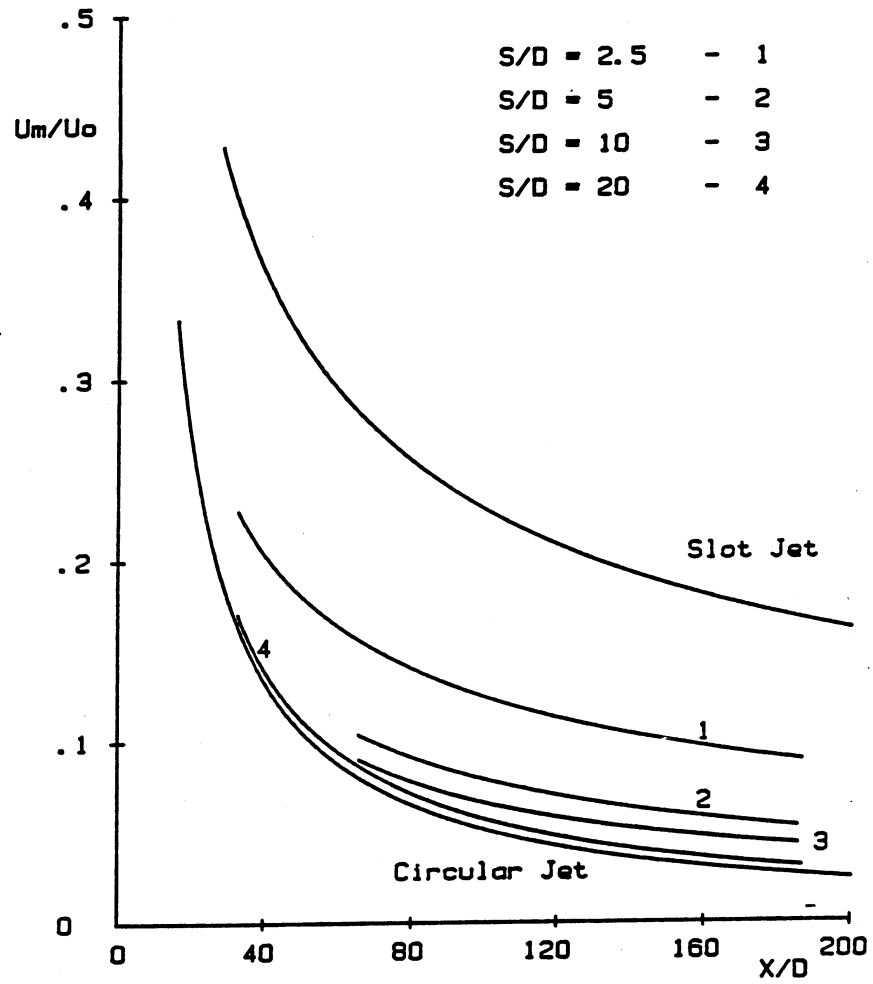
FIGURE 12: Velocity decay rates for different
S/D's
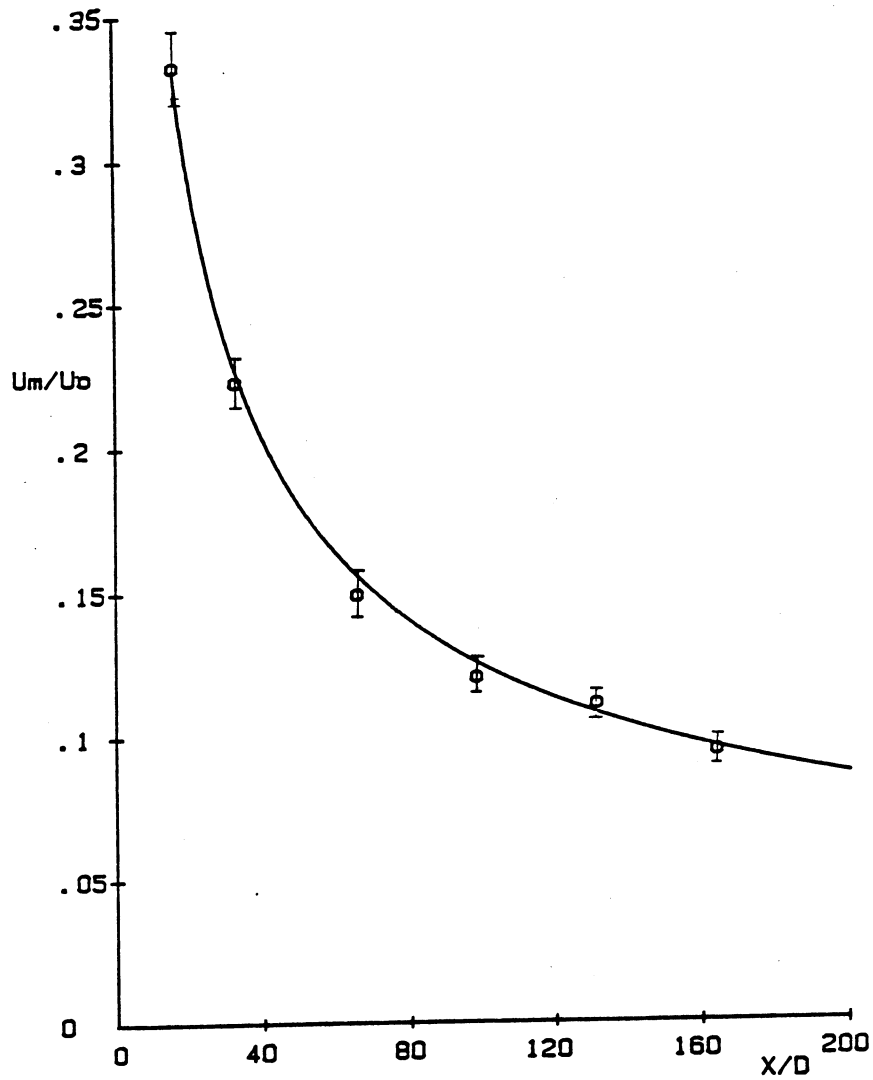
FIGURE 13: Velocity decay rate for S/D = 2.5
least squares fit to data
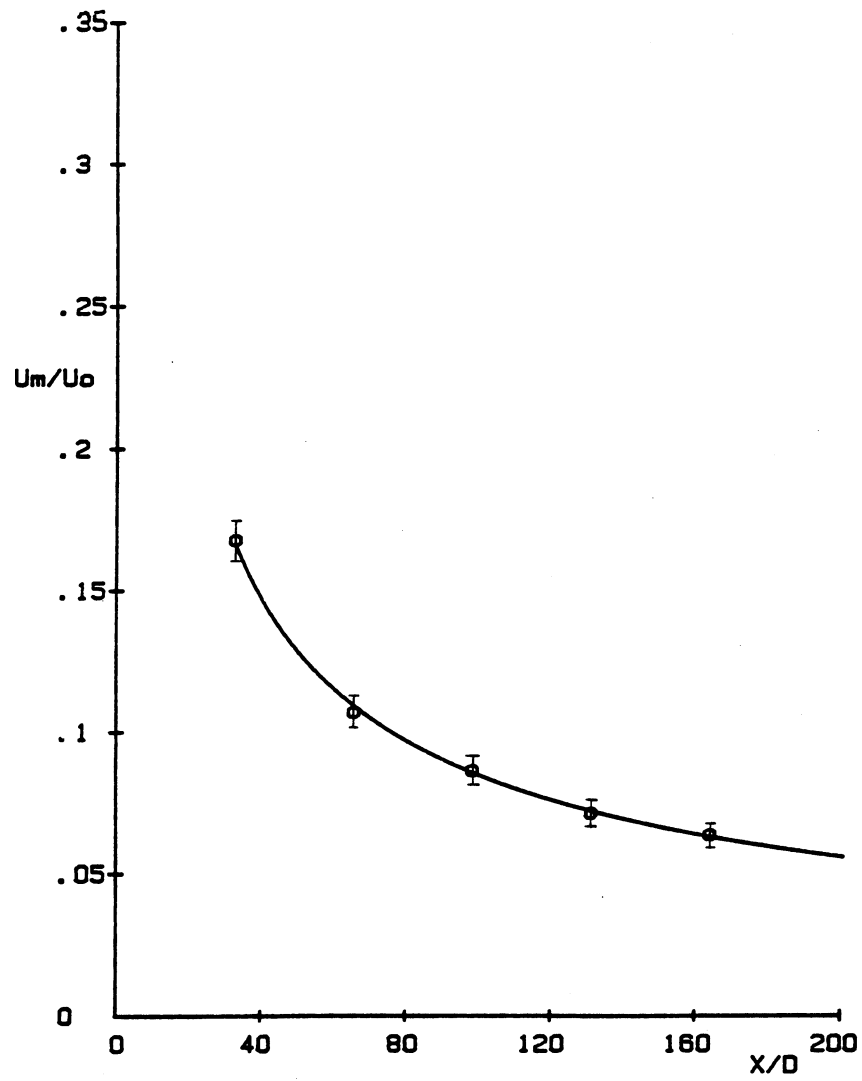
FIGURE 14: Velocity decay rate for S/D = 5
least squares fit to data
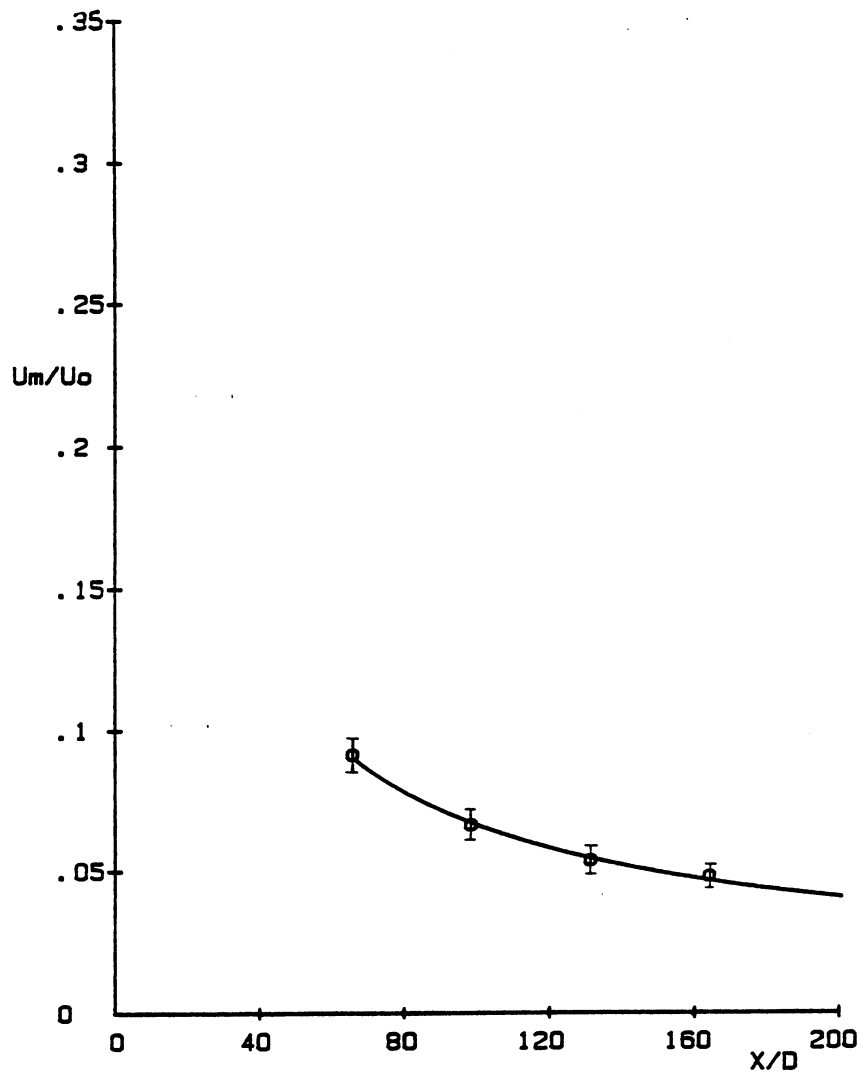
FIGURE 15: Velocity decay rate for S/D = 10
least squares fit to data
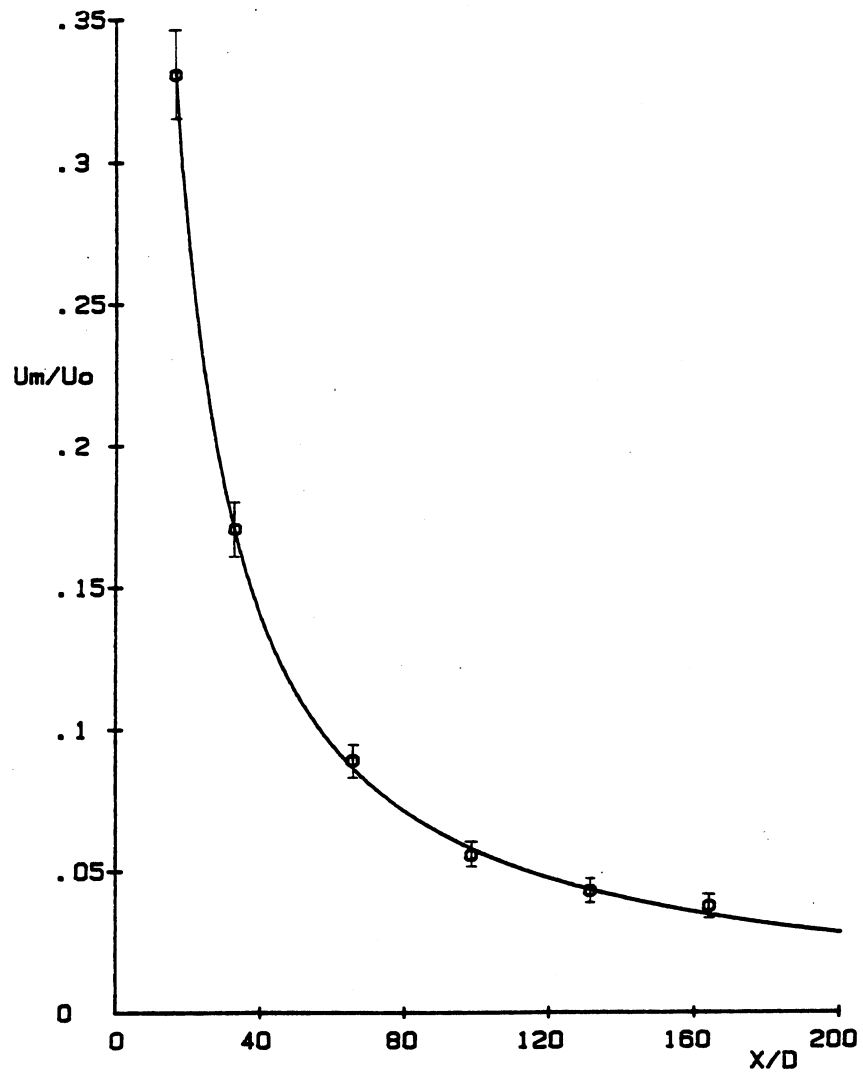
FIGURE 16: Velocity decay rate for S/D = 20
least squares fit to data

FIGURE 17, Self-similarity of velocity distributions for S/D = 2.5
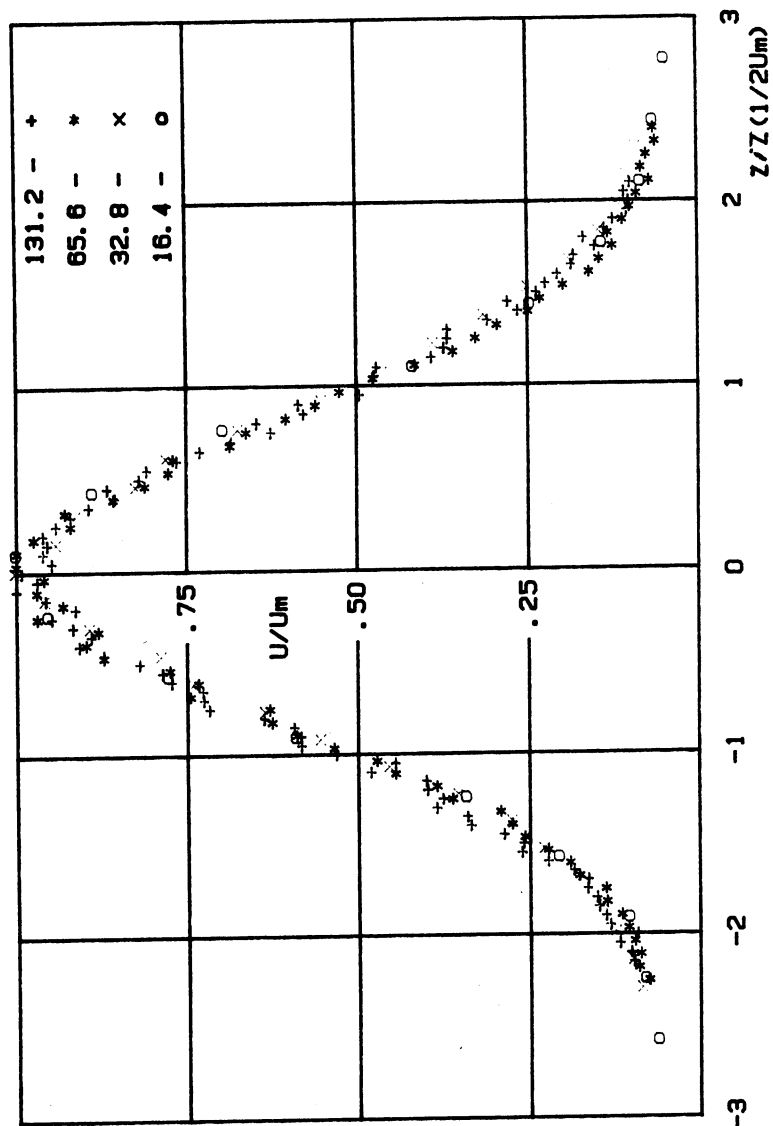
FIGURE 18: Self-similarity of velocity distributions for S/D = 5

50
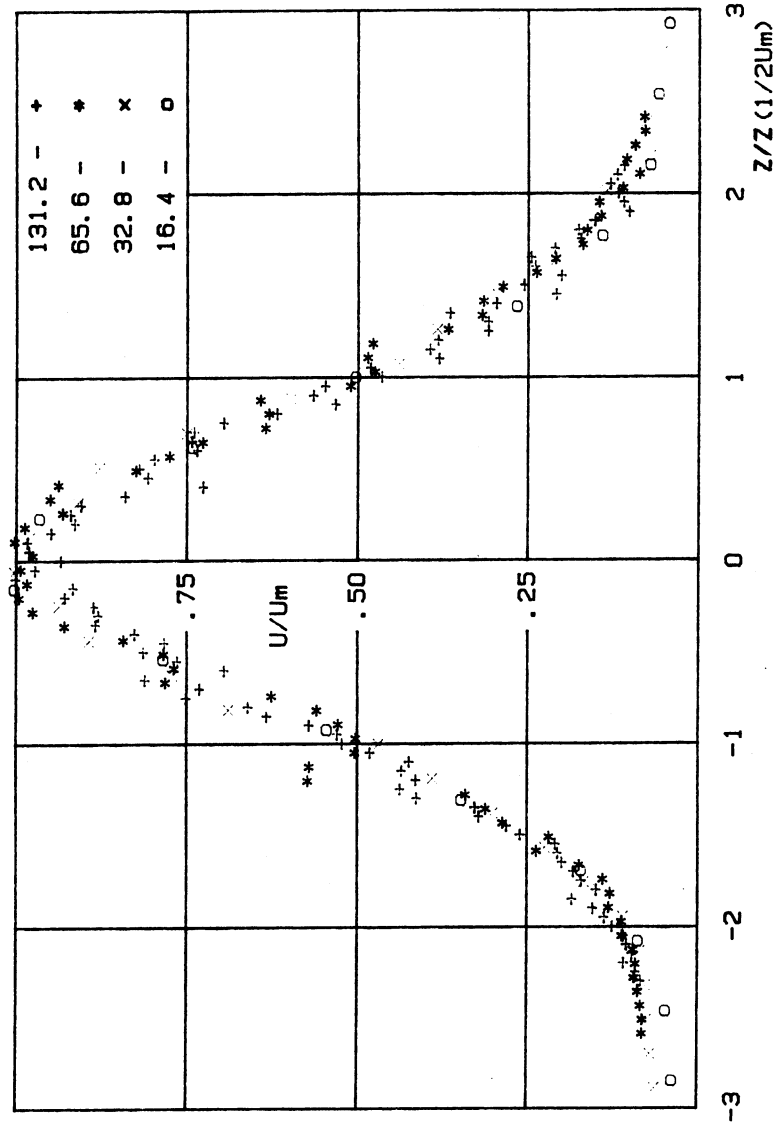


FIGURE 19: Self-similarity of velocity distributions for S/D = 10

51
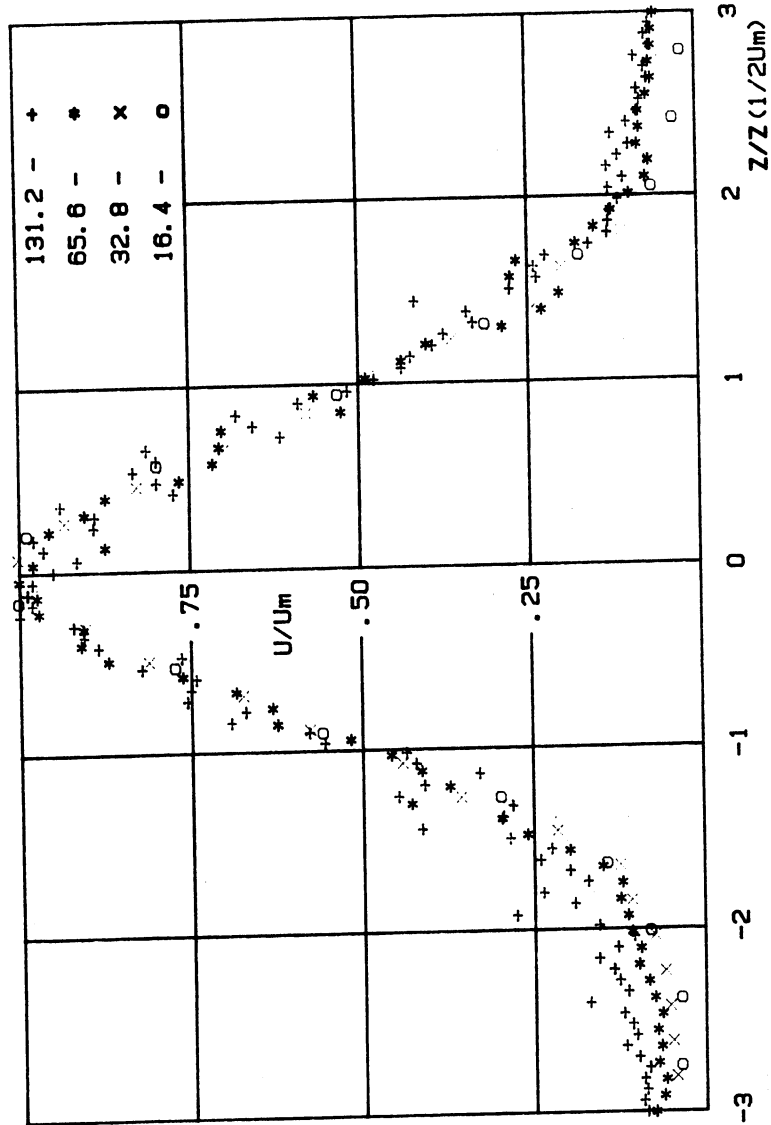


FIGURE 20. Self-similarity of velocity distributions for S/D = 20

FIGURE 21: Volume flux versus jet spacing
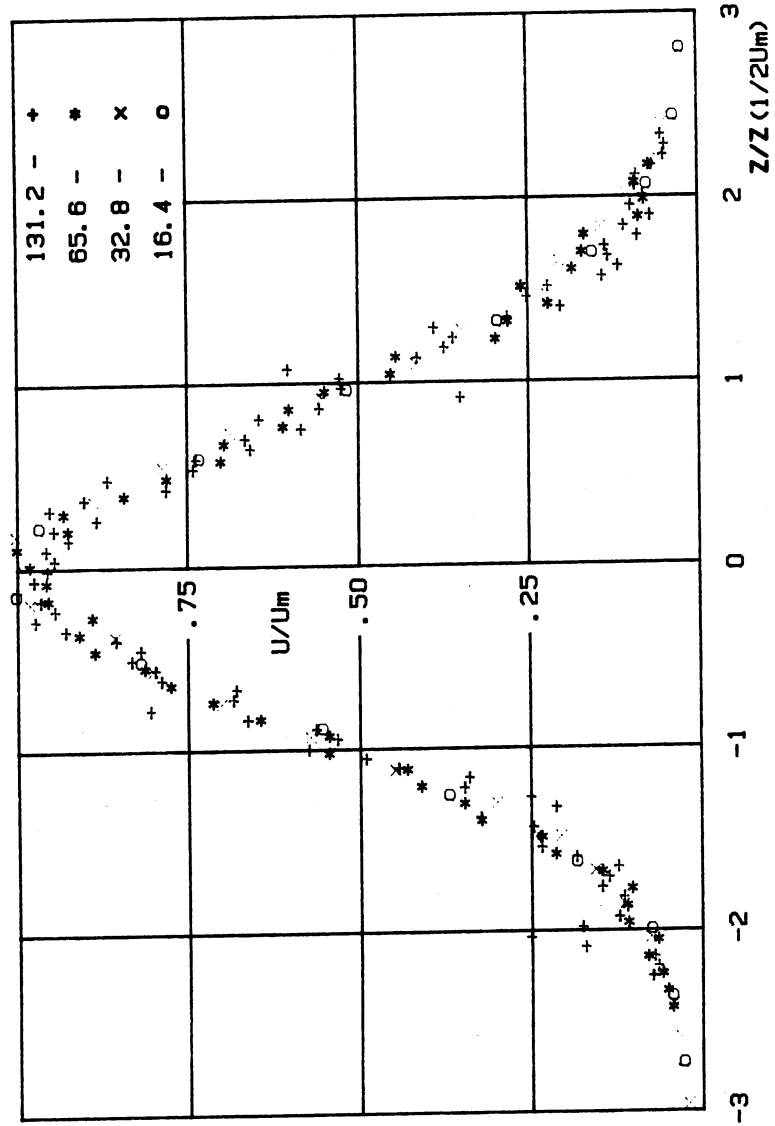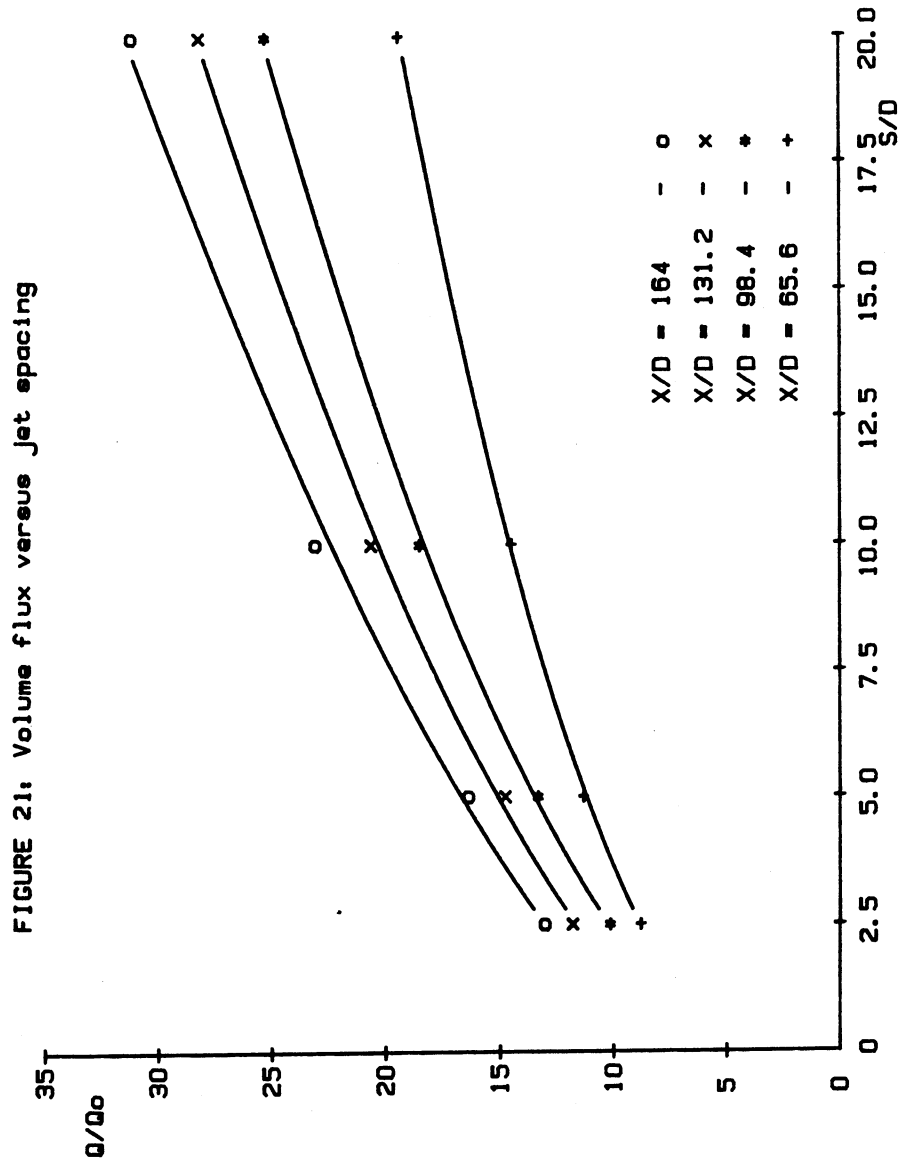
FIGURE 22: Periodicity of velocity distributions through jet center-
line along Y axis for S/D = 5 and 10
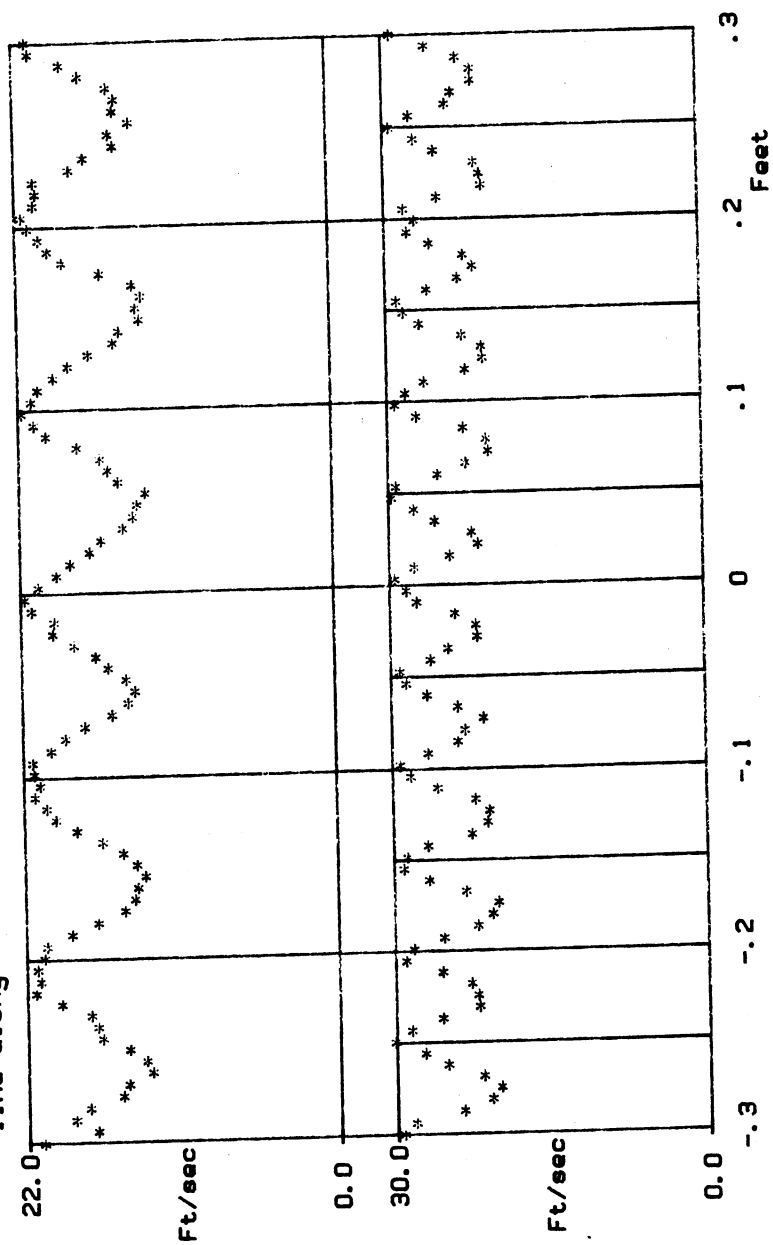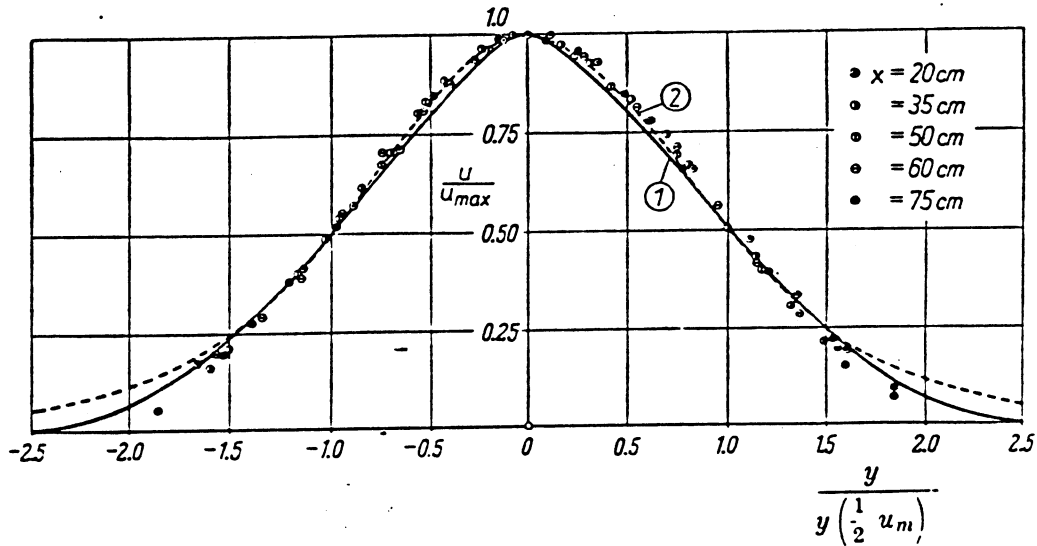
FIGURE 23: Velocity distribution in a two-dimensional turbulent jet. Measurements due to Foerthmann Curve 1 due to theory of Tollmien (ref. 10 . p. 747)
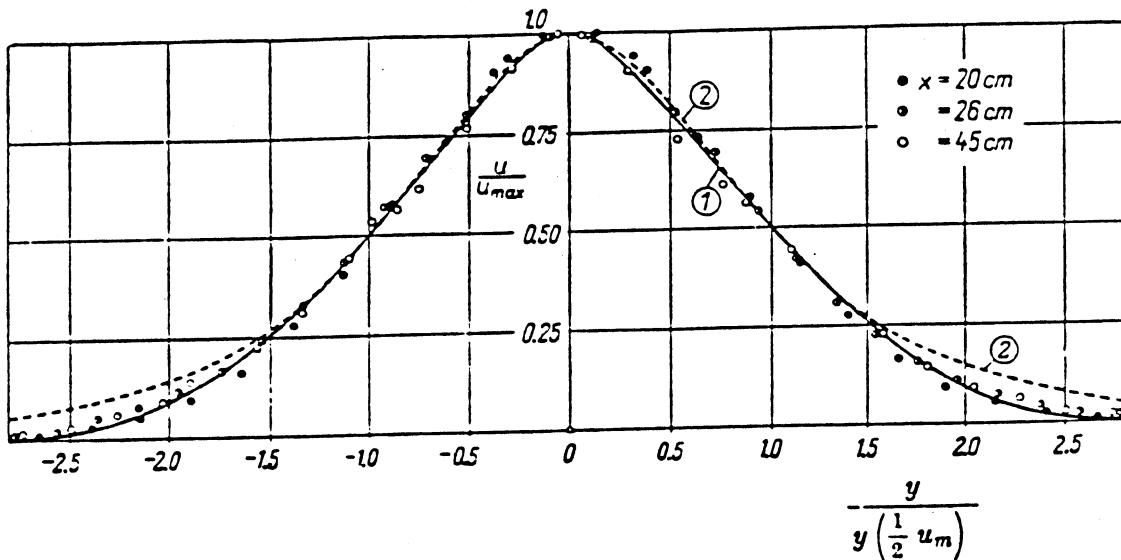


FIGURE 24: Velocity distribution in a circular, turbulent jet. Measurements due to Reichardt. Curve 1 due to theory of Tollmien (ref. 10, p. 749)
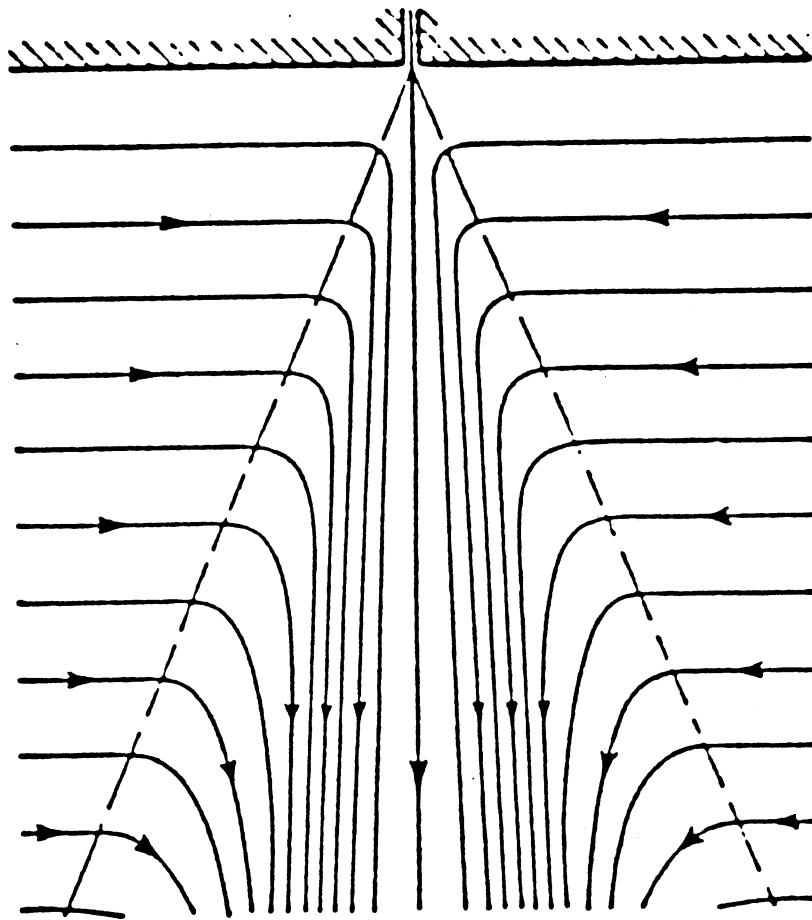
FIGURE 25: Streamline pattern for
circular jet
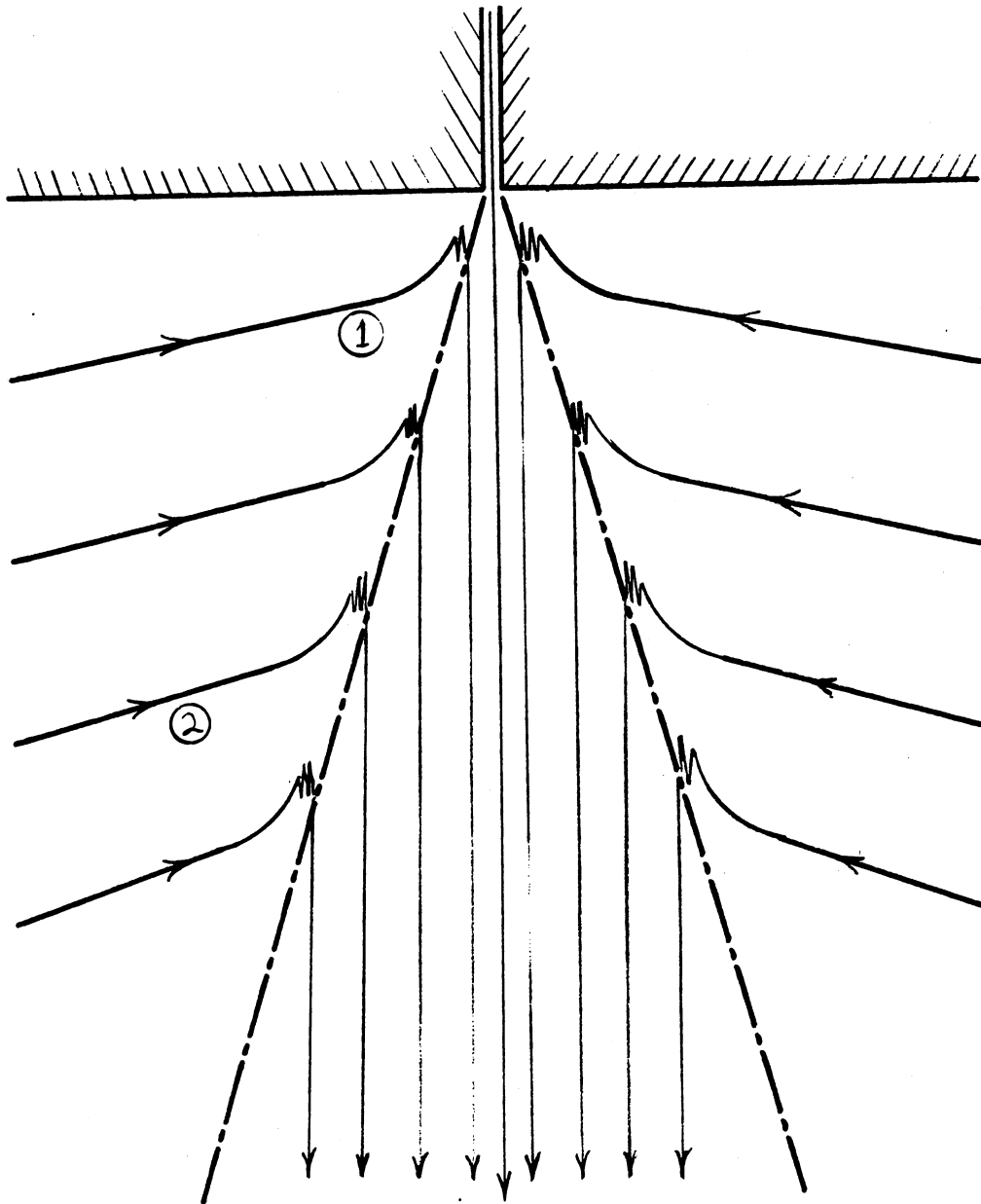
FIGURE 26: Streamline pattern for
row of jets
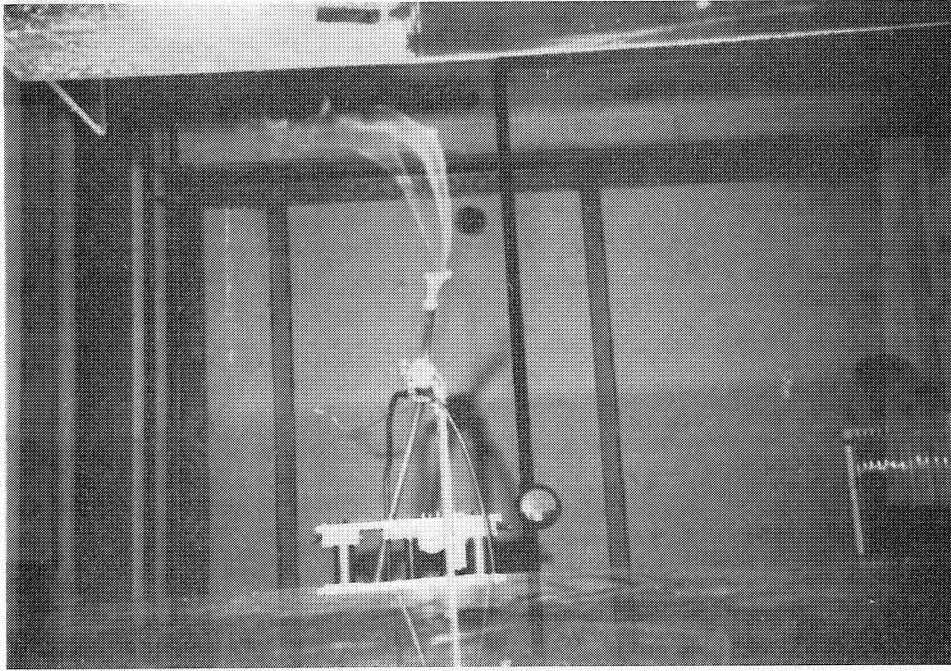
FIGURE 27 Smoke test for circular jet
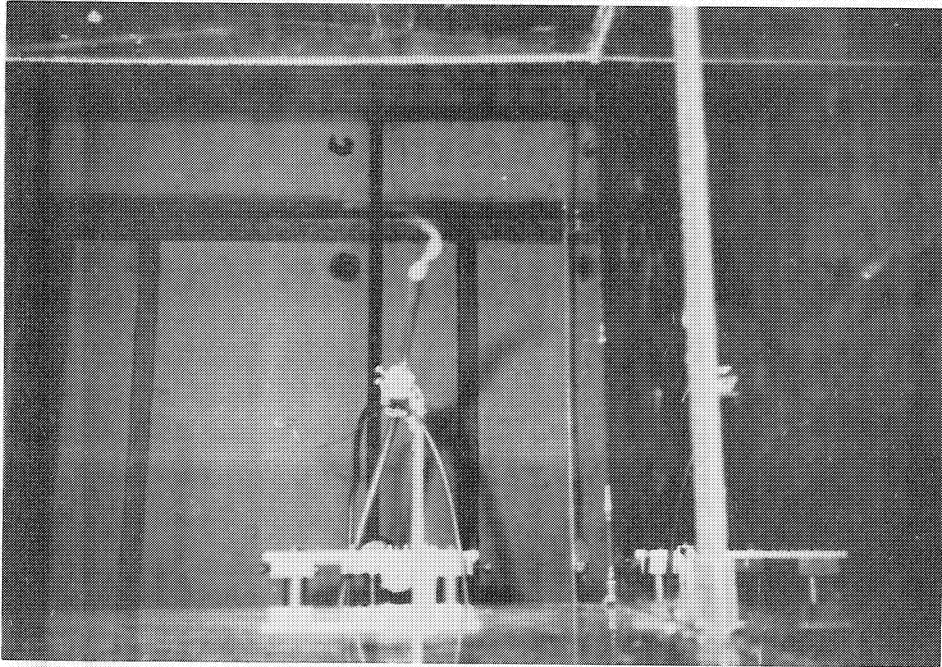
FIGURE 28: Smoke test for S/D = 20
at X/D = 30
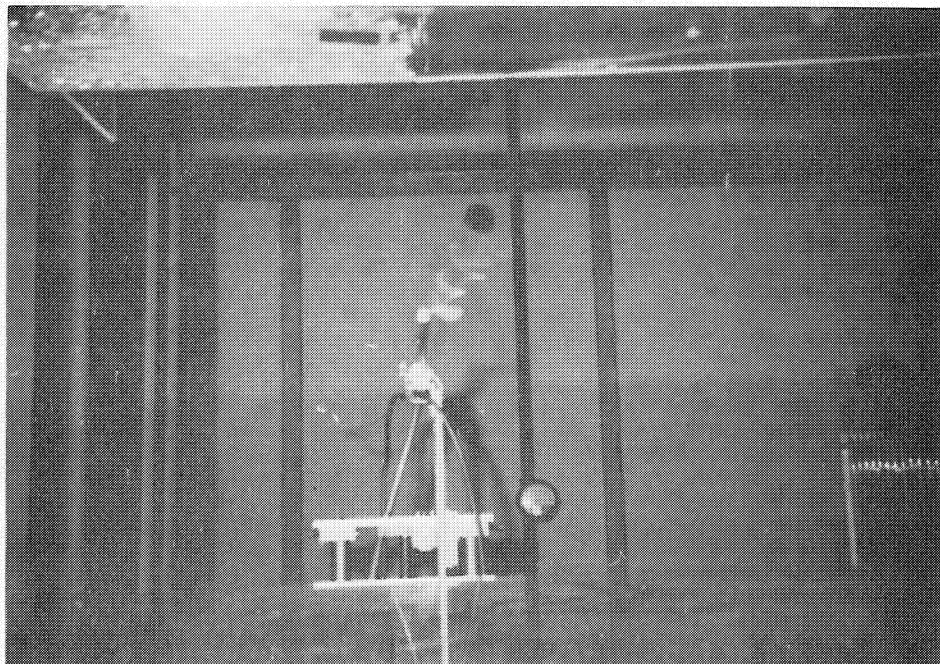
FIGURE 29: Smoke test for S/D = 20
at X/D = 120
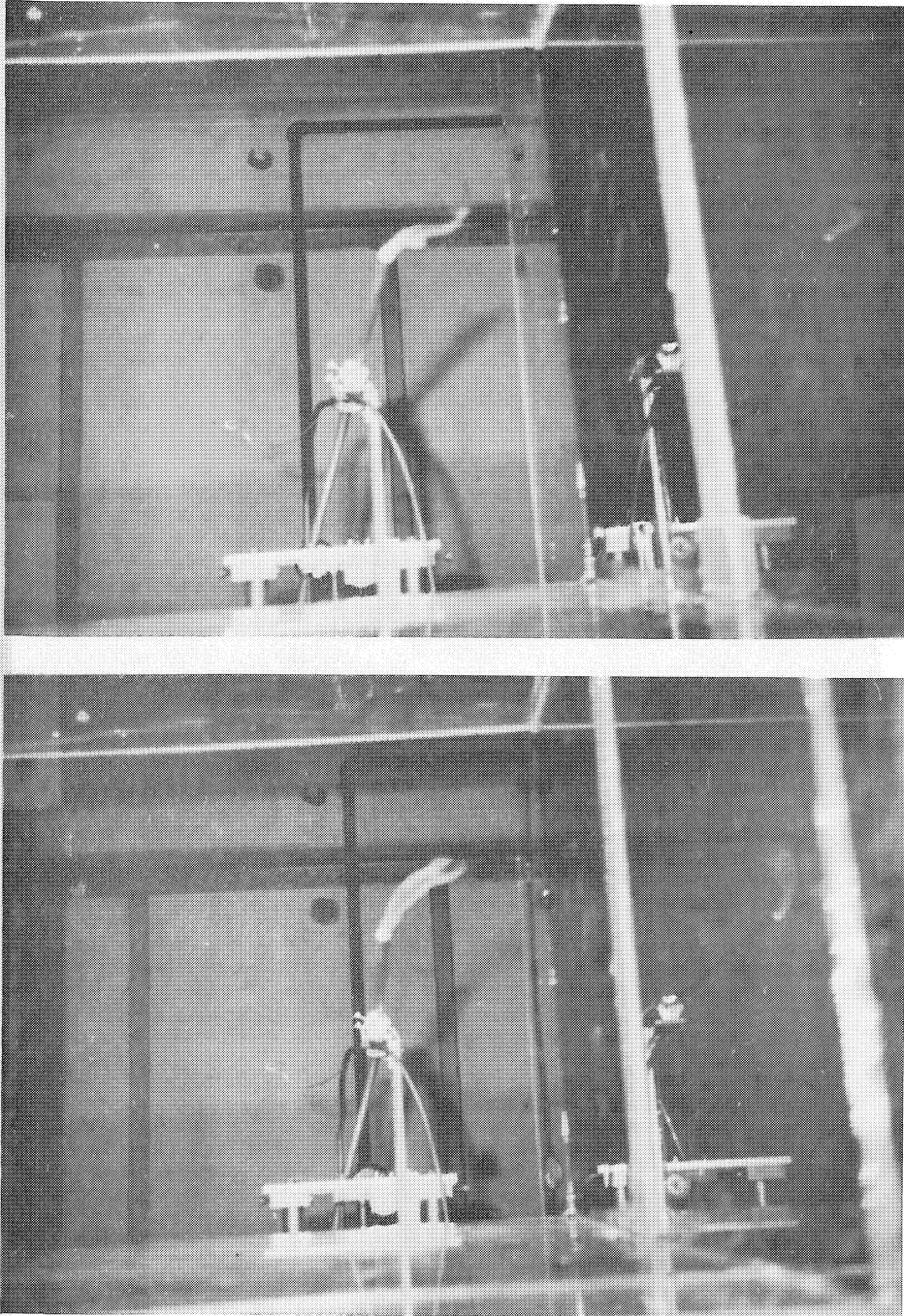
FIGURE 30: Smoke test for S/D = 10
at X/D = 30
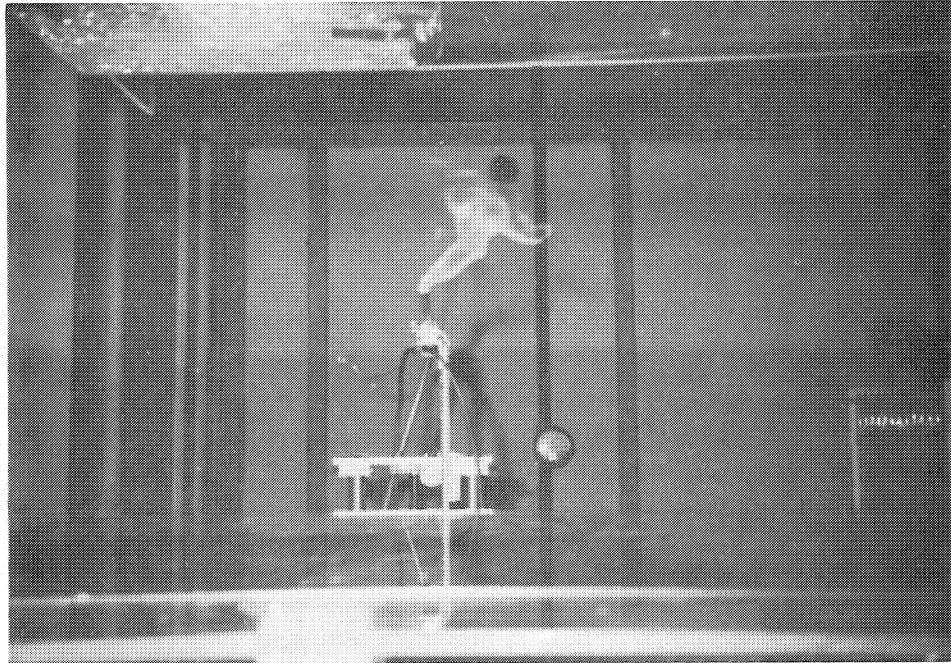
FIGURE 31: Smoke test for S/D = 10
at X/D = 120

62
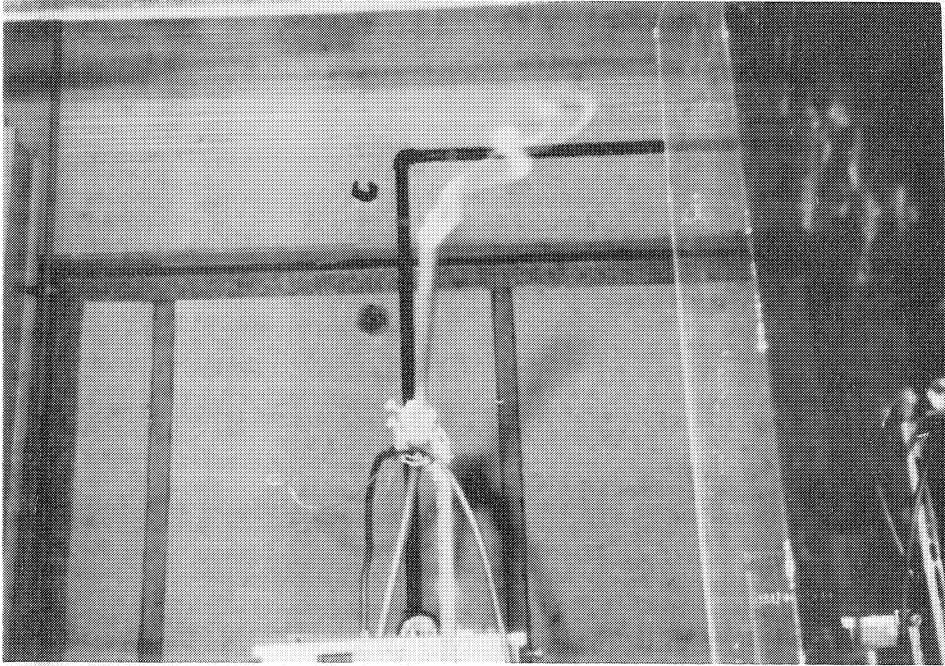


FIGURE 32: Smoke test for S/D = 5
at X/D = 30
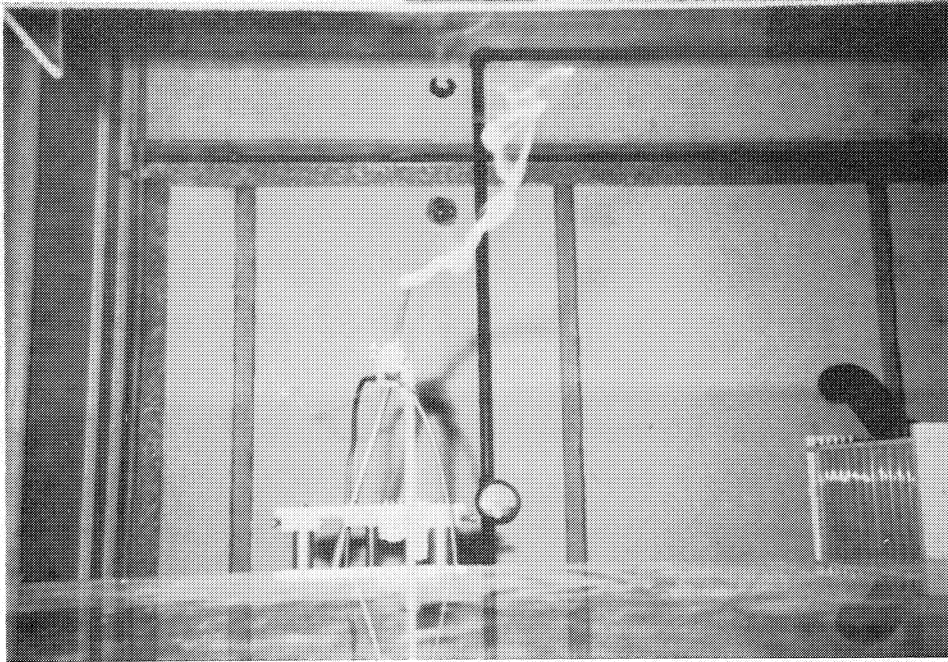
FIGURE 33: Smoke test for S/D = 5
at X/D = 120
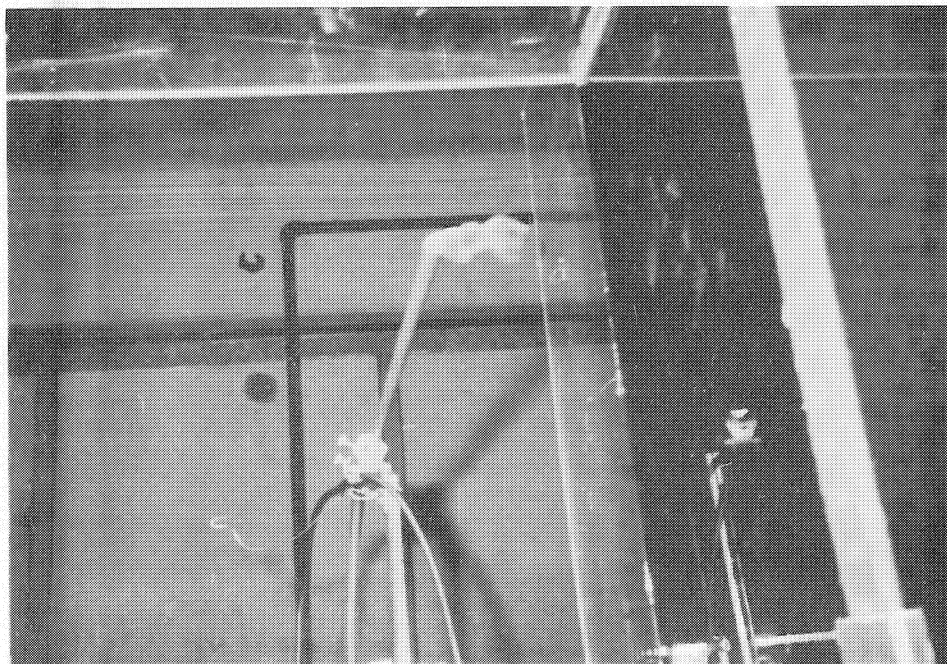
FIGURE 34: Smoke test for S/D = 2.5
at X/D = 30
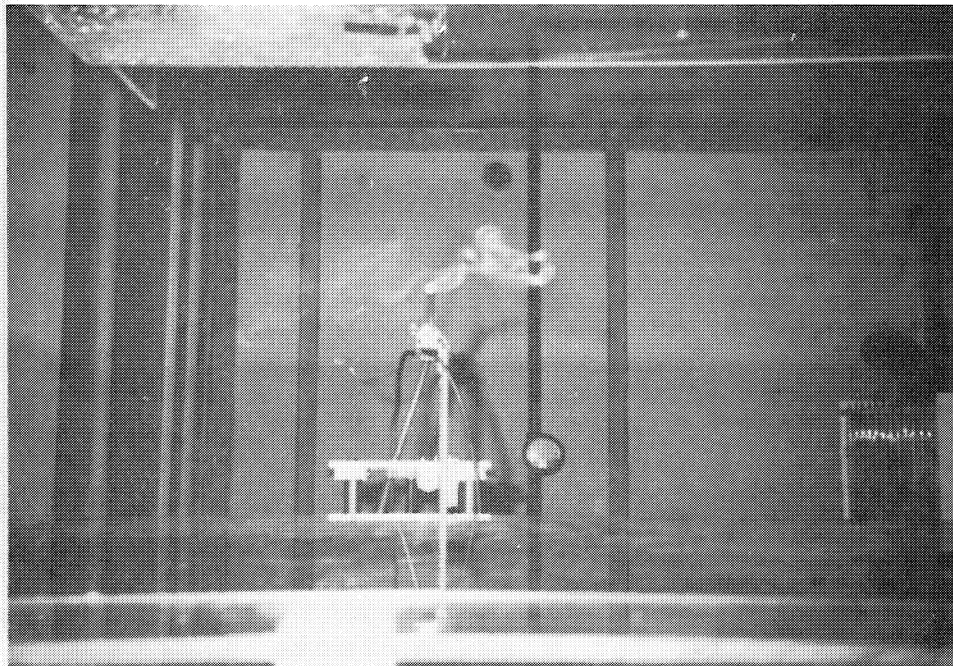
FIGURE 35: Smoke test for S/D = 2.5
at X/D = 120

66

APPENDIX A

Error Due to Experimental Apparatus

The early stages of the present study were spent in an attempt to minimize the effects of misalignment of the jet nozzles first with respect to each other and second with respect to the traversing mechanism which moves the hot wire probe along each of the three axes. Misalignment in the row of jets itself results in momentum losses that - while difficult to quantify - are undoubtedly very significant. Because of the problems generated by jet misalignment, a drilled, threaded rod and tapped aluminum plate assembly was discarded in favor of a solid block of polyvinylchloride in which jet apertures were drilled and reamed on a vertical milling machine.

The length of the row of jets introduces another problem in so far as the study is ideally one of an infinite row of jets. Limitations in compressor flow rates in turn limit the length of the jet row, sinse a minimum turbulent Reynold's number must be maintained. Consequently, barriers were introduced at either end of the row of jets to prevent spreading along the Y axis. The unfortunate side effect of the enclosure is that it introduces a shearing force at the walls. In an attempt

to detect any influence that the walls might have on the central portion of the flow, the hot wire probe was stationed at a location far enough downstream that the flow was essentially two dimensional. The probe was then traversed upward from the bottom to the top wall for the S/D row spacing of 2.5 and 5. In both cases, the velocities measured in the central region of the enclosure showed no tendency to decrease as the probe approached either wall, falling within the standard deviation as calculated for that centerline velocity.

## Error in Directly Measured Variables

The directly measured quantities are the axial location of the probe from the jet source and the nozzle diameter of the jet. The downstream position of the probe, X, is measured on a scale with a resolution of .0625 inches, while the diameter of the jet nozzle is presumed to be within .0001 inches.

The Z and Y locations of the probe are never explicitly taken into account. It is assumed that the relative positioning of the probe due to the stepper operation of the traversing mechanism is accurate to within 5% of the last step, or 5% of 1.8 degrees. 1/200 of a revolution of a 16 thread per inch shaft results in the linear travel of .0003 inches, with 5% of that

value being negligible.

## Error in Calculated Variables

Because the hot wire probe is calibrated at a given temperature, it is not strictly a directly measured variable. A 1 degree Fahrenheit change in the temperature from the 72 degree calibration temperature of the probe results in a .5% error in the anemometer reading. Given a 1 degree Fahrenheit resolution in reading the scale on an alcohol thermometer, the relative error in the velocity reading is .5%. Coupled with .5% relative error associated with the bridge voltage calibration using a micromonometer to read wind tunnel flow speeds and a 2% relative error associated with the linearization of the bridge output, the total relative error for velocity readings is 3%.

The internal error for $U_i$, or its standard deviation of the mean

$$S.D. = [\sum \{(U_i - U)^2 / 199(200)\}]$$

is found to be 2%. At the jet source, the standard deviation is found to be less than 1.3%.

The error in $Q/Q_o$ due to reading error is additive since the anemometer was used to determine each quanti-

ty. The external error alone then is 6%. The internal error in $Q/Q_0$ is also additive, for the same reason. For $S/D$ = 2.5, 5 velocity distributions were determined at each section, giving an internal error of 2%/5 = .4%. This figure is added to 1.3% internal error found in the calculation of $Q_0$ to give a total internal error of 1.7%. Added in quadrature to the external error, the total error in $Q/Q_0$ for $S/D$ = 2.5 is 6.3%. For $S/D$ = 5, 10, and 20 a minimum of 8 velocity distributions were established at each section, resulting in a total internal error of 1.6% for $Q/Q_0$. Again the internal and external errors are added in quadrature to yield a total error of 6.2%

The entrainment formulas are dependent on $X/D$ as well as $Q/Q_0$, and at the near downstream sections of 16.4 and 32.8 the 3% and 1.5% relative errors in $X/D$ must be added in quadrature to give the respective total errors of 7% and 6.3%, all other sections retaining the same value for the total error because of the diminishing relative error in $X/D$ in downstream sections.

APPENDIX B

Velocity magnitude distributions

The graphs presented in this appendix represent
the velocity magnitude distributions from which the
volume fluxes are calculated. Centerline velocity dis-
tributions (Y/S = .5) are given for all sections, while
velocity distributions taken at intermediate locations
between adjacent jets are included for sections in
which flow is still essentially three dimensional.

The graphs plot a dimensionless velocity (U/Uo)
against a dimensionless distance from the jet center-
line along the Z axis (Z/Z(1/2Um), where Z(1/2Um) de-
notes the location at which the velocity in a given
section is half that of the centerline velocity, Um,
for the same section.

The initial velocity profiles for each of the row
of jets tested are also presented in Appendix B. The
velocity is plotted against the nozzle radius, and as
in the case of the total velocity, the distribution was
recorded by traversing the hot wire probe (oriented
along the Y axis) along the Z axis through the jet
centerline.

71



FIGURE 1B: Total velocity distribution for S/D = 2.5

FIGURE 2B: Total velocity distribution for S/D = 2.5
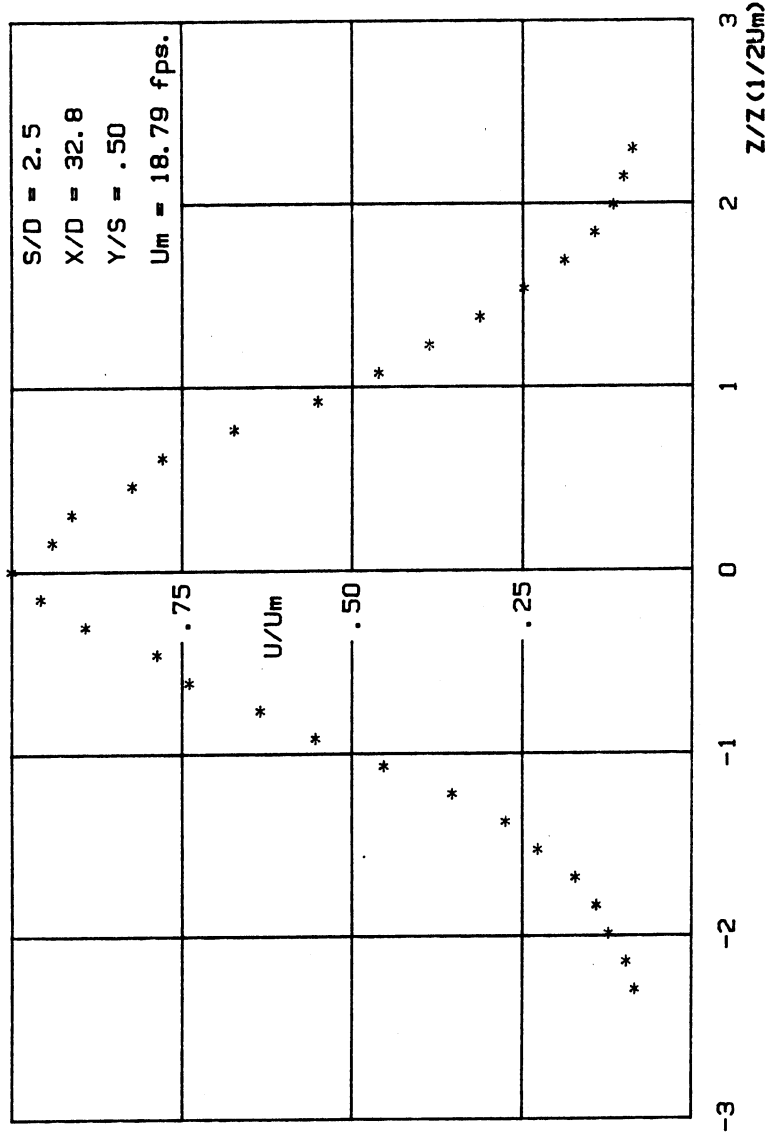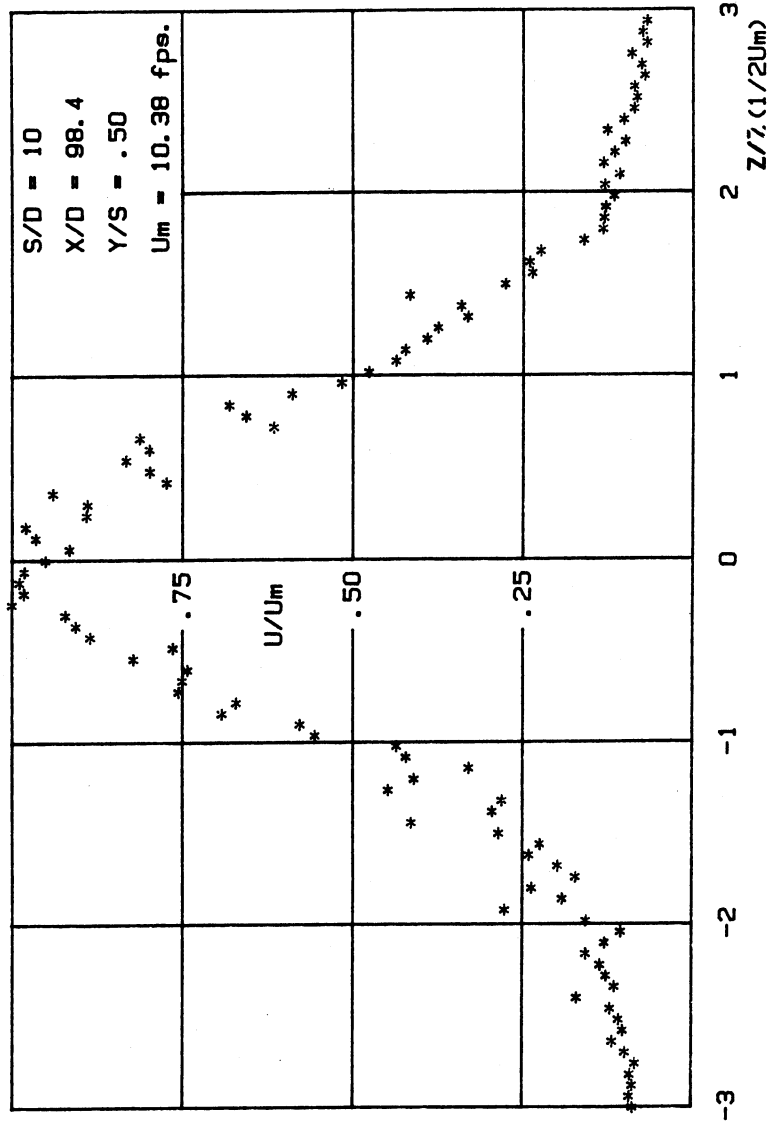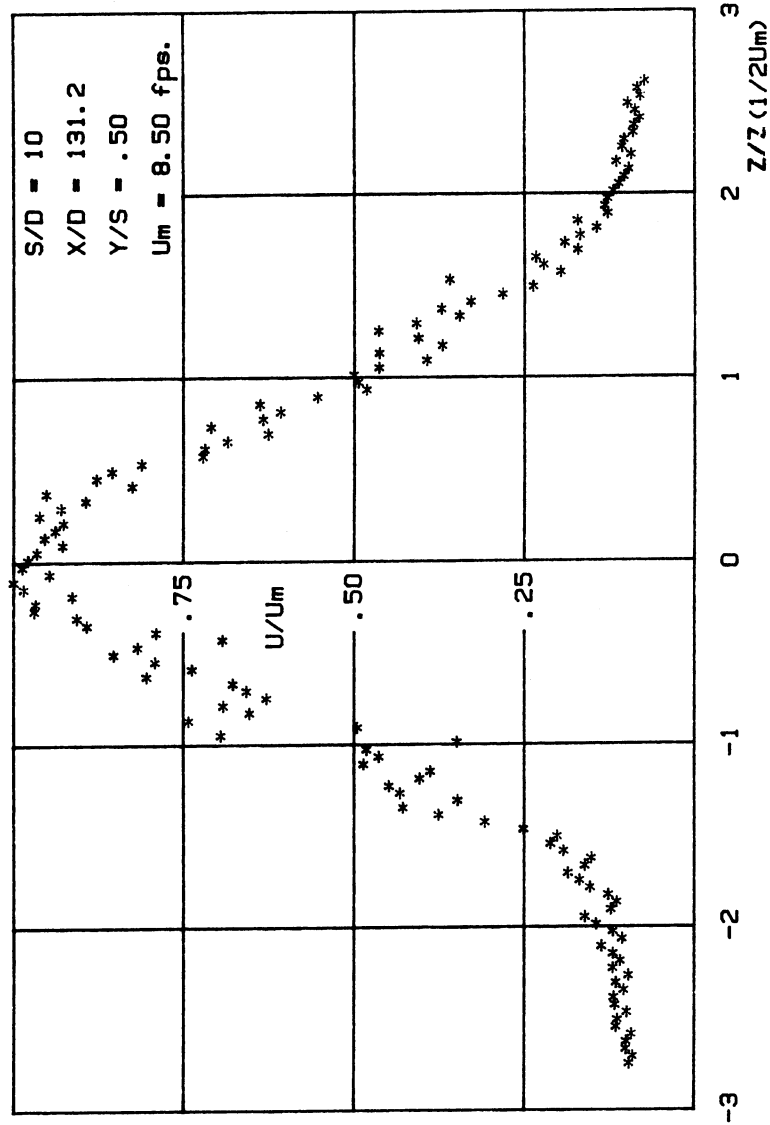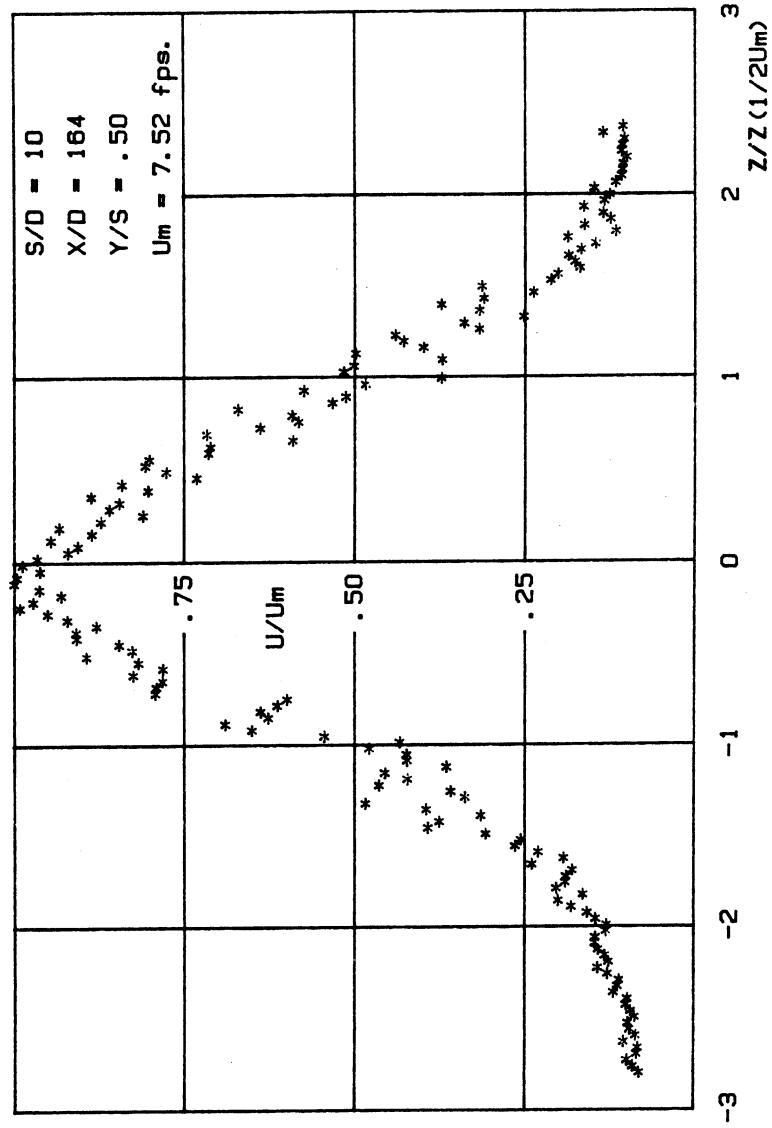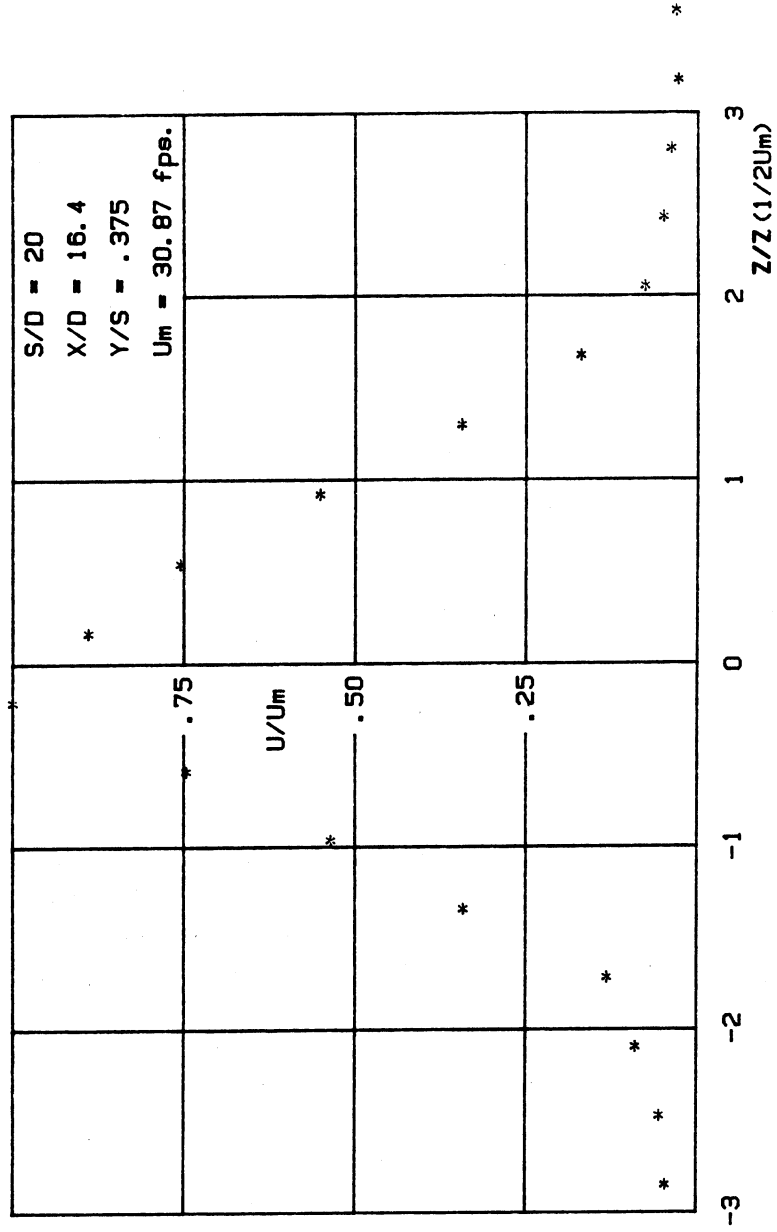
FIGURE 3B: Total velocity distribution for S/D = 2.5

S/D = 2.5
X/D = 65.6
Y/S = .50
Um = 12.58 fps.
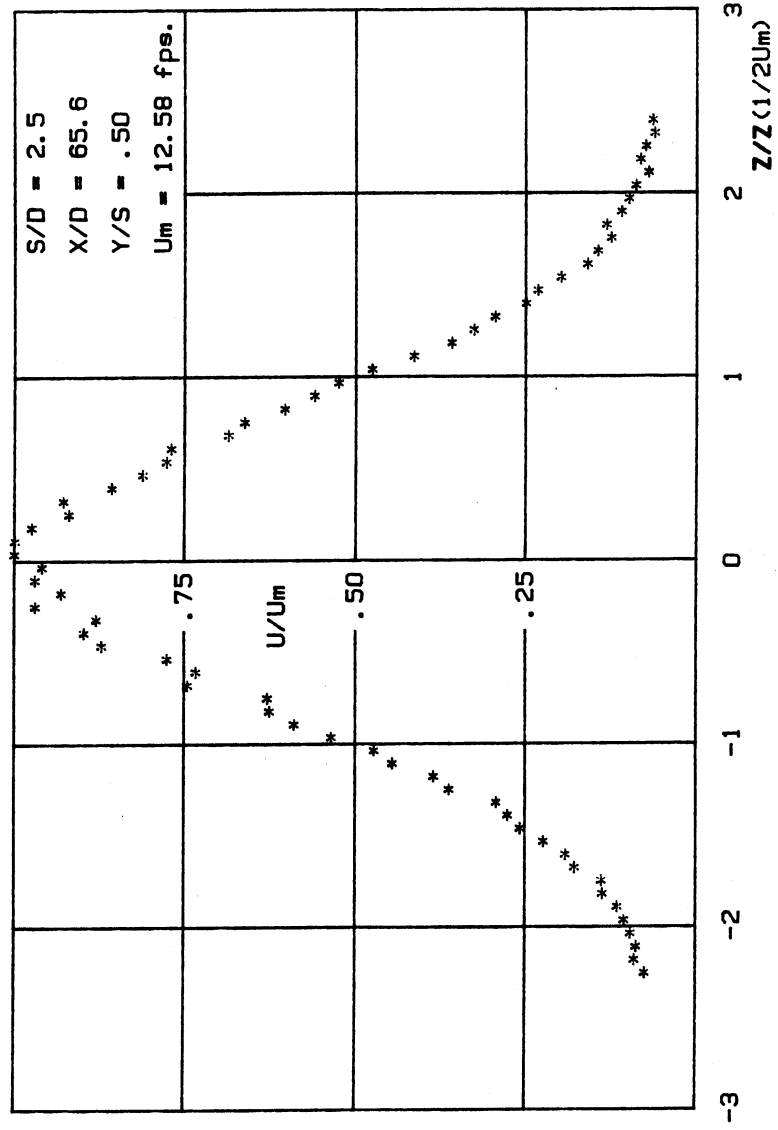
FIGURE 4B: Total velocity distribution for S/D = 2.5

S/D = 2.5
X/D = 98.4
Y/S = .50
Um = 10.14 fps.
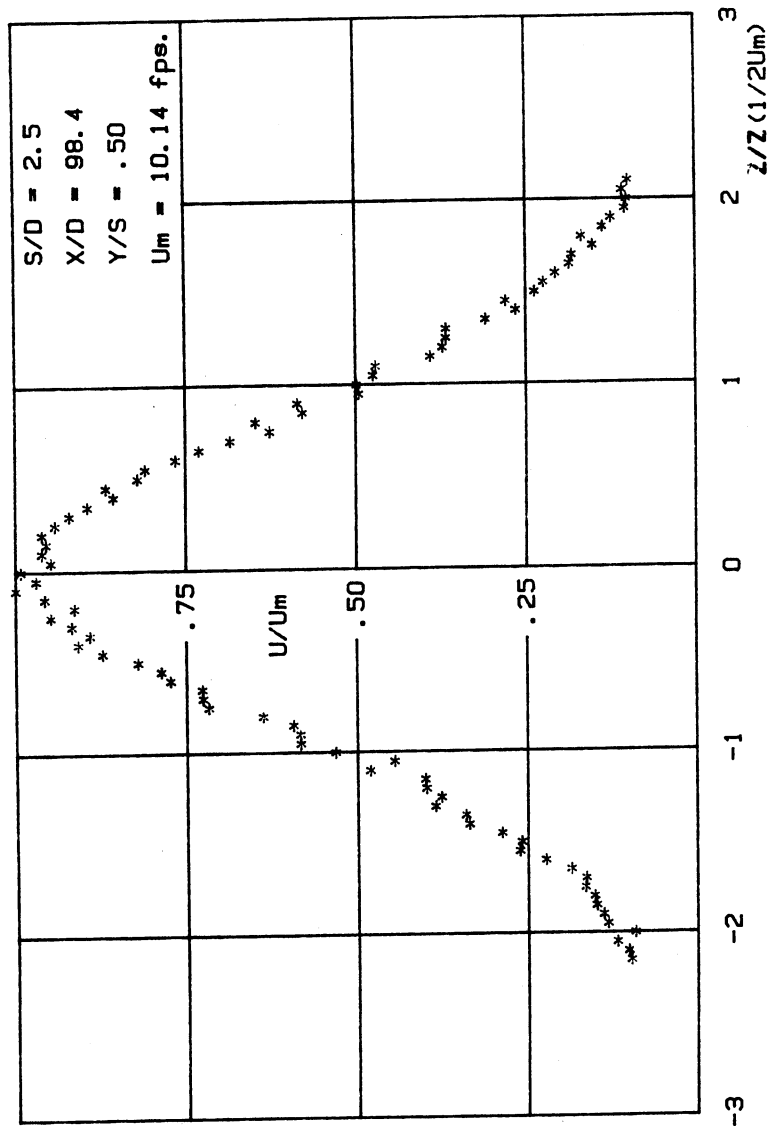
FIGURE 5B: Total velocity distribution for S/D = 2.5

FIGURE 8B: Total velocity distribution for S/D = 2.5

S/D = 2.5
X/D = 164
Y/S = .50
Um = 7.92 fps.

FIGURE 7B: Total velocity distribution for S/D = 5
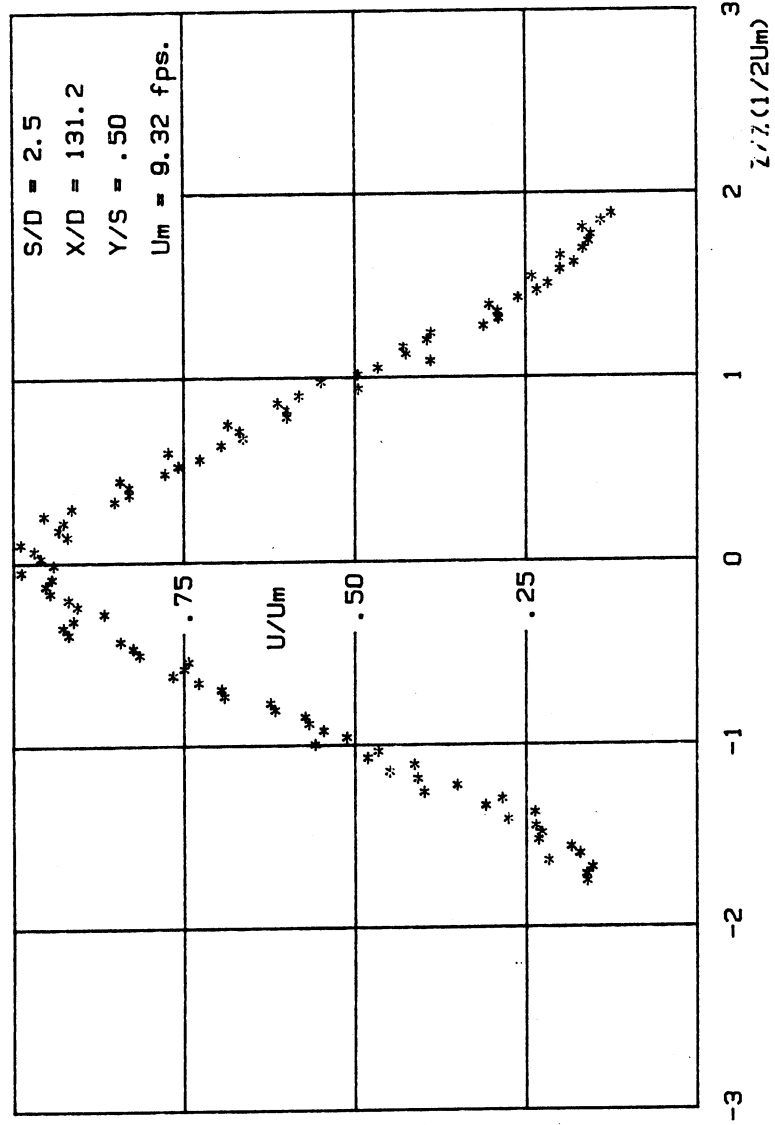
FIGURE 8B: Total velocity distribution for S/D = 5
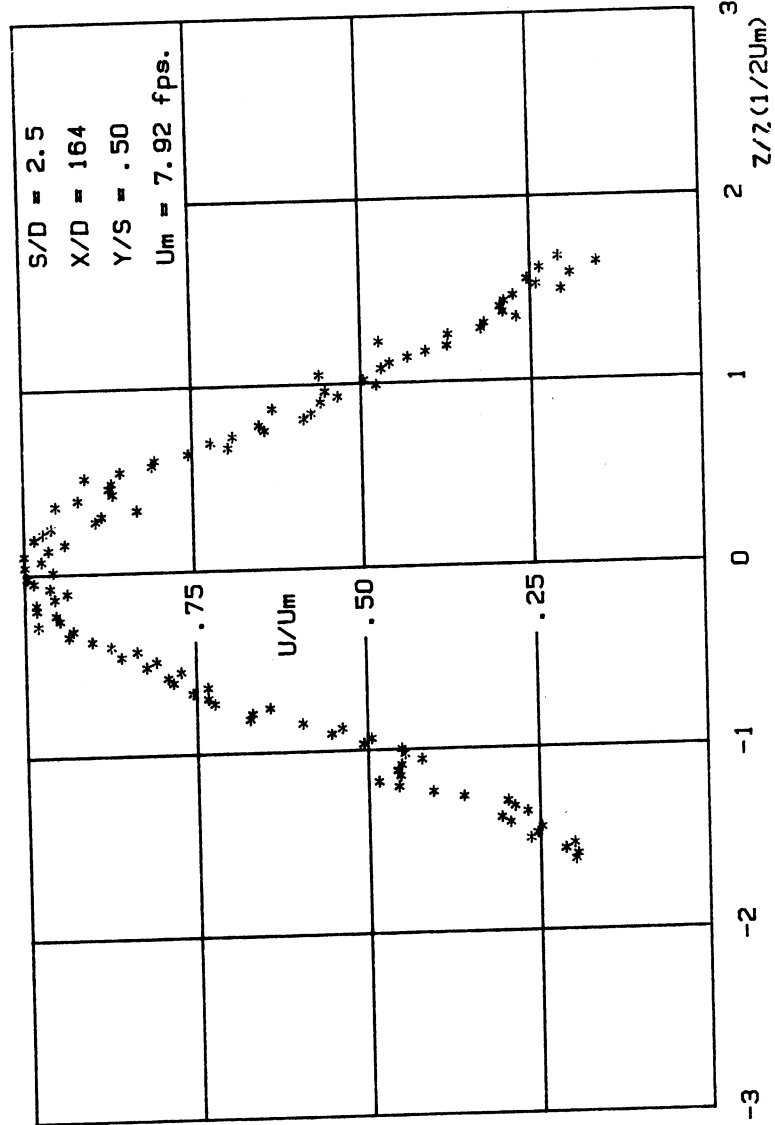
FIGURE 9B: Total velocity distribution for S/D = 5
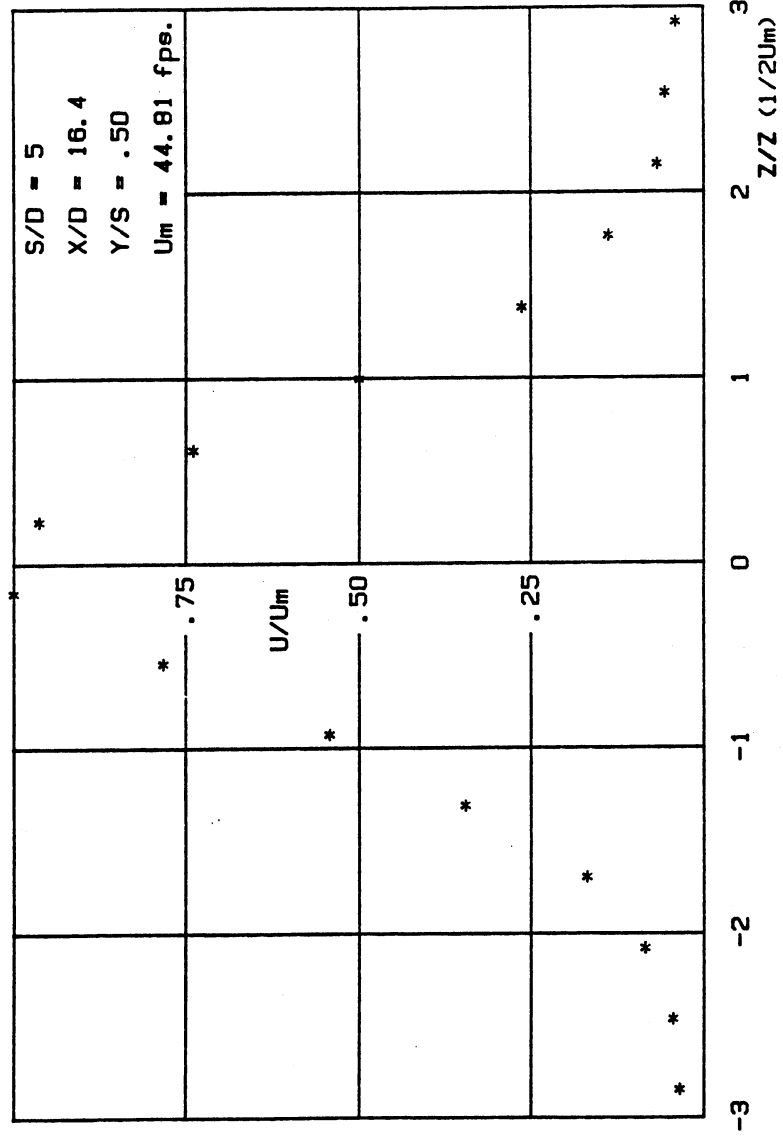
FIGURE 10B: Total velocity distribution for S/D = 5
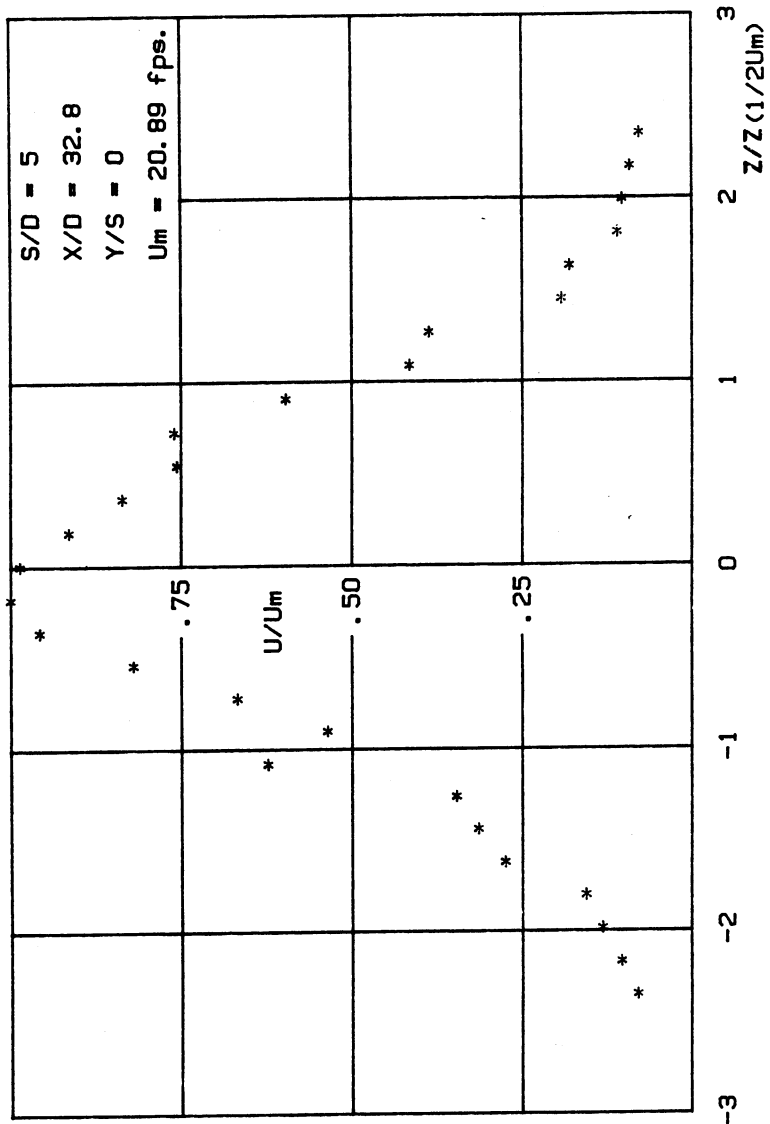
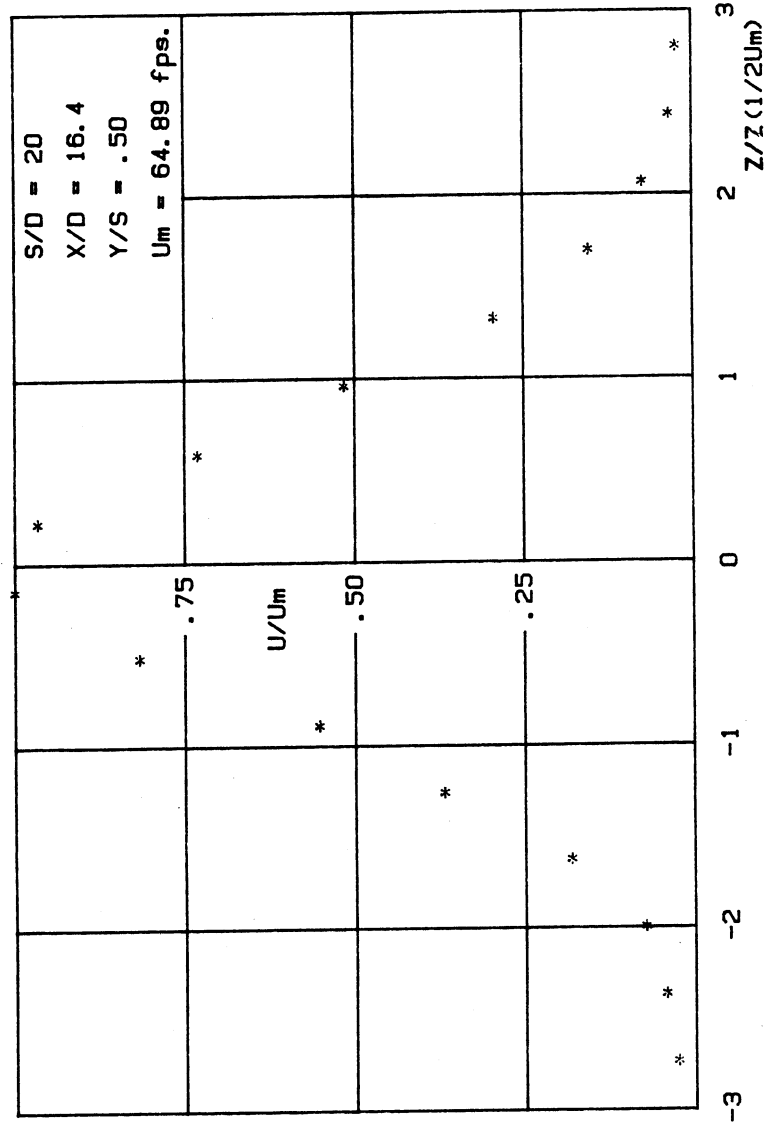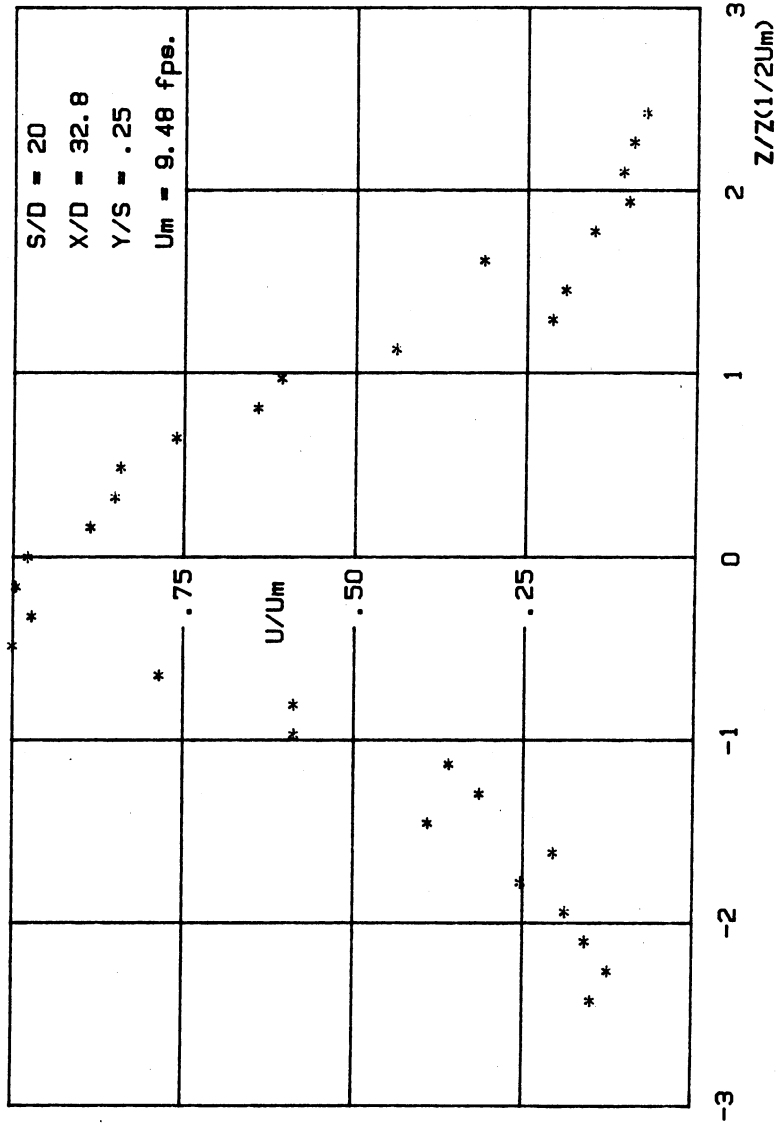FIGURE 11B: Total velocity distribution for S/D = 5

82
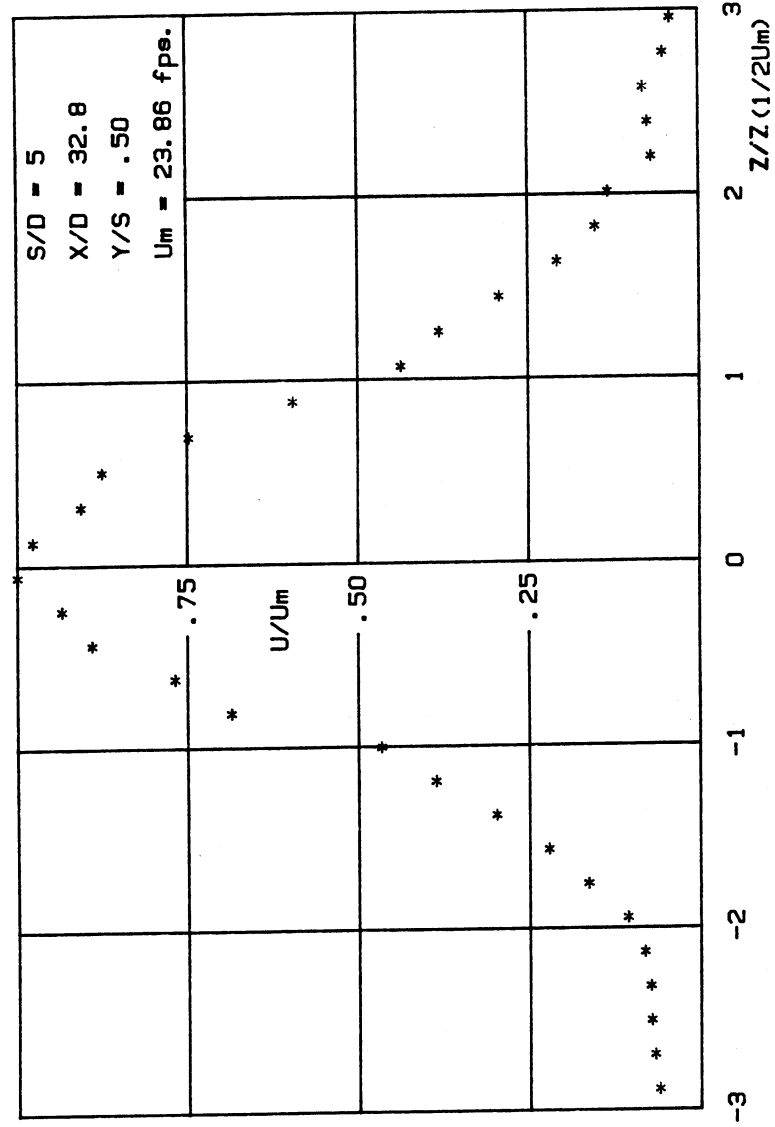


FIGURE 12B: Total velocity distribution for S/D = 5
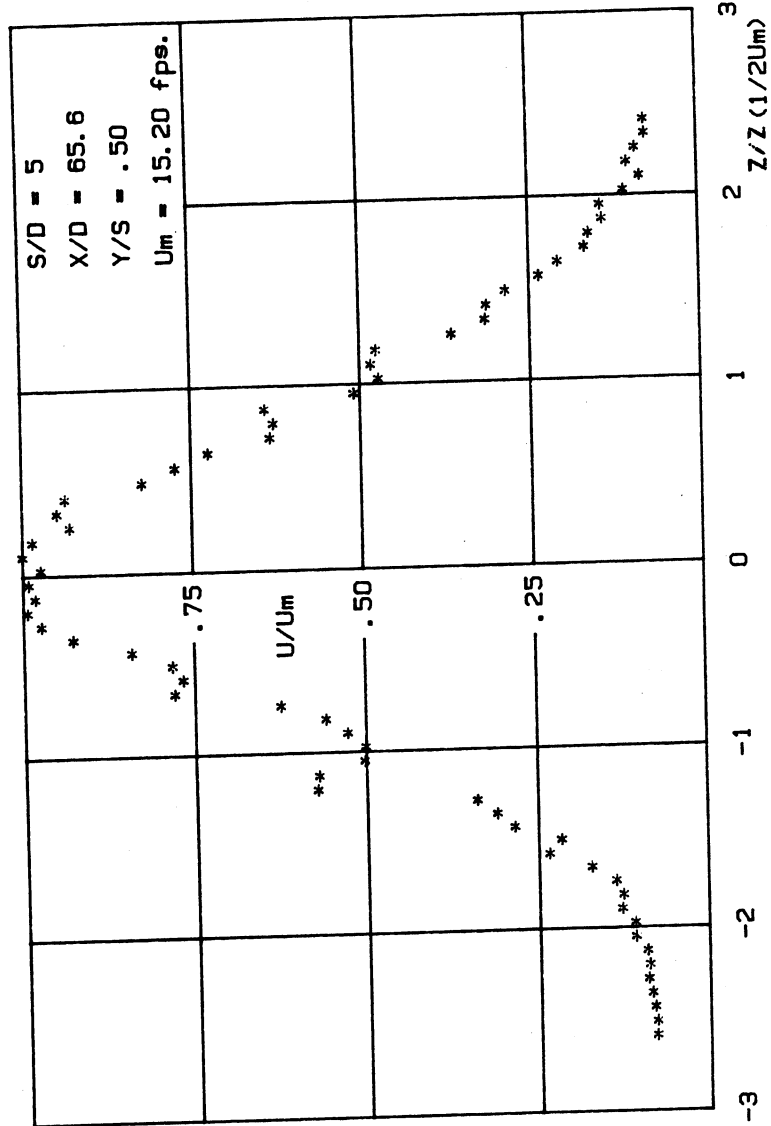
FIGURE 13B: Total velocity distribution for S/D = 5



S/D = 5
X/D = 98.4
Y/S = .50
Um = 12.24 fps.
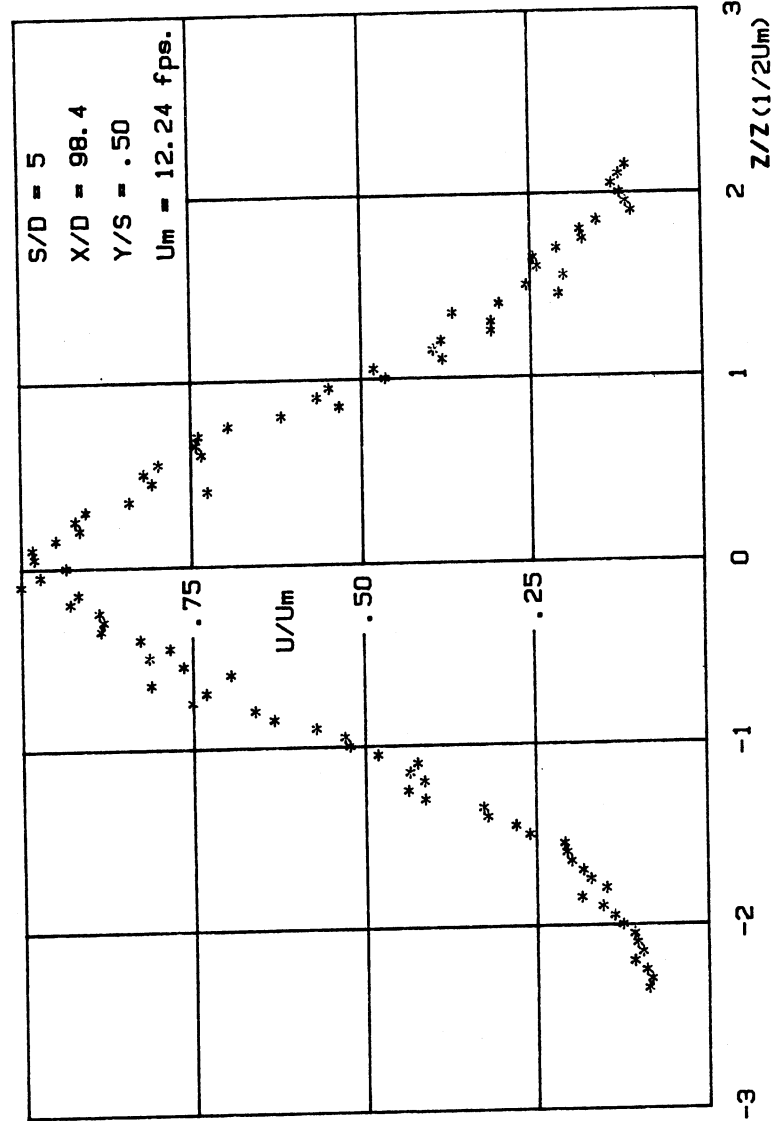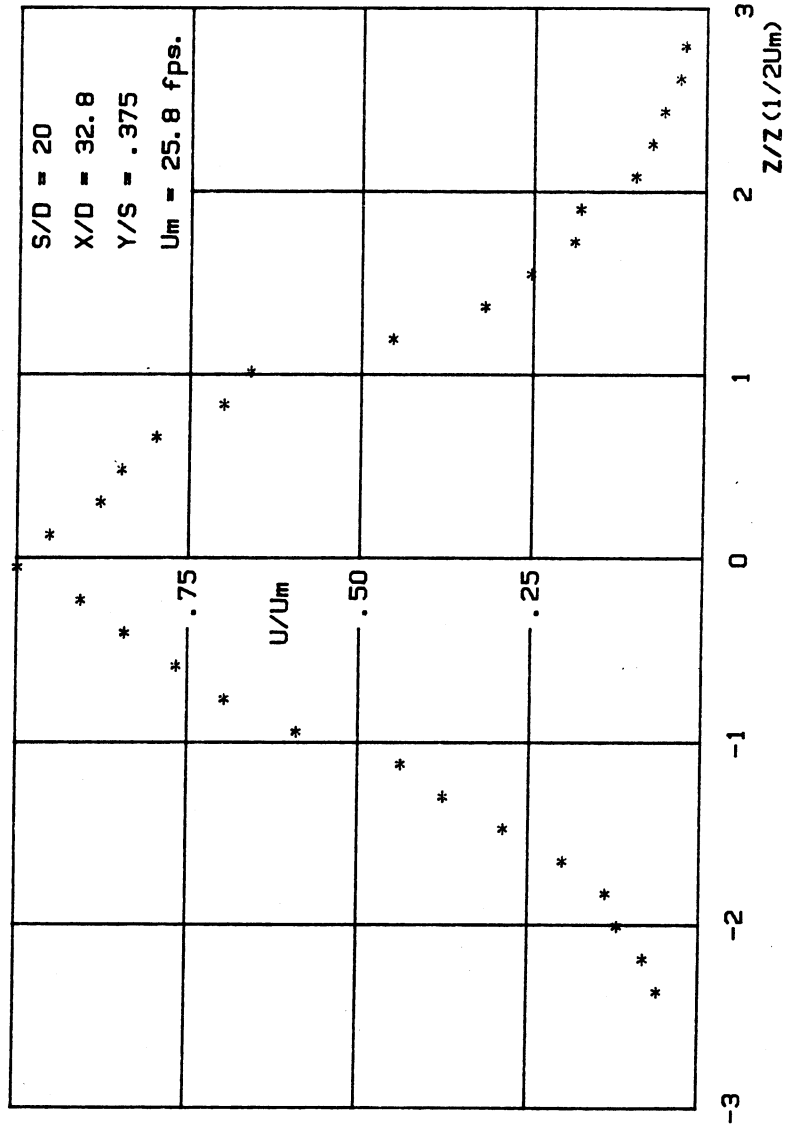
FIGURE 14B: Total velocity distribution for S/D = 5
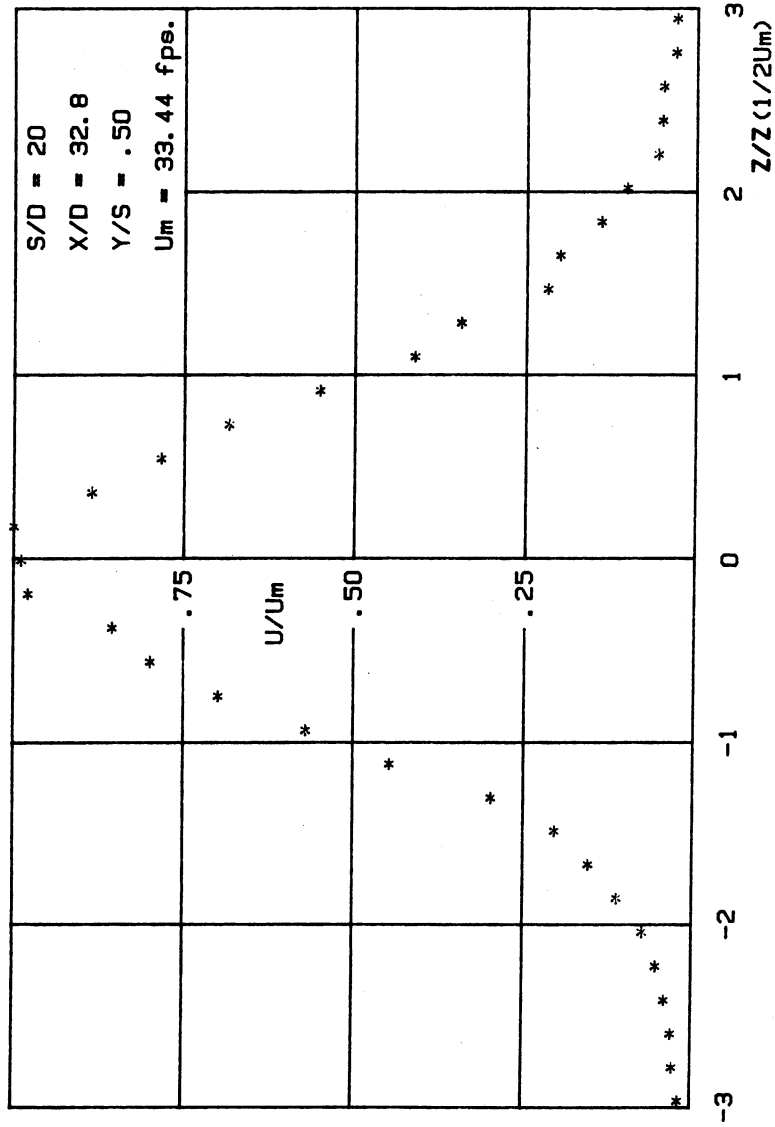
FIGURE 15B: Total velocity distribution for S/D = 10
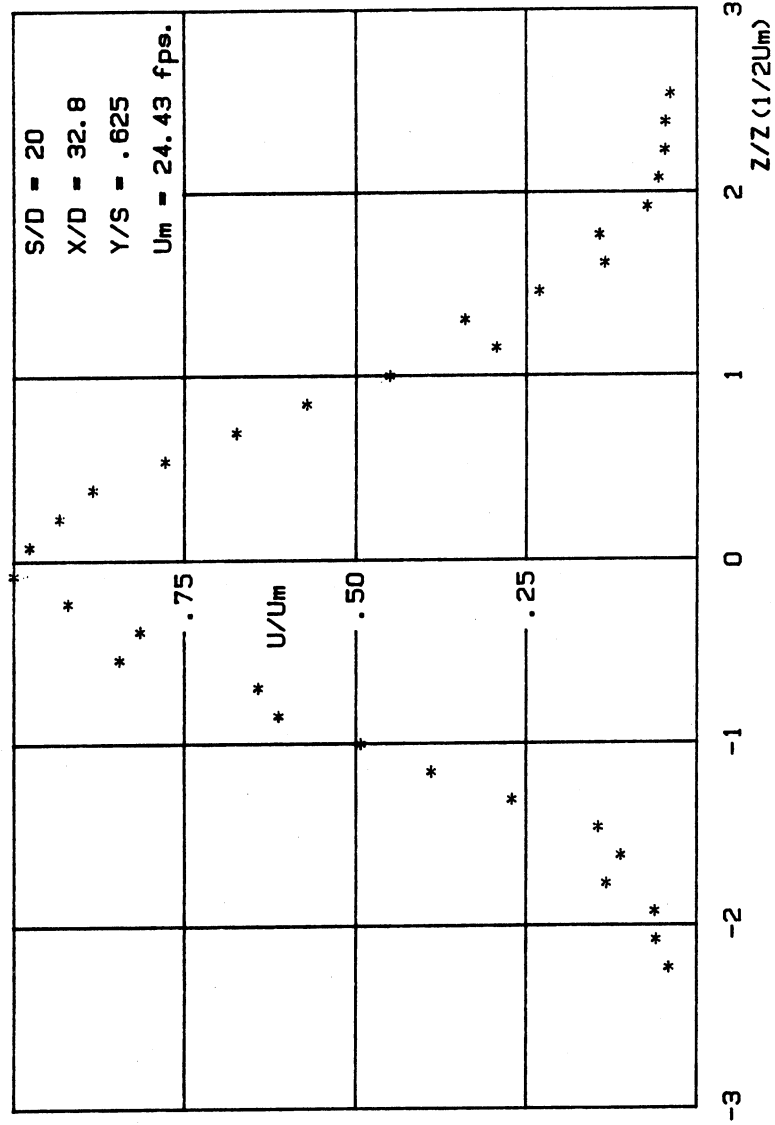
FIGURE 16B: Total velocity distribution for S/D = 10

FIGURE 17B: Total velocity distribution for S/D = 10
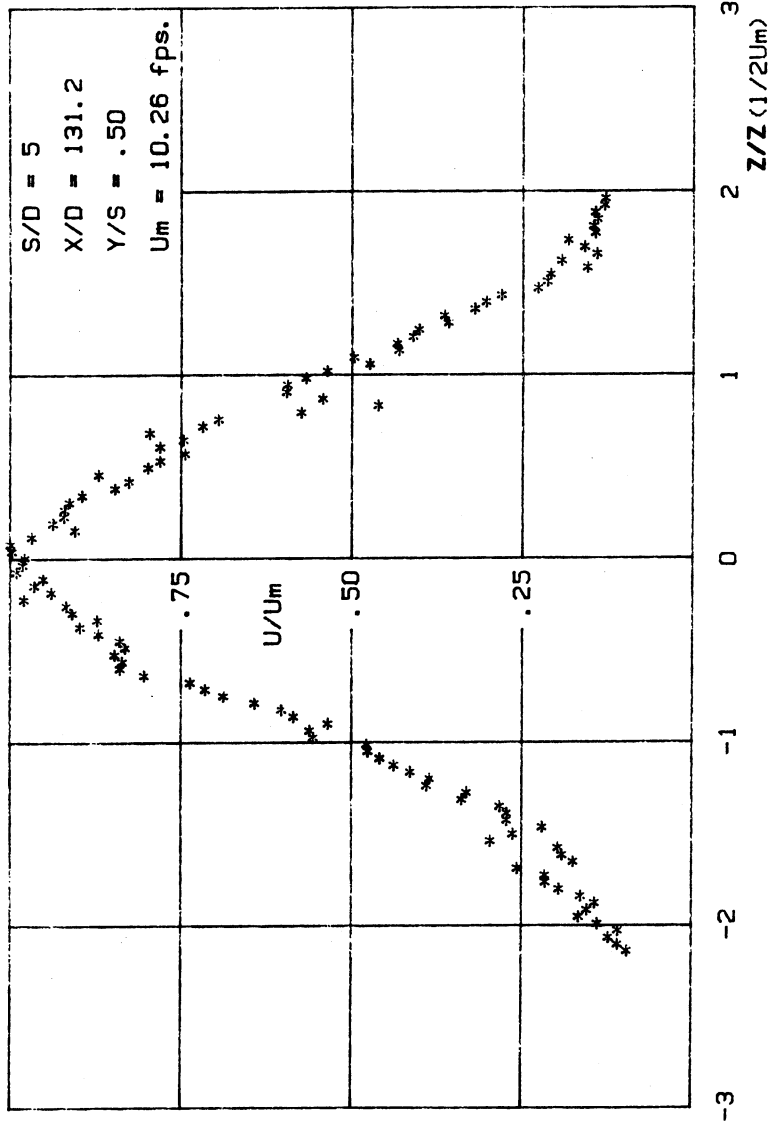
FIGURE 18B: Total velocity distribution for S/D = 10
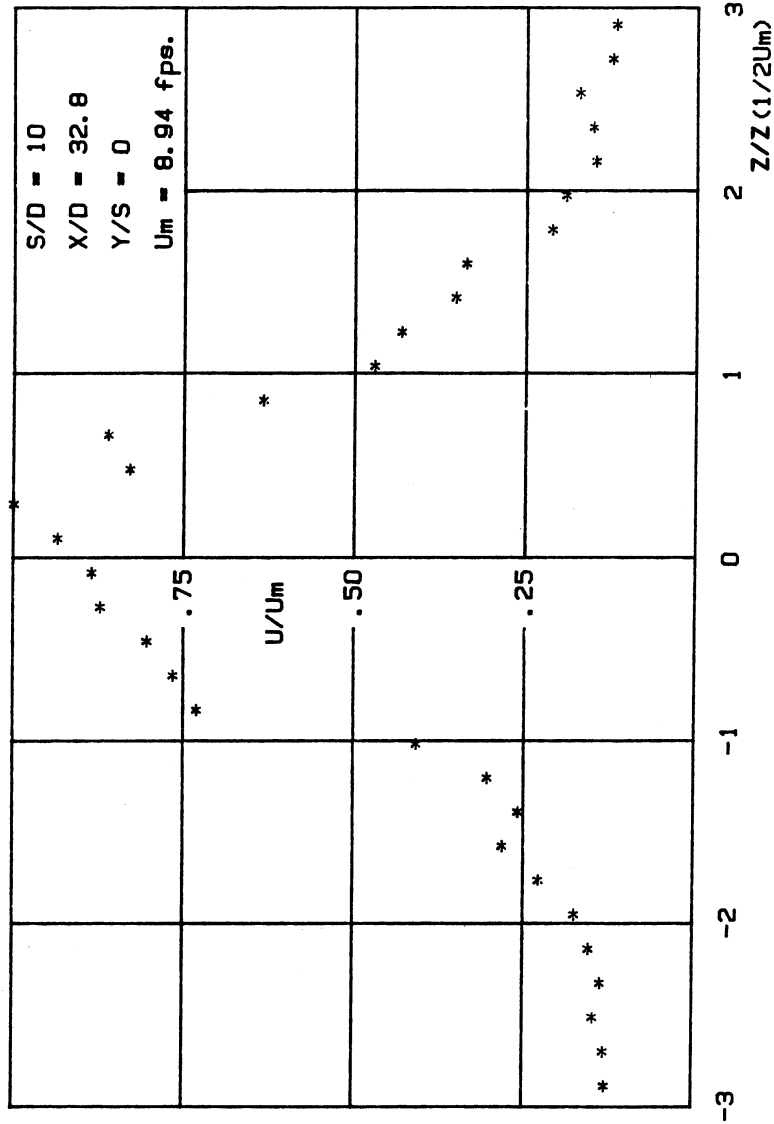
FIGURE 19B: Total velocity distribution for S/D = 10
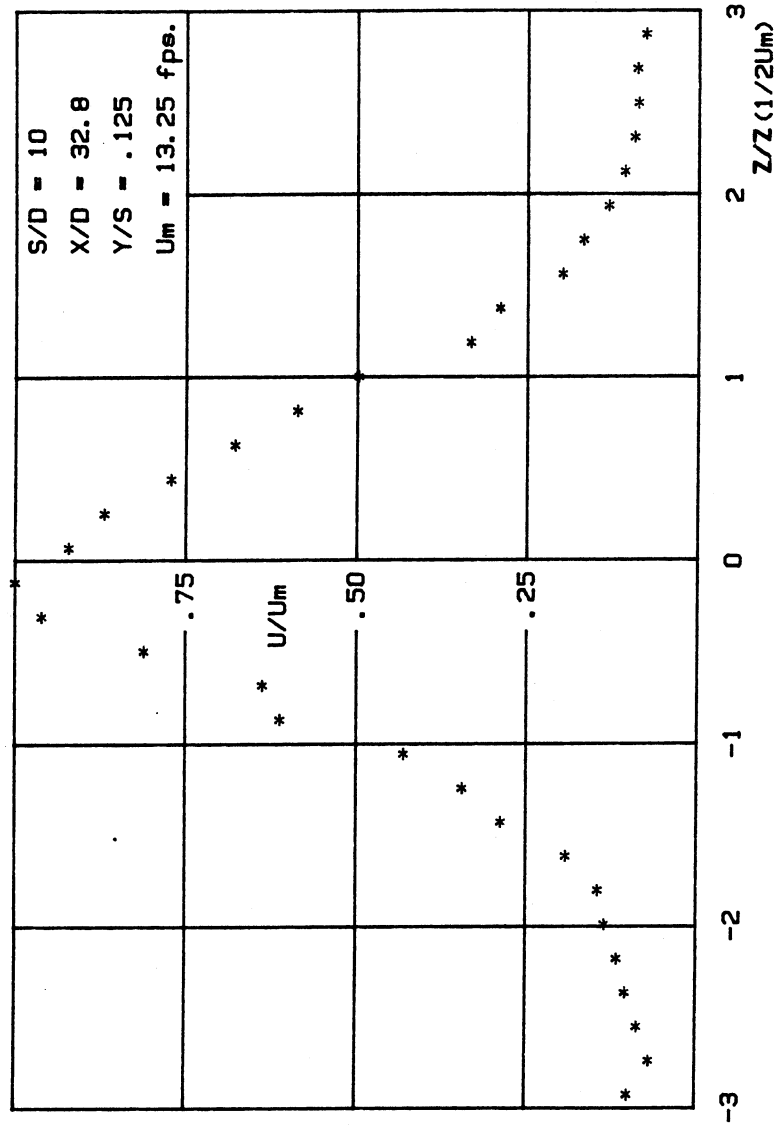
FIGURE 20B: Total velocity distribution for S/D = 10

S/D = 10
X/D = 32.8
Y/S = .25
Um = 19.17 fps.
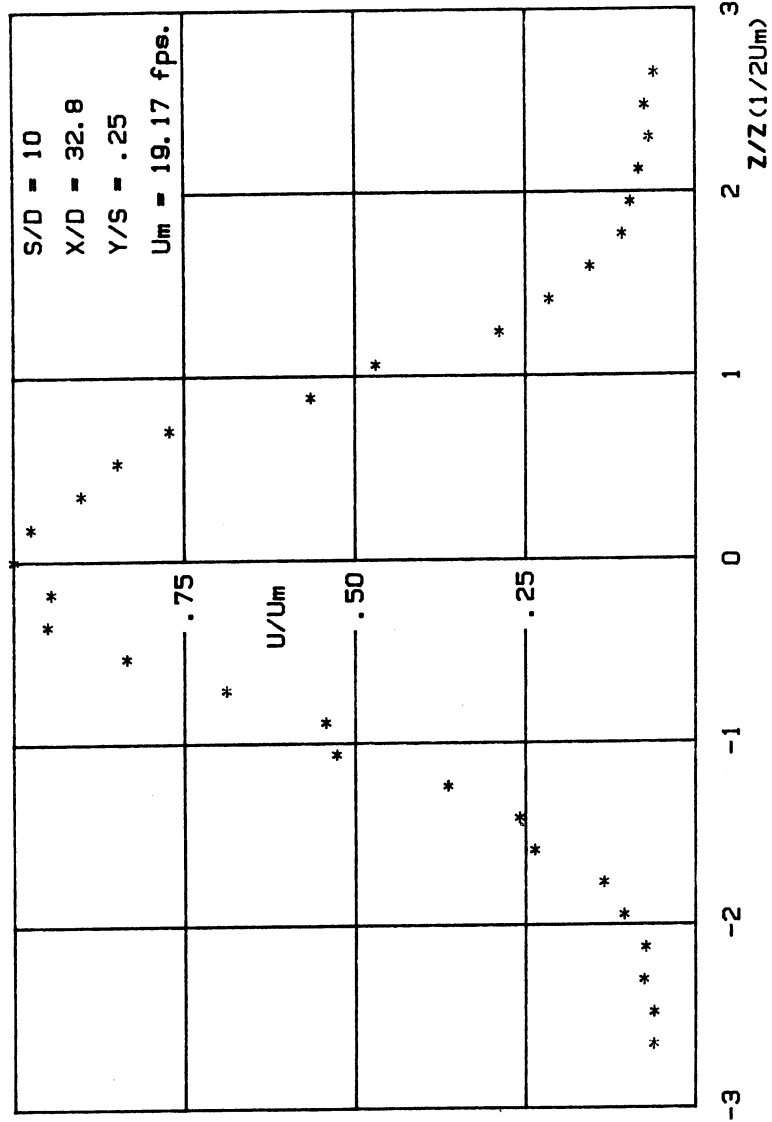
FIGURE 21B: Total velocity distribution for S/D = 10

92
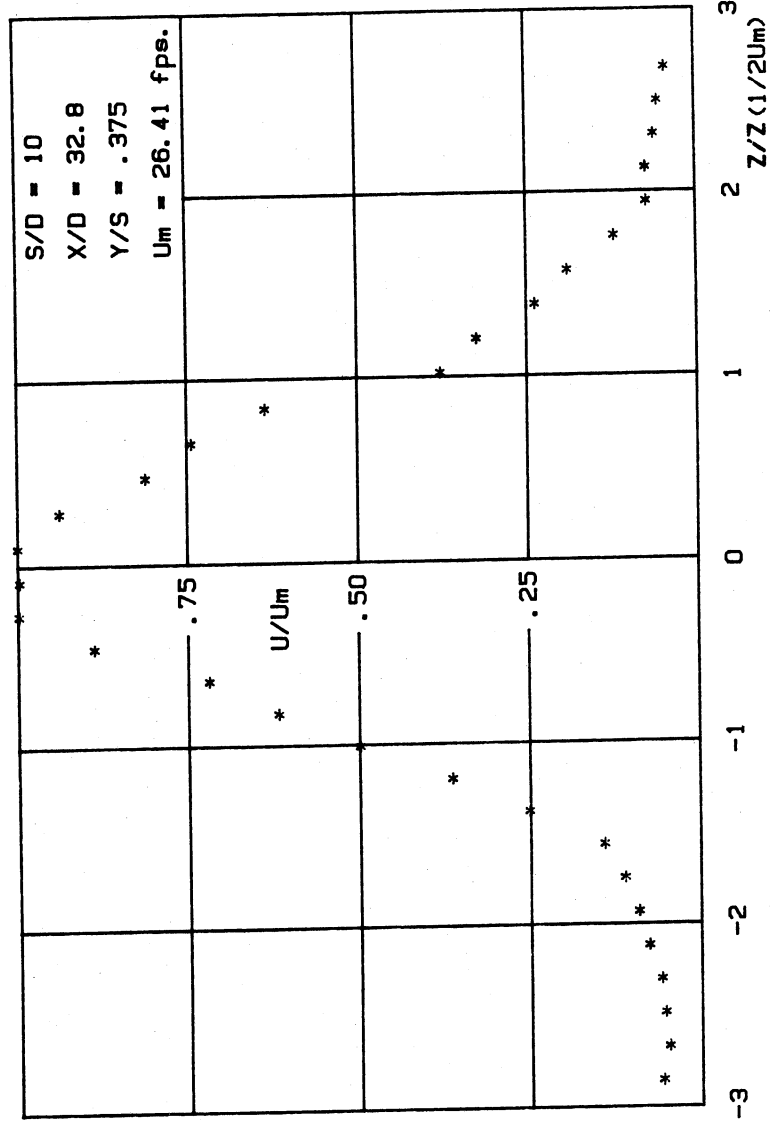


FIGURE 22B: Total velocity distribution for S/D = 10

93
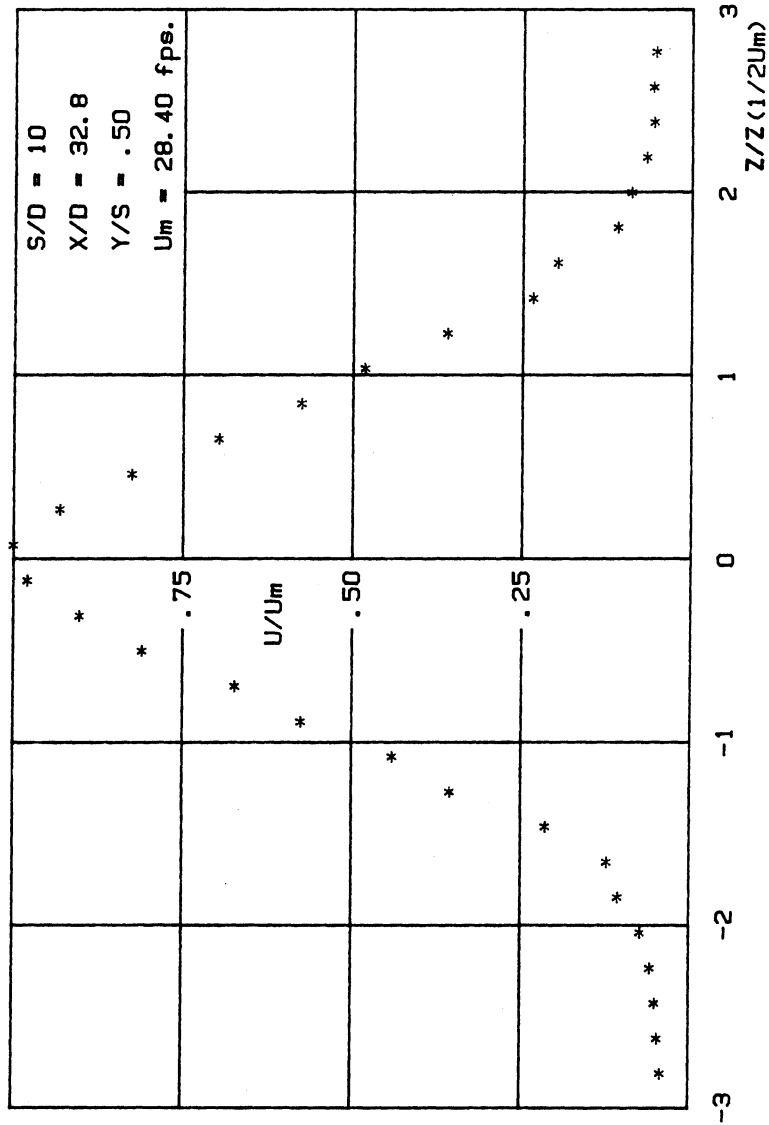


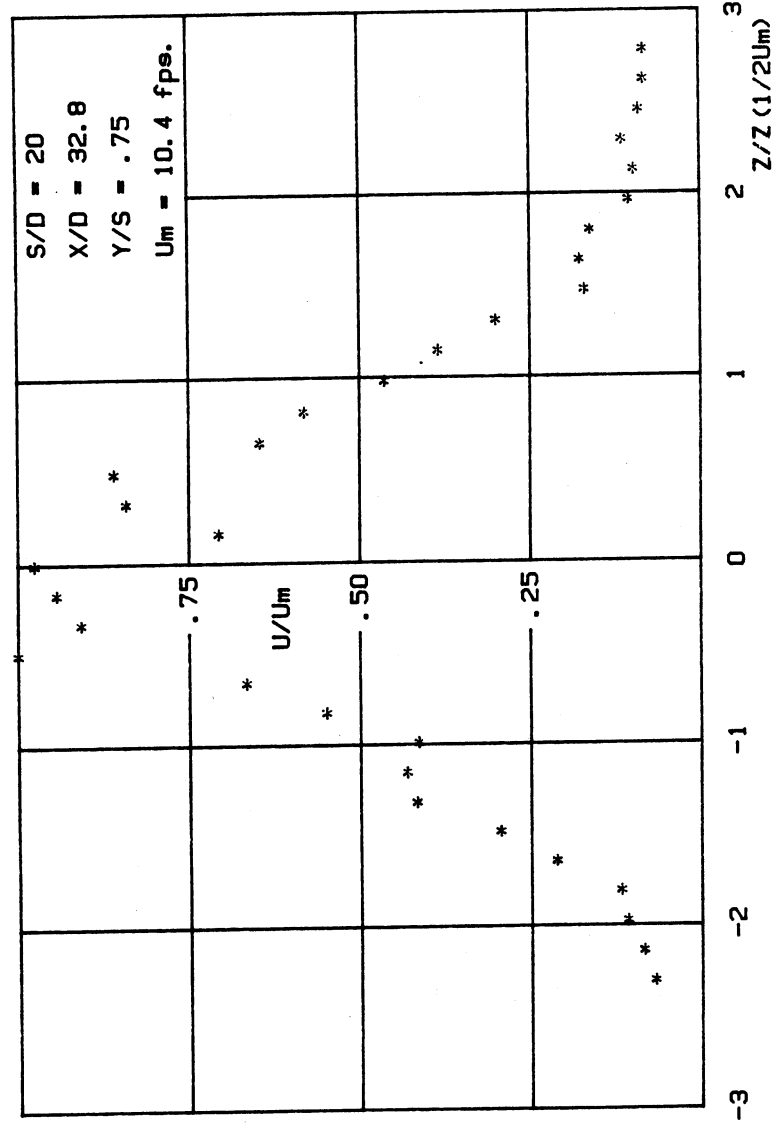FIGURE 23B: Total velocity distribution for S/D = 10

S/D = 10
X/D = 65.6
Y/S = 0
Um = 12.54 fps.

U/Um

.75

.50

.25

Z/Z (1/2Um)

94
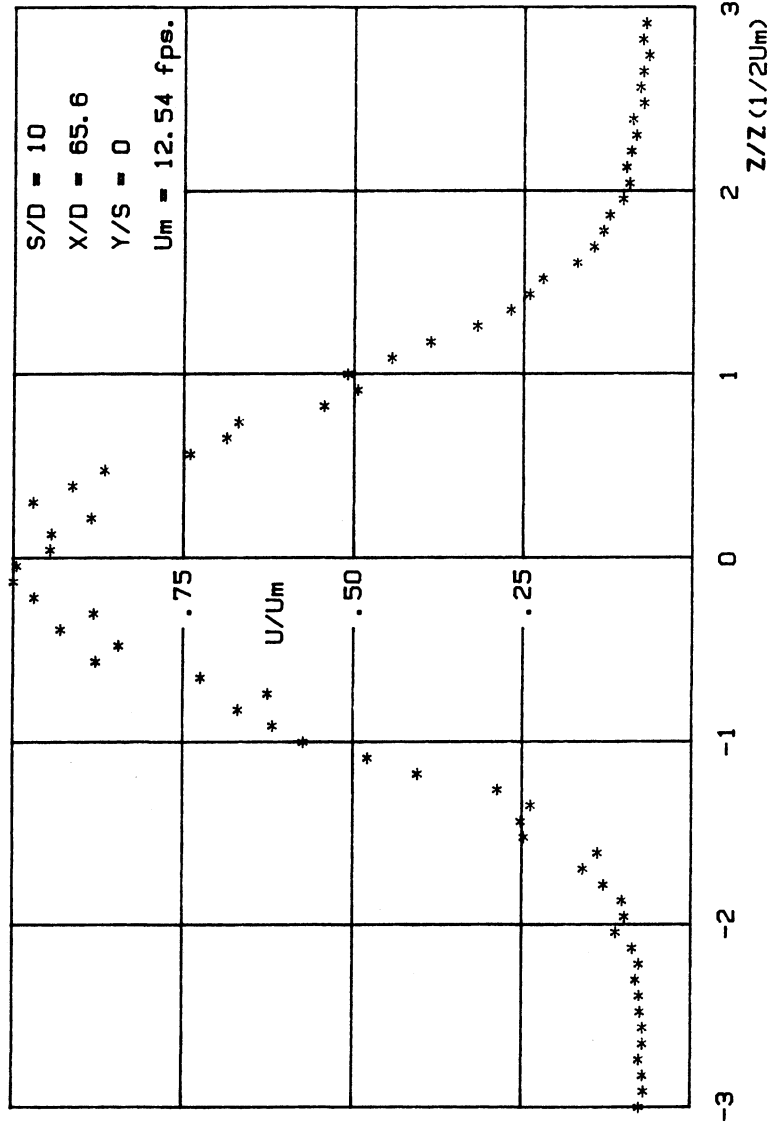


FIGURE 24B: Total velocity distribution for S/D = 10
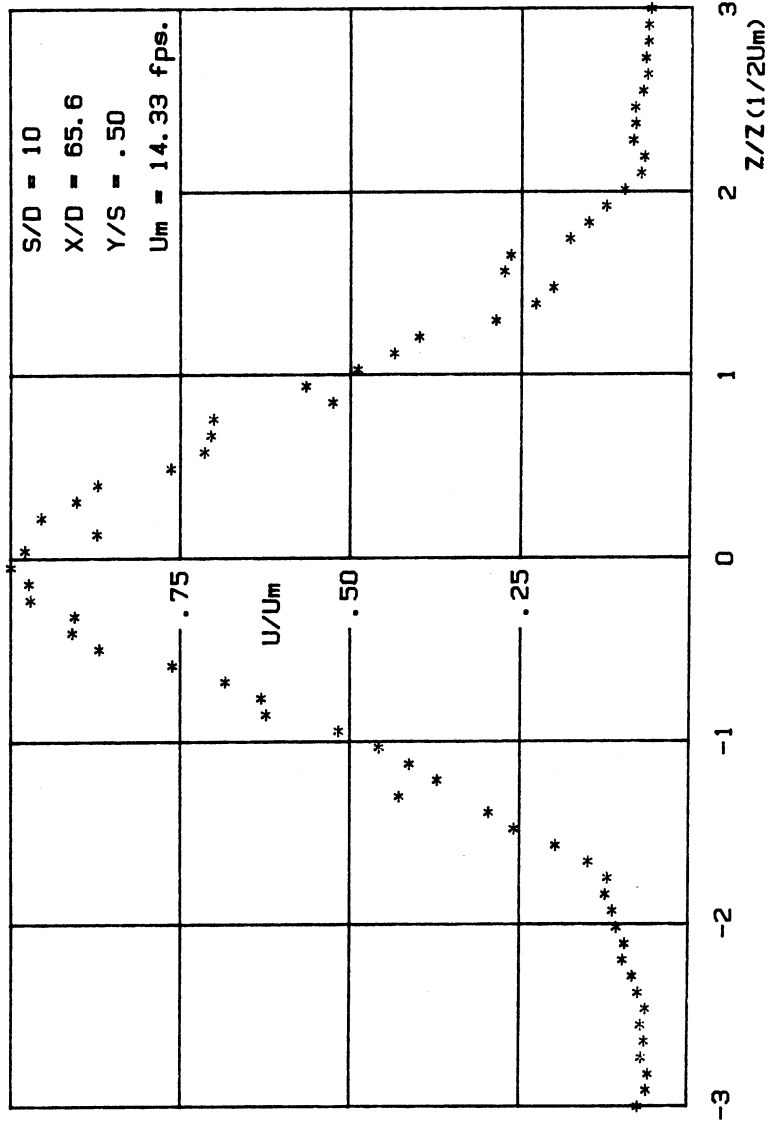
FIGURE 25B: Total velocity distribution for S/D = 10
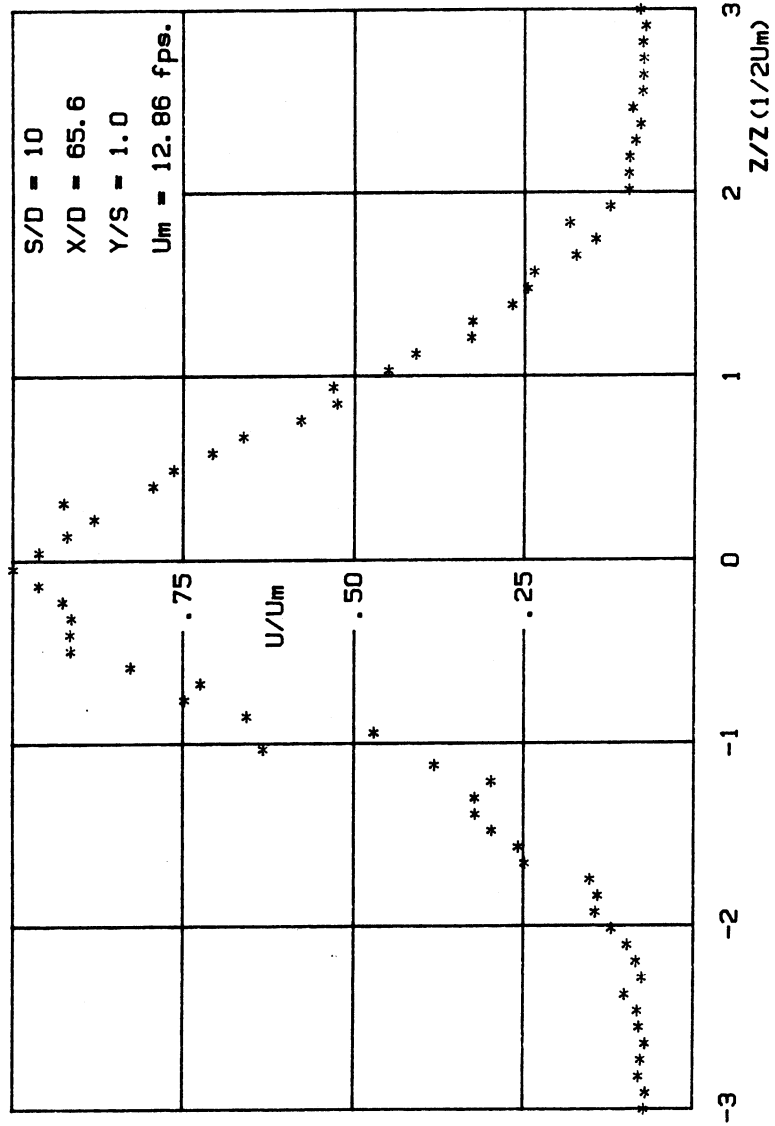
FIGURE 26B: Total velocity distribution for S/D = 10

FIGURE 27B: Total velocity distribution for S/D = 10

FIGURE 28B: Total velocity distribution for S/D = 10

FIGURE 29B: Total velocity distribution for S/D = 20
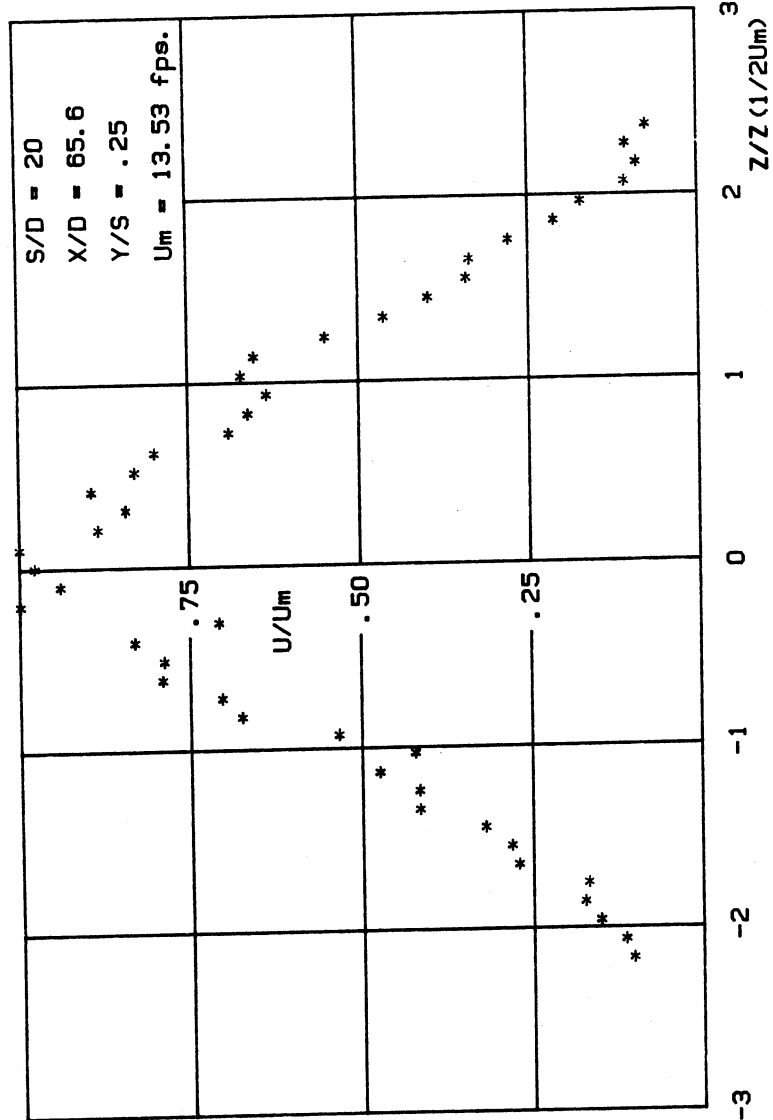
FIGURE 30B: Total velocity distribution for S/D = 20
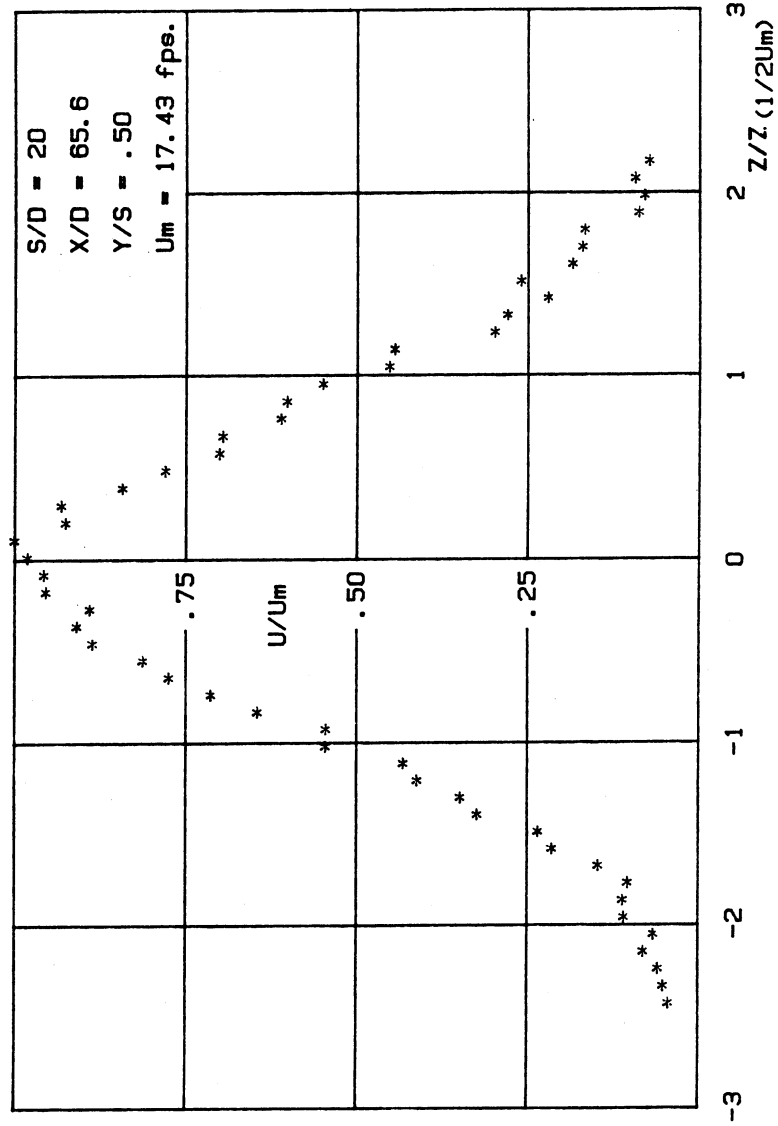
S/D = 20
X/D = 16.4
Y/S = .4375
Um = 44.06 fps.

FIGURE 31B: Total velocity distribution for S/D = 20

FIGURE 32B: Total velocity distribution for S/D = 20
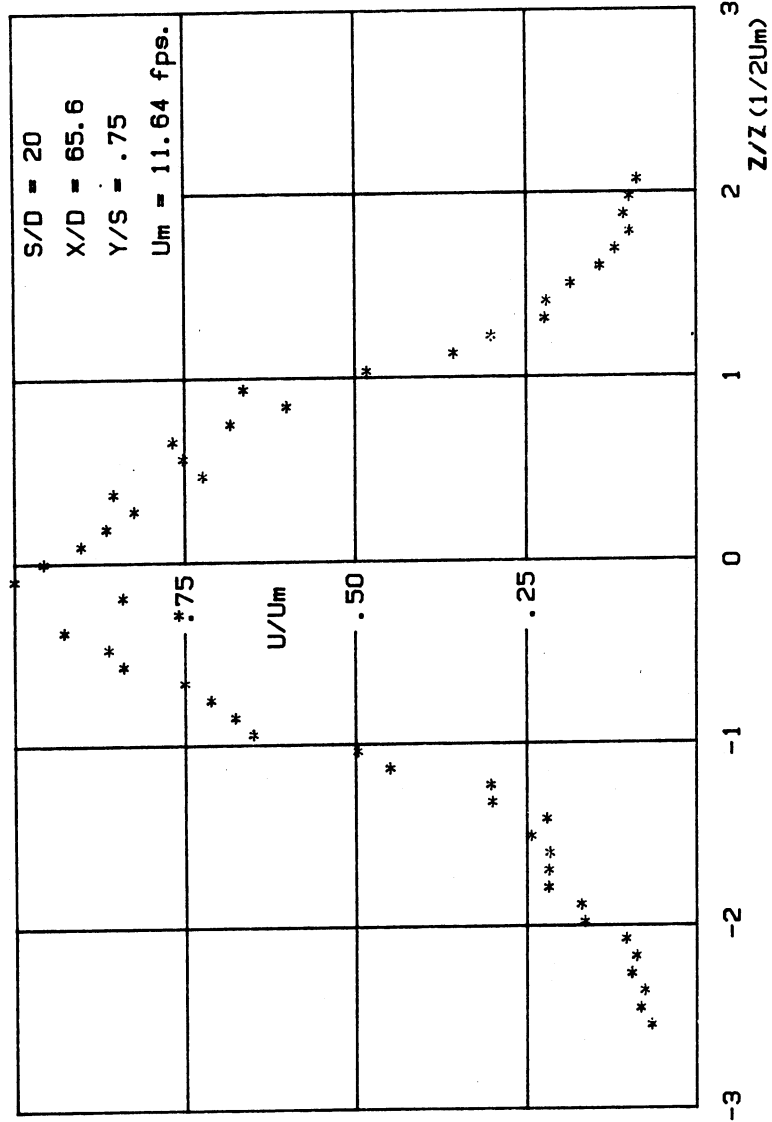
FIGURE 33B: Total velocity distribution for S/D = 20

S/D = 20
X/D = 16.4
Y/S = .625
Um = 31.49 fps.

U/Um

.75

.50

.25

Z/Z (1/2Um)

-3  -2  -1  0  1  2  3

FIGURE 34B: Total velocity distribution for S/D = 20

FIGURE 35B: Total velocity distribution for S/D = 20
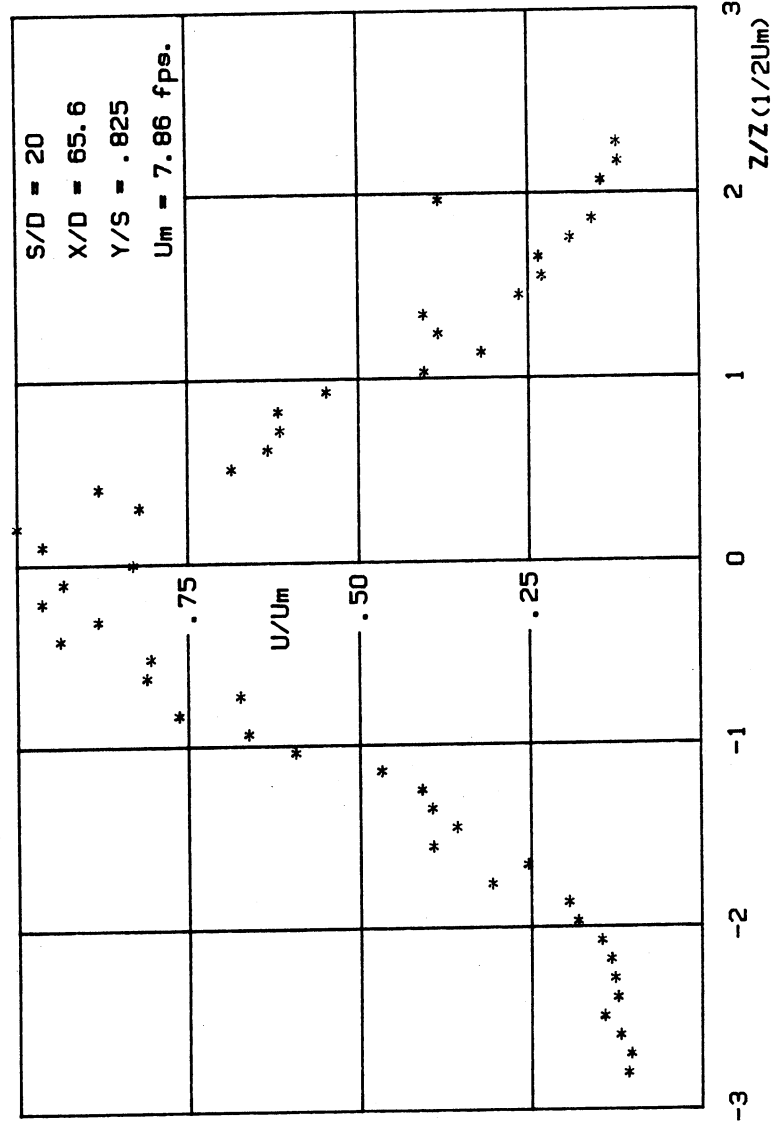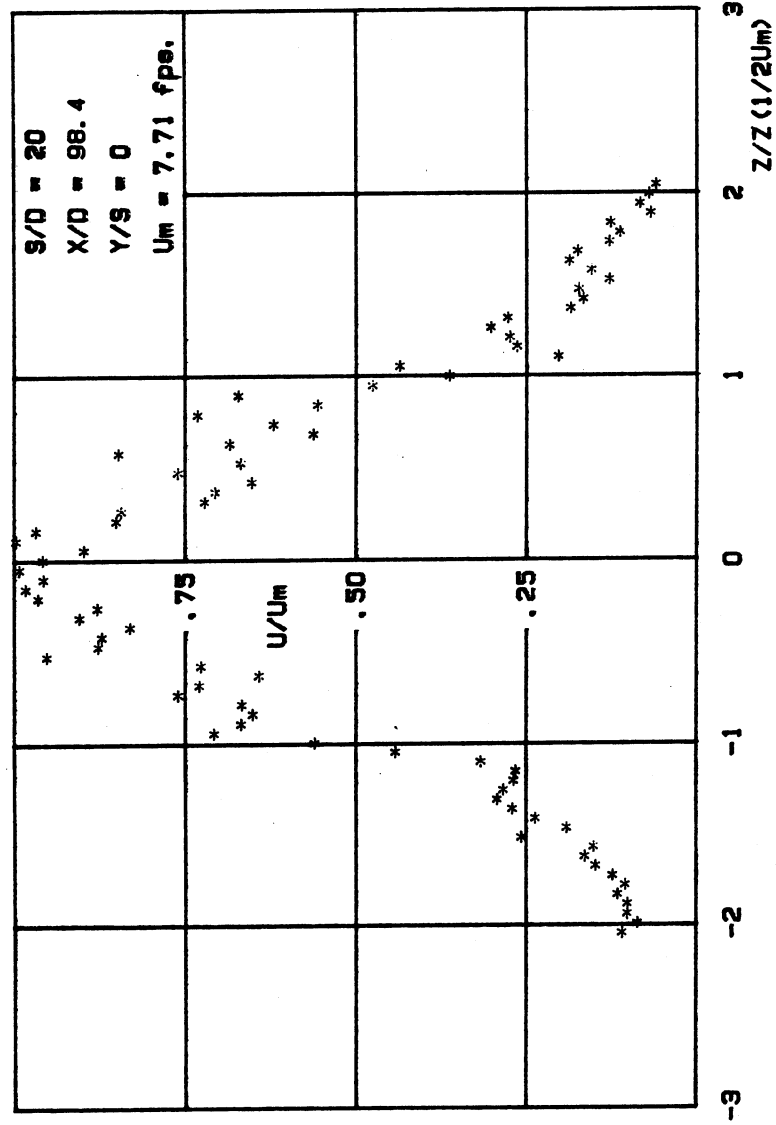
FIGURE 36B: Total velocity distribution for S/D = 20

FIGURE 37B: Total velocity distribution for S/D = 20

108



FIGURE 38B: Total velocity distribution for S/D = 20

FIGURE 39B: Total velocity distribution for S/D = 20
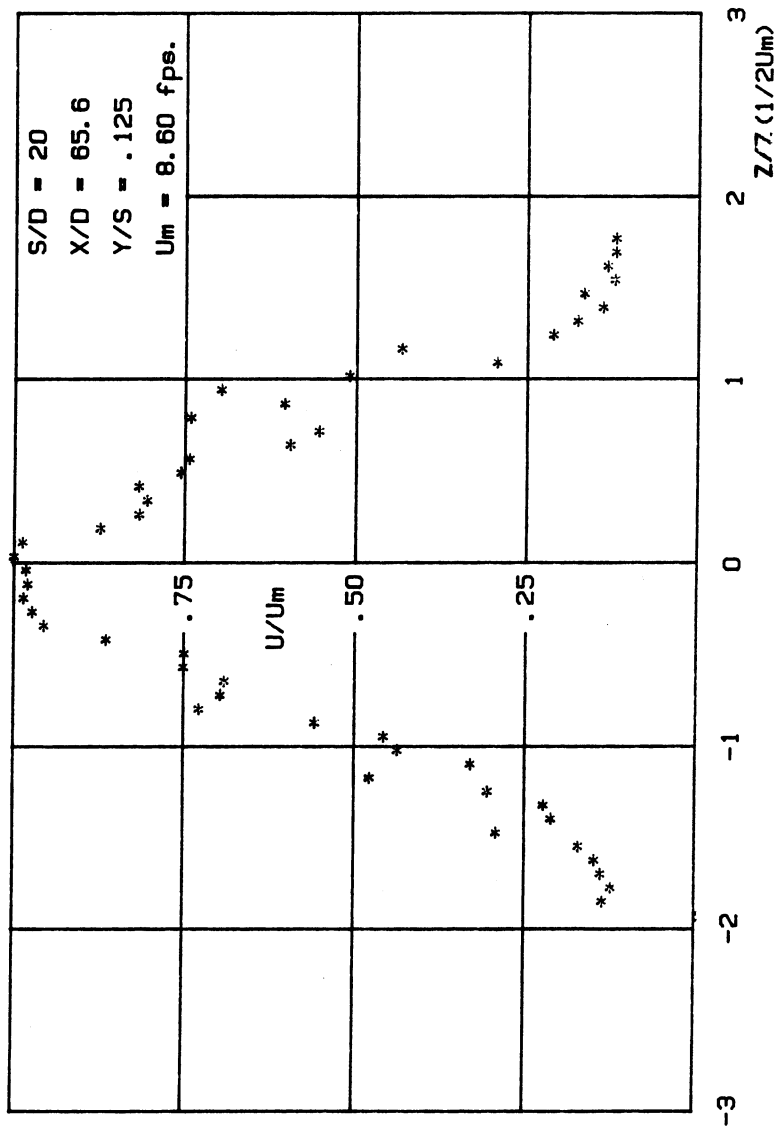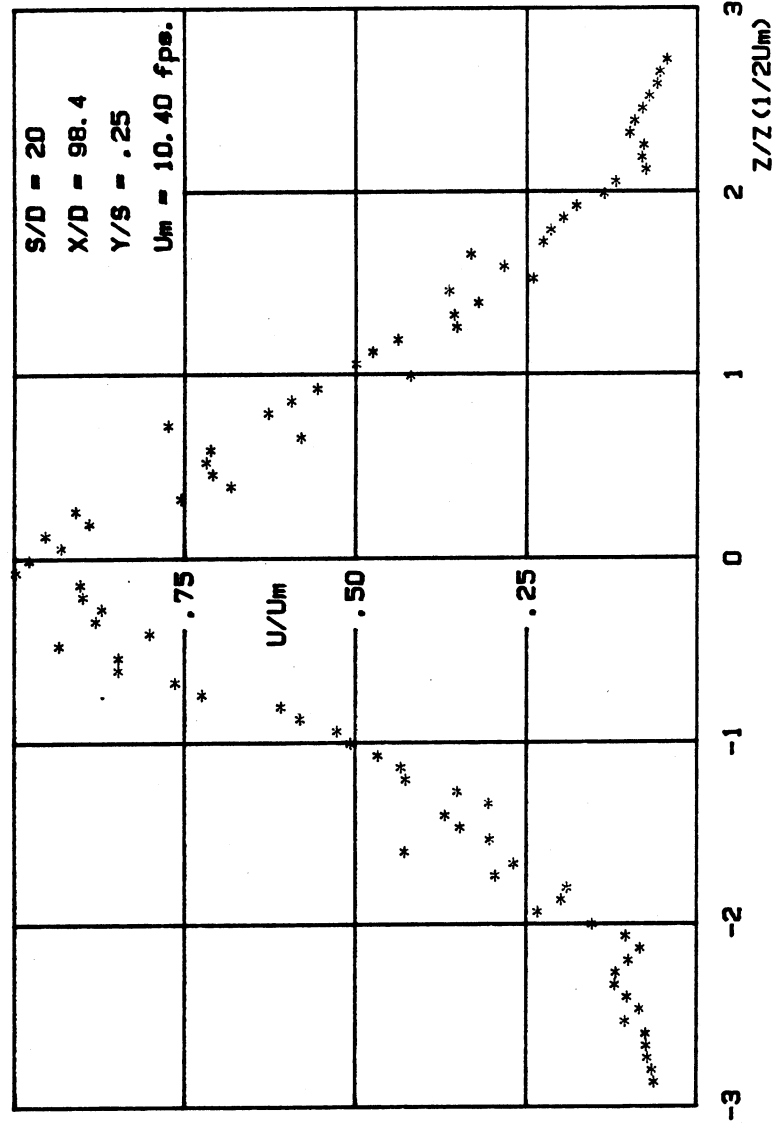
FIGURE 40B: Total velocity distribution for S/D = 20

S/D = 20
X/D = 65.6
Y/S = .25
Um = 13.53 fps.

U/Um

Z/Z (1/2Um)

FIGURE 41B: Total velocity distribution for S/D = 20

S/D = 20
X/D = 65.6
Y/S = .50
Um = 17.43 fps.

U/Um

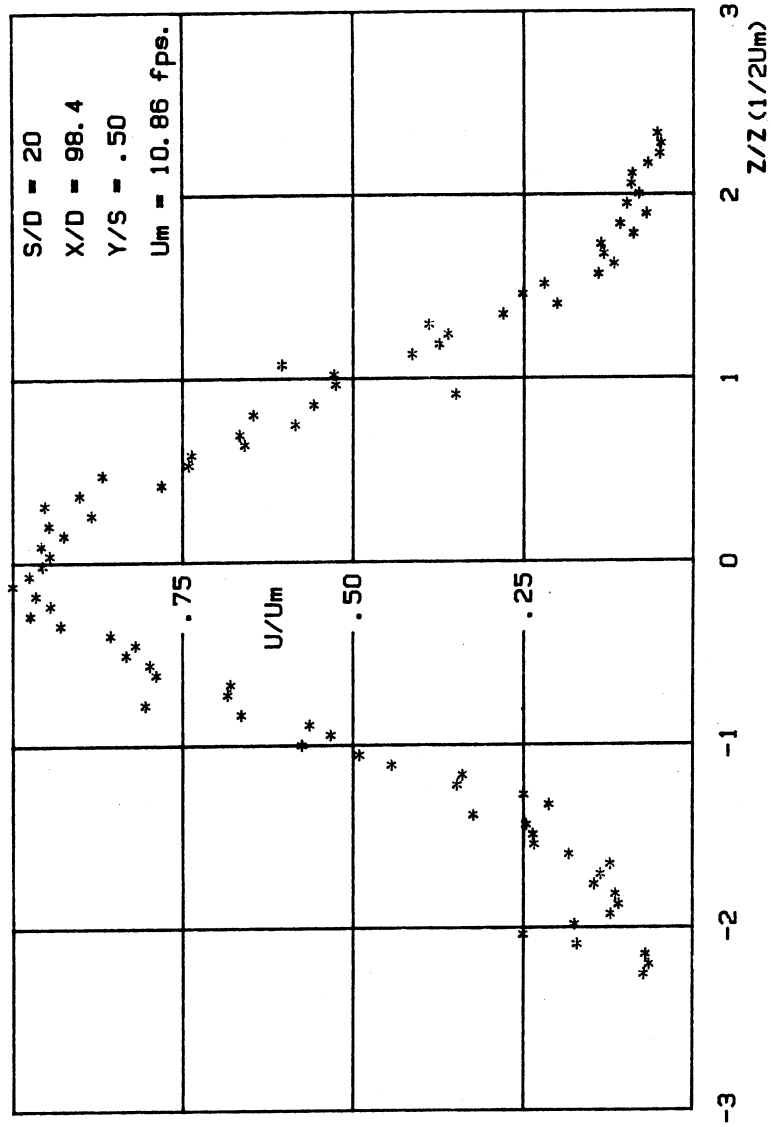Z/Z (1/2Um)

FIGURE 42: Total velocity distribution for S/D = 20

FIGURE 43: Total velocity distribution for S/D = 20

FIGURE 44B: Total velocity distribution for S/D = 20

FIGURE 45B: Total velocity distribution for S/D = 20
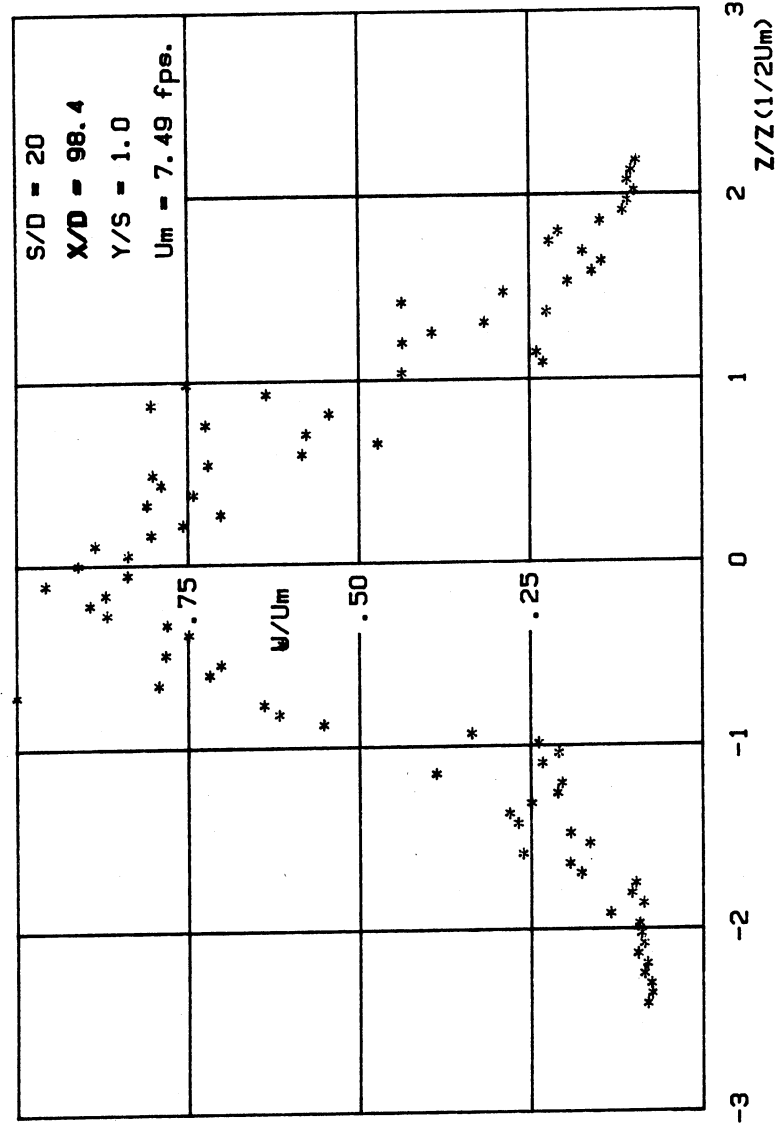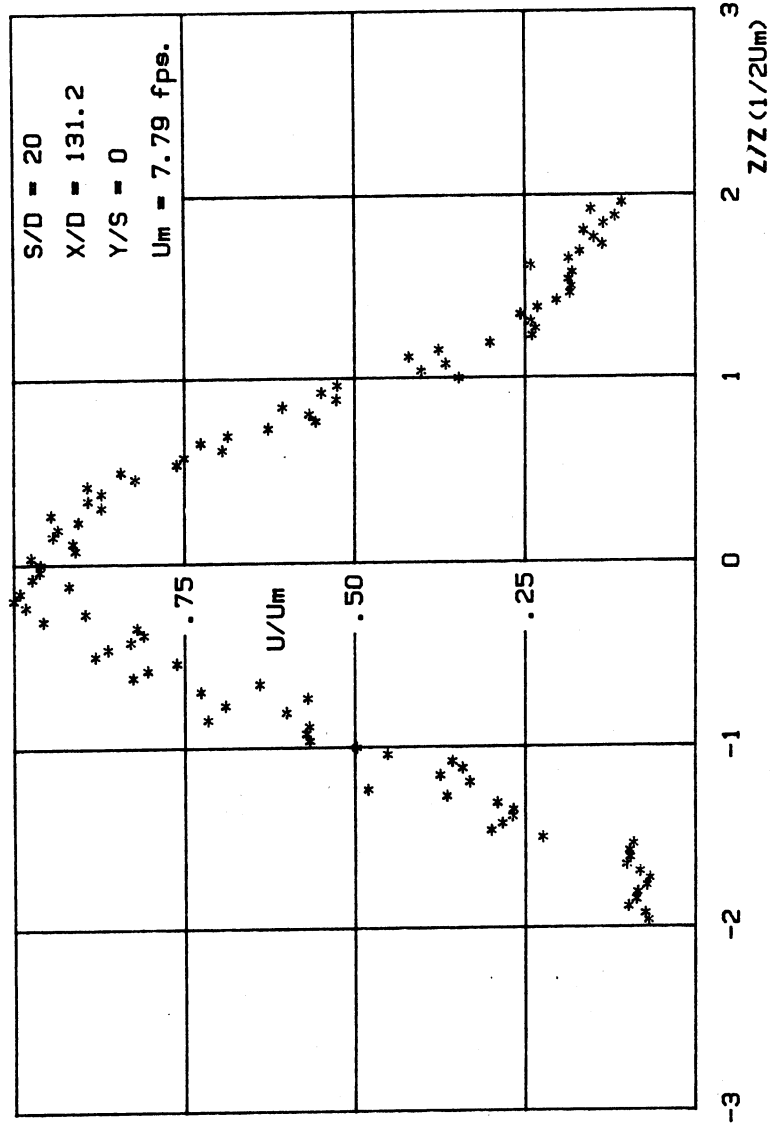
FIGURE 46B: Total velocity distribution for S/D = 20

S/D = 20
X/D = 98.4
Y/S = .50
Um = 10.86 fps.

U/Um

Z/Z (1/2Um)

FIGURE 47B: Total velocity distribution for S/D = 20

FIGURE 48B: Total velocity distribution for S/D = 20
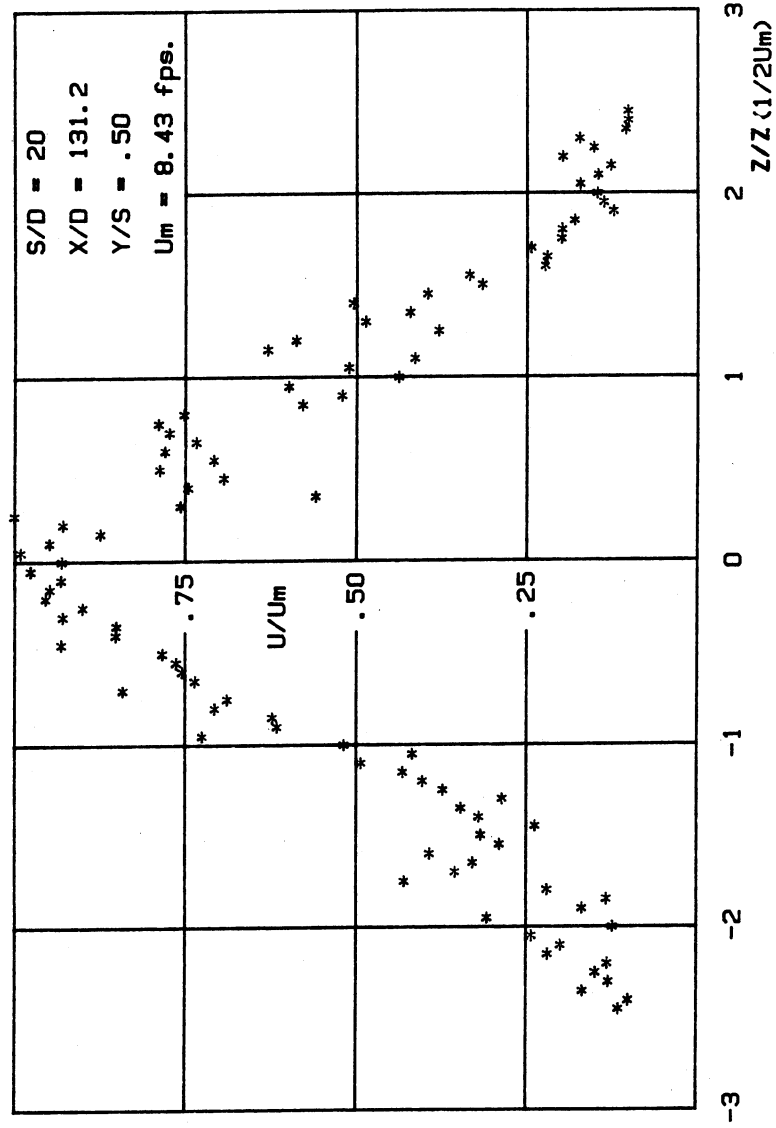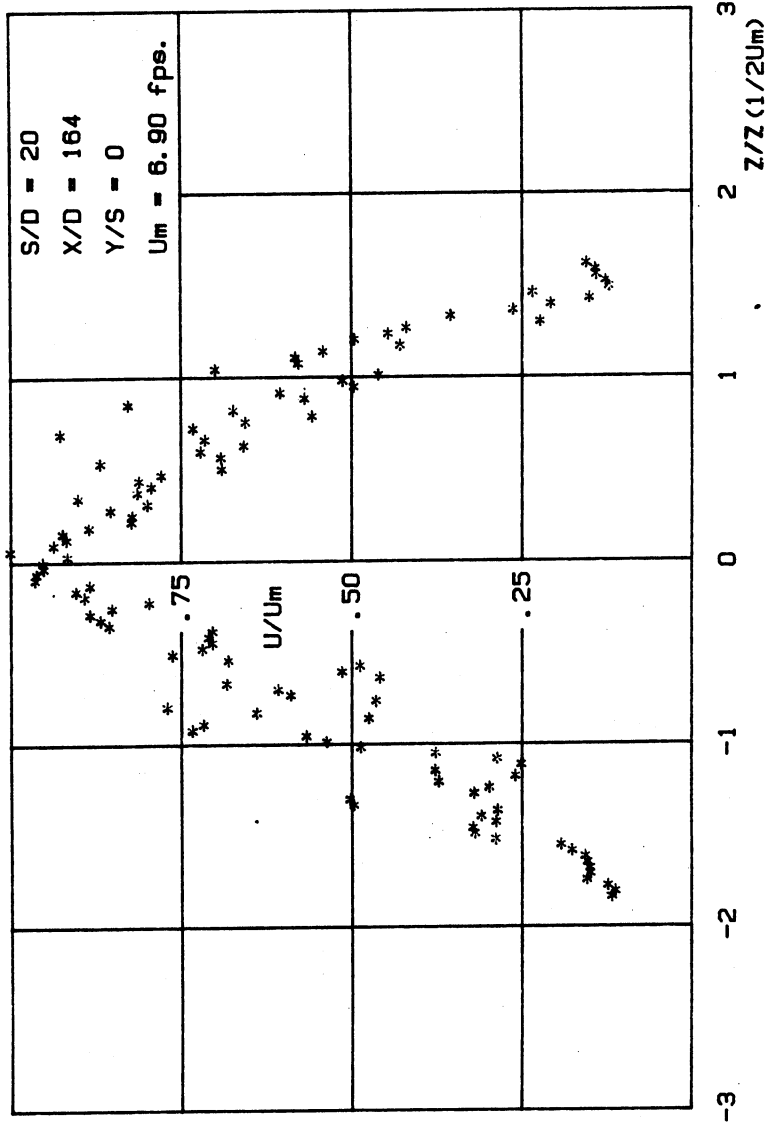
FIGURE 49B: Total velocity distribution for S/D = 20

FIGURE 50B: Total velocity distribution for S/D = 20
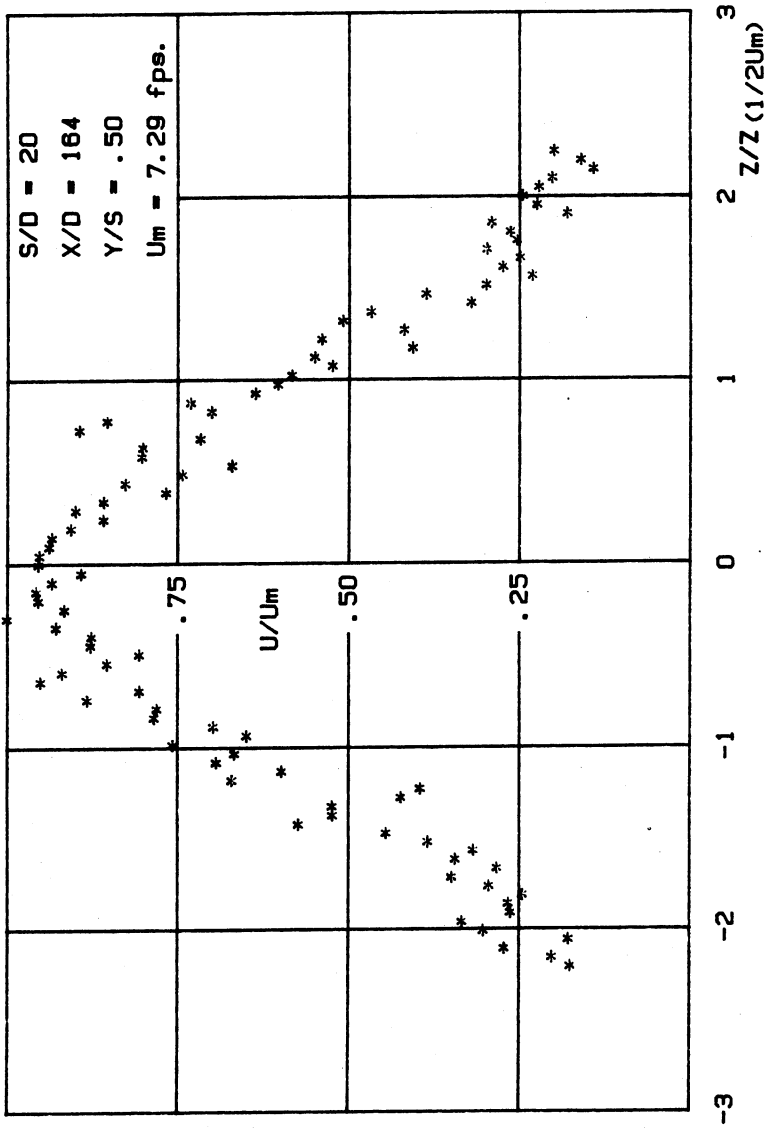
FIGURE 51B: Total velocity distribution for S/D = 20

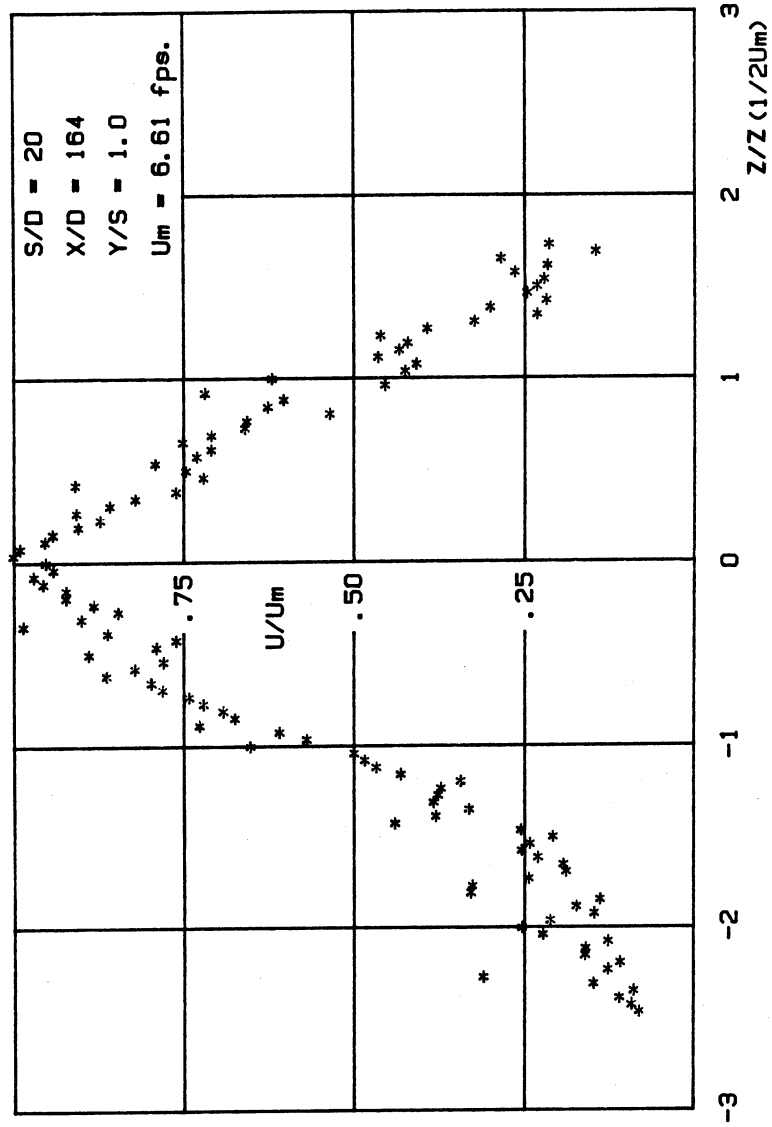FIGURE 528: Total velocity distribution for S/D = 20

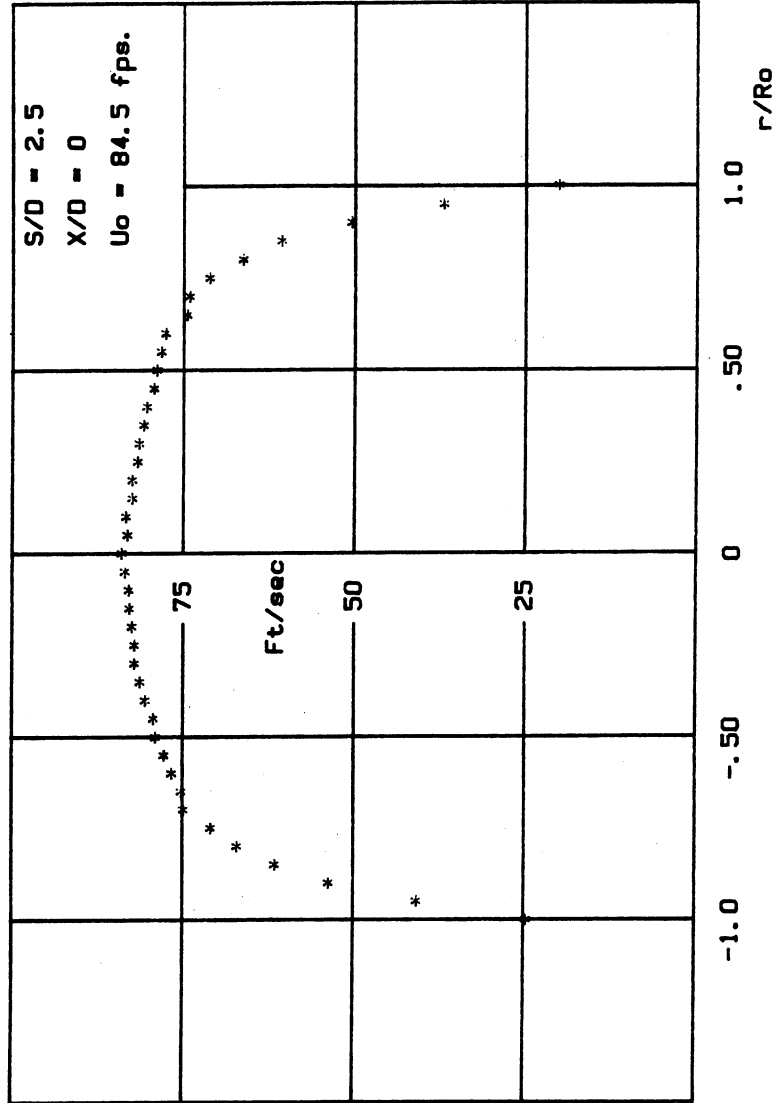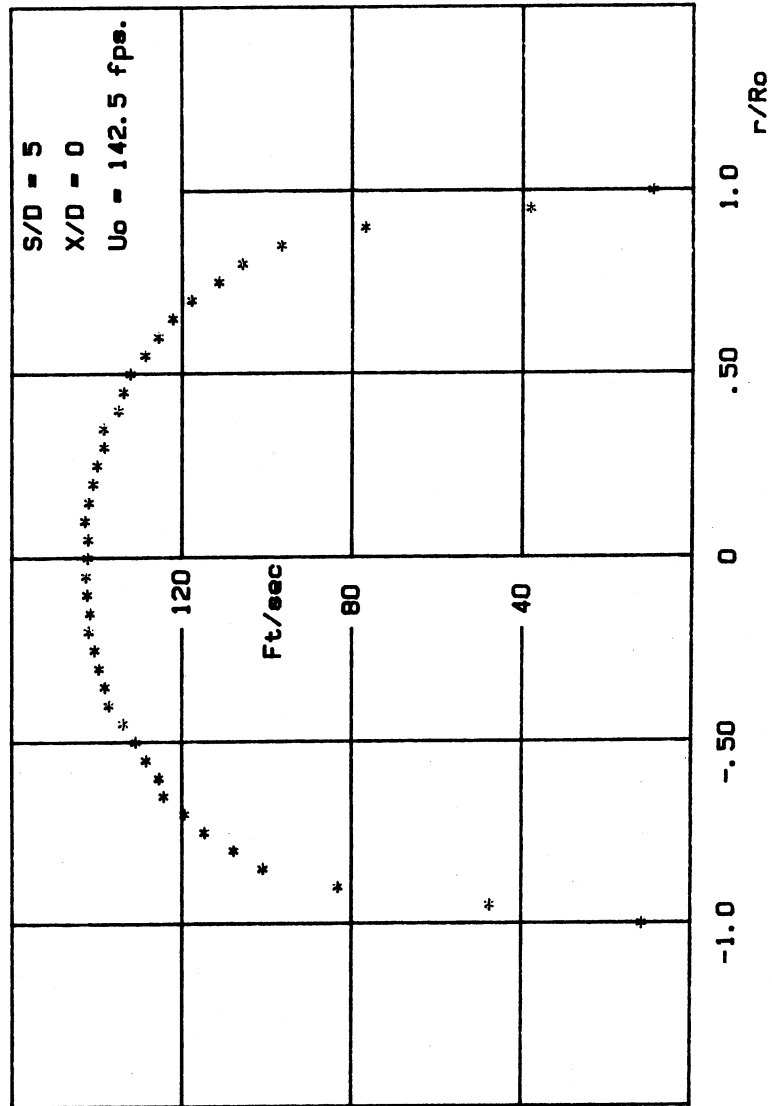FIGURE 53B: Initial velocity distribution for S/D = 2.5

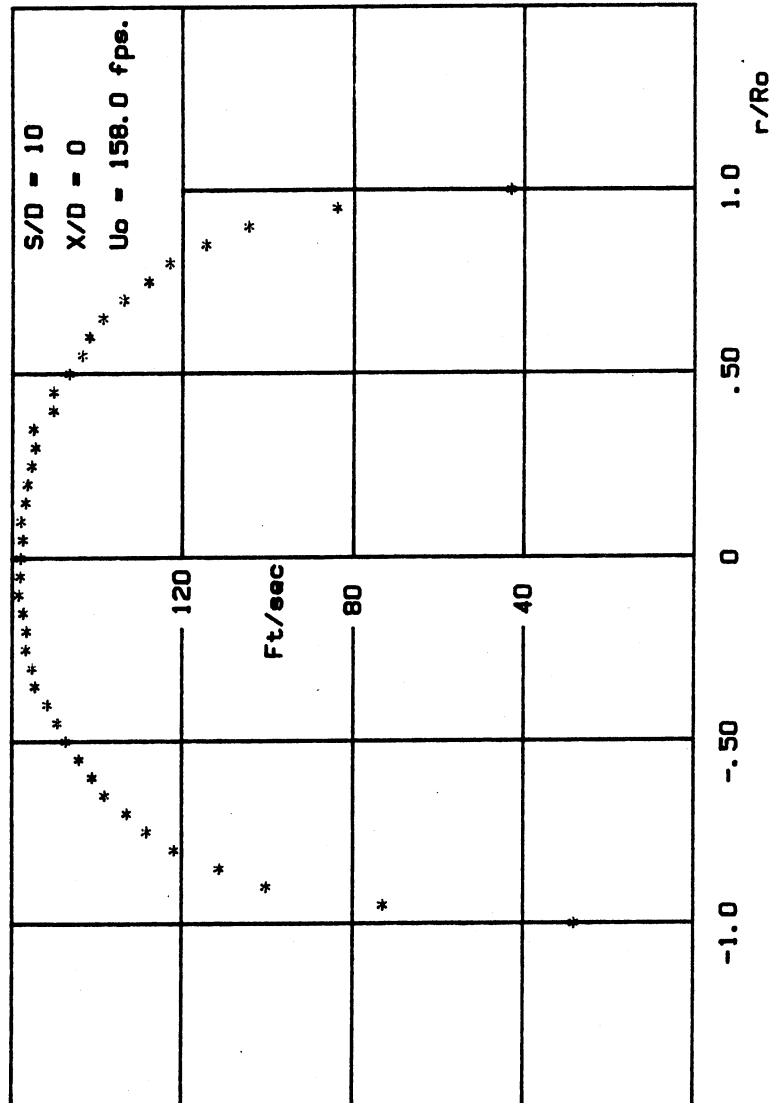124



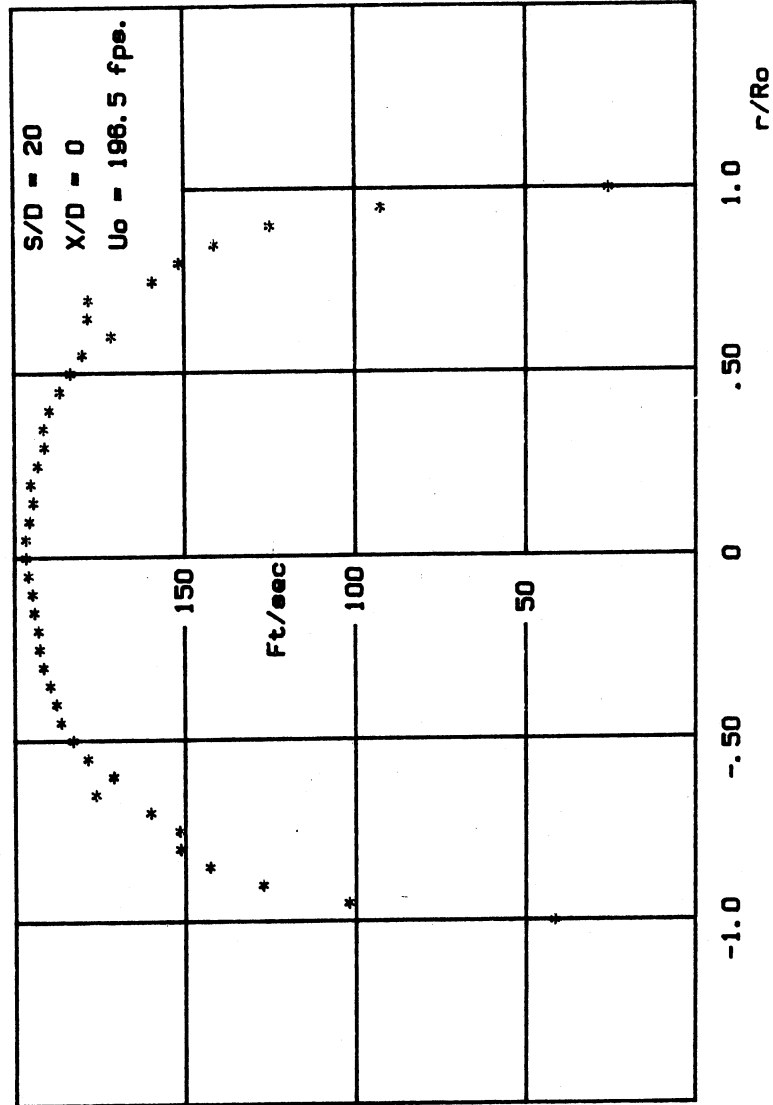FIGURE 54B: Initial velocity distribution for S/D = 5

FIGURE 55B: Initial velocity distribution for S/D = 10

126



FIGURE 56B: Initial velocity distribution for S/D = 20

# REFERENCES

1. Abramovich, G.N., The Theory of Turbulent Jets, M.I.T. Press, Cambridge, Mass., 1963.

2. Albertson, M.L., Dai, Y.B., Jensen, R.A., and Rouse, H., "Diffusion of Submerged Jets", Trans. ASCE, pp. 639-697, 1950.

3. Hinze, J.O., Turbulence, McGraw-Hill Book Co., New York, New York, 1975.

4. Kamotani, Y., and Greber, I., "Experiments on a Turbulent Jet in a Cross Flow", AIAA Journal, Vol. 10, No. 11, 1972.

5. Lipshitz, A., "Dilution Jets in Accelerated Cross Flows", Ph.D. Thesis, Case Western Reserve Univ., 1981.

6. Lipshitz, A., and Greber, I., "Dilution Jets in Accelerated Cross Flows", NASA Contractor Report 174717, June 1984.

7. Nash, M.V., "The Entrainment Rate for a Row of Turbulent Jets", M.S. Thesis, Case Western Reserve Univ., 1984.

8. Pai, S., Fluid Dynamics of Jets, Van Nostrand Co., New York, New York, 1954.

9. Ricou, F.P., and Spalding, D.B., "Measurements of Entrainment by Axisymmetrical Turbulent Jets", Journal of Fluid Mechanics, Vol. 11, pp. 21-32, 1961.

10. Schenck, H., Theories of Engineering Experimentation, McGraw-Hill Book Co., New York, New York, 1968.

11.   Schlicting, H., _Boundary Layer Theory_,
      McGraw-Hill Book Co., 1955.

# Report Documentation Page

| 1. Report No. NASA CR-185278 | 2. Government Accession No. | 3. Recipient's Catalog No. |
|---|---|---|

| 4. Title and Subtitle | 5. Report Date |
|---|---|
| The Entrainment Rate for a Row of Turbulent Jets | September 1990 |
| | 6. Performing Organization Code |

| 7. Author(s) | 8. Performing Organization Report No. |
|---|---|
| Eliott B. Gordon and Isaac Greber | None |
| | 10. Work Unit No. 505-62-21 |

| 9. Performing Organization Name and Address | 11. Contract or Grant No. |
|---|---|
| Case Western Reserve University Department of Mechanical and Aerospace Engineering Cleveland, Ohio 44106 | NAG3-251 |
| | 13. Type of Report and Period Covered Contractor Report Final |

| 12. Sponsoring Agency Name and Address | 14. Sponsoring Agency Code |
|---|---|
| National Aeronautics and Space Administration Lewis Research Center Cleveland, Ohio 44135-3191 | |

**15. Supplementary Notes**

Project Manager, James D. Holdeman, Internal Fluid Mechanics Division, NASA Lewis Research Center.

**16. Abstract**

Entrainment rates for a row of isothermal circular air jets issuing into a quiescent environment are found by integrating velocity distributions measured by a linearized hot wire anemometer. Jet spacing to jet diameter ratios of 2.5, 5, 10, and 20 are studied at jet Reynold's numbers ranging from 5110 to 12 070. Velocity distributions are determined at regular downstream intervals at axial distances equal to 16.4 to 164 jet diameters from the jet source. The entrainment rates for the four spacing configurations vary monotonically with increasing S/D between the liniting case of the slot jet entrainment rate (where the jet spacing to diameter ratio is zero) and the circular jet entrainment rate (in which case the spacing to diameter ratio is infinity).

| 17. Key Words (Suggested by Author(s)) | 18. Distribution Statement |
|---|---|
| Jets Cross flow Entrainment Experimental | Unclassified – Unlimited Subject Category 02 |

| 19. Security Classif. (of this report) | 20. Security Classif. (of this page) | 21. No. of pages | 22. Price* |
|---|---|---|---|
| Unclassified | Unclassified | 133 | A07 |